AALBORG UNIVERSITY

DENMARK

Estimation of Wave Disturbance in Harbours

Helm-Petersen, Jacob

Publication date:
1998

Document Version
Publisher's PDF, also known as Version of record

[Link to publication from Aalborg University](#)

Jacob Helm-Petersen

Estimation of
Wave Disturbance in Harbours

Hydraulics & Coastal Engineering Laboratory
Department of Civil Engineering
Aalborg University

October 1998

Estimation of
Wave Disturbance in Harbours

by

Jacob Helm–Petersen

October 1998

Preface

The present thesis *Estimation of Wave Disturbance in Harbours* is submitted as one of the requirements for obtaining the degree of Ph.D. according to Order No. 989 of 11 December 1992 from the Danish Ministry of Education.

The study was supported by the Danish Technical Research Council (STVF) as part of the frame work programme Marine Techniques 2 (Marin Teknik 2) and was carried out in the period from November 1993 to July 1997.

Associate professor Michael Brorsen, Department of Civil Engineering, Aalborg University, acted as supervisor during the study. Further associate professor Peter Frigaard has been involved in the project. Their interest and patience is greatly acknowledged.

During a 5 month stay at the School of Civil and Structural Engineering, University of Plymouth, UK, prototype measurements were analysed and permission was granted to publish results from selected measurements in the present thesis. This gesture is highly appreciated.

Data from physical measurements have also been made available from a combined MAST, LIP, and TAW project carried out at Delft Hydraulics, the Netherlands. The collaboration of the involved partners is greatly acknowledged.

Last but not least the author wishes to thank his colleagues and the technical staff within the department.

Aalborg, October 1998.

Jacob Helm–Petersen.

Contents

Symbols

The following list of symbols contains the majority of symbols applied in the present report. To a wide extent the symbols follow the IAHR–guidelines as proposed in Frigaard et al. (1997). A small number of assisting symbols are defined throughout the text and have not been included in the list.

a	wave amplitude
A	area
c	wave celerity
C_R	reflection coefficient (amplitude)
E	energy
$E[\ ]$	expected value
f	wave frequency
f_c	carrier frequency
g	acceleration due to gravity
h	depth of water
H	wave height
H_s	significant wave height
$H(f, \theta)$	directional spreading function
i	imaginary unit
k	wave number
L	wave length
$L(\ )$	likelihood function
p	probability
q	flow

R	cross-correlation
R_c	crest height
s	directional spreading parameter
s	wave steepness
S_η	spectral density of surface elev.
t	time
T	wave period
u	hyperparameter in BDM
u, v, w	velocity components
x, y, z	geometric co-ordinates
α	slope angle
δ	variational derivative
ε	error
η	surface elevation
θ	wave direction
θ_m	mean wave direction
ρ	density
σ	standard deviation
ω	angular frequency
ϕ	velocity potential
μ	reduction factor
ξ	surf similarity parameter
Φ	phase

Abstract

The motivation for the present study has been to improve the reliability in using numerical wave propagation models as a tool for estimating wave disturbance in harbours. Attention has been directed towards the importance of the modelling of reflection in the applied mild-slope model.

Methods have been presented for the analysis of reflected wave fields in 2D and 3D. The Bayesian Directional Wave Spectrum Estimation Method has been applied throughout the study.

Reflection characteristics have been investigated by use of physical models for three types of coastal structures with vertical fronts. The analyses include mainly directional waves. Analysis of field measurements has also taken place.

Simulations with a mild-slope model have been carried out with individual structures and a complete harbour. The analyses clarify to a wide extent the behaviour of the sponge layers applied in the model. Information on how the sponge layers perform with respect to reflection of short-crested waves are presented mainly in terms of overall reflection coefficients and main directions as functions of incident main direction relative to the structure. The influence of a irregular structure front has also been investigated. Within the limitations of the performed simulations the numerical model showed very good behaviour with respect to reflection of short-crested waves.

Simulations with a harbour gave an indication of the influence reflection can have on the estimated wave disturbance. Significant differences were seen for small changes in reflection coefficients. This points in the direction of a need for improvements of wave reflection prediction formulae.

Finally comparisons between results from the numerical model and physical scale measurements from earlier experiments with the same harbour show satisfactory agreement.

Sammenfatning

Baggrunden for nærværende studie har været at forbedre pålideligheden ved at anvende numeriske bølgeudbredelsesmodeller som et værktøj til at estimere bølgeuro i havne. Opmærksomheden har været rettet mod vigtigheden af at modellere refleksionen i den anvendte mild-slope model.

Metoder til analyse af reflekterede 2D og 3D bølgefelter er blevet presenteret. The Bayesian Directional Wave Spectrum Estimation Method er blevet anvendt i studieforløbet.

Refleksions-karakteristikker for tre typer af kystkonstruktioner med lodret front er blevet undersøgt ved brug af fysiske modelforsøg. Analysen inkluderer hovedsageligt retningsspredte bølger. Analyse af felt målinger har også fundet sted.

Simuleringer med mild-slope modellen er blevet udført med individuelle konstruktioner og med en komplet havn. Analysen klarlægger i et bredt omfang karakteristika for de i modellen anvendte svampelag. Information om hvordan svampelagene opfører sig med hensyn til refleksion af kortkammede bølger er præsenteret i form af refleksions koefficienter og hovedudbredelses-retninger som funktion af indkommende hovedudbredelses-retning relativ til konstruktionen. Betydningen af en irregulær konstruktions-front er også blevet undersøgt. Indenfor begrænsningerne for simuleringerne viste den numeriske model tilfredsstillende resultater.

Simuleringer med en havn giver en indikation af den betydning bølge-refleksion kan have på den estimerede bølgeuro. Der ses betydelig forskel for små ændringer i refleksions-koefficienter. Dette peger i retningen af et behov for forbedringer af formler til forudsigelse af bølgerefleksion.

Afsluttende sammenligninger mellem resultater af den numeriske model og fysiske skala-målinger fra tidligere forsøg med den samme havn viser tilfredsstillende overensstemmelse.

SAMMENFATNING

1

Introduction

1.1 Motivation

The design of a modern port or harbour is a complicated task. As engineers have gained better understanding in the design of breakwaters and quays, the demand to the wave conditions in a harbour has been pushed forward. In addition a demand for larger water depths has arisen due to the increased draft of the large vessels. Consequently, there is a continuous need for building new harbours and extending existing ones.

The major difficulty in designing a harbour is not so much to design the individual structures, but to determine an optimal layout of the harbour taking into consideration the resulting performance of the structures altogether. Another difficult problem is to determine the environmental loads, which the individual structures have to resist. This subject will, however, not be addressed further in this study.

As a design criterion the wave disturbance (or tranquillity) plays an important role, as it concerns the usefulness and hence the quality of the harbour. In practice estimates of the wave disturbance in a harbour can be achieved either through physical modelling or numerical simulation. Applying a physical model introduces uncertainties mainly due to scale effects, whereas it is various theoretical shortcomings, which introduce uncertainties in numerical methods. It is clear though that both approaches are approximate.

One can be tempted to consider numerical models to replace the use of physical models in the future. Although numerical models have developed rapidly during the last decade, many problems do remain to be solved, and subsequently implemented into the models. Hence, there is still a significant need for carrying out physical experiments. Thus numerical models have not yet replaced, but rather encourage to the use of physical models.

There is no doubt, however, that the role of numerical models as a design tool will continue to grow. At present numerical wave propagation models are already being used in the design of harbours, but in many cases simulations are accompanied with physical small scale experiments. This obviously emphasises the insufficiency in either the performance of numerical wave propagation models or in the validation of the available models.

The present study has been initiated in order to improve the reliability in results obtained by use of numerical wave propagation models. The study will focus on conditions related to wave reflection from marine structures, particularly by involving the following subjects.

- Determination of reflection coefficients for various marine structures, ranging from typical harbour structures for berthing (vertical face structures) to porous sloping structures like breakwaters. There is in particular a significant need to investigate the influence of wave directionality on wave reflection.

- Investigation of the capability of existing numerical models to model oblique wave reflection as well as reflection of directional waves (3D waves). The model to be considered implements a wave reflection technique, which is based on considerations of a two dimensional case. There is a possibility that this technique can perform satisfactory also in the general three dimensional case. If so, this should be verified thoroughly.

1.2   Reflection from Marine Structures

The reflection of waves is a physical process taking place, when waves approach a boundary preventing the waves to continue undisturbed. At such a boundary the waves can also be dissipated or transmitted, but most often a combination of these effects will take place. From an engineering point of view the only condition is that the energy of the reflected, dissipated and transmitted waves altogether will correspond to the incident wave energy.

Problems with reflection in a harbour can be reduced using structures with a high dissipation of wave energy. This encourages the use of sloping or porous

structures, as these will cause either wave breaking or turbulence, which, in this case, are useful energy dissipating processes. Common harbour structures like quays and wharf's are, however, usually constructed with a vertical face, so as to provide optimal conditions for loading and unloading ships. These structures must resist considerable vertical loads from various cargo handling equipment, making it difficult to use porous or perforated structures.

Although these considerations are very general, it is clear that it is the conflict between wave dissipation and load capacity, which makes it unfavourable to design the perfect harbour (structure). The wave reflection characteristic for some typical harbour structures are reproduced in Table 1.1 clearly showing a significant variation in reflection.

Type of structure	C_R
Vertical wall with crown above water	0.7~1.0
Vertical wall with submerged crown	0.5~0.7
Slope of rubble stones (slope of 1 on 2 to 3)	0.3~0.6
Slope of energy dissipating concrete blocks	0.3~0.5
Vertical structure of energy dissipating type	0.3~0.8
Natural beach	0.05~0.2

Table 1.1: Typical ranges of reflection, from Goda (1985).

In addition the highly reflective structures create an inhomogeneous pattern between incident and reflective waves, i.e. some areas will be rough and other areas calm. This is also known as phase-locking. The effect is less pronounced for a low reflective structure, where the point of reflection varies for the different wave components in an irregular sea. Further, this effect is less for short–crested waves than for long–crested waves.

For a reflected monochromatic wave it is easy to calculate a reflection coefficient, but introducing irregular waves and wave directionality it becomes a more complicated task. Many sophisticated methods, among which none are perfect, have been presented. However, considering those methods which estimate reflection coefficients on the basis of measured or simulated wave kinematics, a reasonable level has been reached.

Wave reflection characteristics have often been investigated through experiments either in the laboratory or in the field. Both have their advantages and disadvantages. In the laboratory experiments are easily controlled but will often be carried out as small–scale experiments, hence introducing scale effects. In the field the opposite situation occurs. Although a large amount of experiments have been done, information of reflection of short–crested waves in particular are still lacking.

1.3   Numerical Wave Propagation Models

Numerous wave propagation models have been presented in the past, many of them based on the same theory but still different due to different boundary conditions or other assumptions. Having developed since the late fifties the most important type of models are the Boussinesq models. The variability of these models is considerable, each of them focussing on a particular phenomenon like e.g. wave breaking. The combination of many complex phenomena in one model is not yet without difficulties not to mention the cost in simulation time.

Another widespread model is the Mild-Slope model, which also exist in various versions. The Mild-Slope models are less developed than the Boussinesq models, but for many purposes they are sufficient in accuracy and have the advantage of being less complicated and use less simulation time.

A good understanding of the performance of a proposed harbour layout can, however, be obtained with these models despite the inaccuracy. Wave disturbance is in general evaluated for many incident wave conditions, only few of them related to extreme events, which will often cause major problems for the models due to especially increased non-linear effects. Thus, the harbour layout can be designed to avoid wave energy being concentrated in certain areas, which may be a problem even for less wave activity.

1.4   Scope of Thesis

As it may already appear the present work involves several subjects in order to follow up on the motivation given earlier. Thus some subjects will be treated thoroughly, whereas others will be treated only superficially. This approach has been adapted so as to provide a smooth reading of the thesis.

In the following the scope of the thesis will be outlined.

Chapter 2 contains theories on reflection analysis. Attention will be paid mainly to 3D wave spectrum estimation methods, which enables reflection analysis in the 3D case, i.e. short-crested waves. The Maximum Likelihood Method considering 3D wave spectra on standard form including reflection will be presented, followed by a description of the Bayesian Directional Spectrum Estimation Method.

In Chapter 3 results from physical scale experiments will be presented. This may be considered as an example of how to obtain reflection coefficients for short-crested waves. Two vertical face structures have been investigated, namely a porous structure and a caisson with plain and perforated front.

The subsequent Chapter 4 contains a presentation of field measurements collected at Alderney by the University of Plymouth, UK. These results are in themselves very valuable in not being affected by scale effects, but other inaccuracies and uncertainties are inevitably introduced. However, results of reflection coefficients are presented for the considered breakwater. More data and more work would possibly decrease the scatter of these results, but that have fallen beyond the present study.

Chapter 5 introduces the Mild-Slope wave propagation model in its main principle, but a really thorough description of the theory must be found elsewhere. A large number of simulations of various boundaries (structures) are carried out and results are presented. The purpose has been to clarify what happens when short-crested waves are being reflected in the model.

Hereafter, in Chapter 6, comparisons between results from the numerical model and a physical scale model are presented. A harbour for which data from physical scale measurements were already available has been selected for the simulations.

The thesis ends with summary and conclusions.

Appendices contain a literature survey on reflection coefficients for various coastal structures, theory on MLM and BDM, data from the field measurements, results from the numerical simulations, and finally a note on the performance of the BDM method.

2

Reflection Analysis

2.1 Introduction

Reflection of waves is conveniently expressed in reflection coefficients, which relates the size of reflected waves to the size of the corresponding incident waves. Hence reflection coefficients ought to be expressed as a function depending on a number of controlling parameters. Then it would be possible to determine the reflection at a given structure for an arbitrary known incident wave. This will, however, involve a great deal of parameters, of which some will be less important than others. Hence it is general practice to express the reflection coefficient for a certain structure as one of the following simplifications.

- An overall reflection coefficient, i.e. a scalar (weighted or plain average).

- A frequency dependent reflection coefficient.

- A reflection coefficient depending on frequency and angle of wave attack, or at least main direction of wave attack.

Factors like amplitude, steepness, or non-linearity of the incident waves are often ignored for vertical face structures, as the effect on the reflection is believed to be within the accuracy of the available methods at present.

Further, reflection can be expressed in terms of amplitude or energy. This is only a matter of a square root, but it does sometimes lead to misunderstandings

anyway. Where nothing else is specified, reflection will be based on amplitude throughout this thesis.

In some situations reflection coefficients may be derived analytically, but such results will always depend on theoretical shortcomings. Hence it is more common to estimate reflection coefficients based on physical scale experiments or proto-type measurements. The main difficulty is, however, that incident and reflected waves cannot be measured individually.

The following sections will contain a description of methods for reflection ana-lysis of longcrested as well as shortcrested waves. The latter includes methods originally proposed for estimation of directional wave spectra, but some of these may also be used to estimate reflection coefficients in the 3D domain.

2.2   Reflection Methods in 2D

The development of methods for reflection analysis of irregular waves began in the late 60's. The methods presented by Kajima (1969), and Thornton and Calhoun (1972) were among the first to be presented. The method by Kajima was improved significantly by Goda and Suzuki (1976), who introduced the FFT[1] algorithm. Mansard and Funke (1980) once again improved the method by introducing an optimisation procedure accounting for noise in the signals. Due to the simple implementation of the methods by Goda and Suzuki & Mansard and Funke, these have been used extensively ever since.

The above mentioned methods to be used in the analysis of reflected two di-mensional waves are based on the assumption, that the wave elevation can be considered as a sum of waves propagating with different frequencies, amplitudes, phases and wavelengths according to the 1st order wave theory. Further for each incident wave a reflected wave will travel in the opposite direction.

Thus, the wave elevation can be expressed as in (2.1).

$$
\begin{aligned}
\eta(x,t) &= \sum_{n=1}^{N} a_{I,n} \cos(k_n x - \omega_n t + \Phi_{I,n}) \\
&\quad + \sum_{n=1}^{N} a_{R,n} \cos(k_n x + \omega_n t + \Phi_{R,n})
\end{aligned}
\tag{2.1}
$$

Goda and Suzuki (1976) suggested to solve (2.1) by use of Fourier analysis of two elevation time series recorded simultaneously at two distinct points. This yields the solution in (2.2) with respect to amplitudes.

---

[1]Fast Fourier Transformation

$$
\begin{aligned}
a_I &= \frac{1}{2|\sin(kx_{12})|} \sqrt{(A_2 - A_1\cos(kx_{12}) - B_1\sin(kx_{12}))^2} \\
&\quad \overline{+(B_2 + A_1\sin(kx_{12}) - B_1\cos(kx_{12}))^2} \\
a_R &= \frac{1}{2|\sin(kx_{12})|} \sqrt{(A_2 - A_1\cos(kx_{12}) + B_1\sin(kx_{12}))^2} \\
&\quad \overline{+(B_2 - A_1\sin(kx_{12}) - B_1\cos(kx_{12}))^2}
\end{aligned}
\tag{2.2}
$$

where the introduced coefficients are obtained from the Fourier analysis.

Mansard and Funke (1980) recognised, that any measurements are likely to contain noise and hence included an error in the method by Goda and Suzuki. The error is expressed in (2.3) as $\Omega(t)$.

$$
\begin{aligned}
\eta(x,t) &= \sum_{n=1}^{N} a_{I,n}\cos(k_n x - \omega_n t + \Phi_n) \\
&\quad + \sum_{n=1}^{N} a_{R,n}\cos(k_n(x + 2x_R) + \omega_n t + \Phi_n + \theta_s) + \Omega(t)
\end{aligned}
\tag{2.3}
$$

In (2.3) x_R is the distance to the reflector and θ_s is a possible phase shift at the reflector.

Results are then obtained by minimising the noise e.g. in a least squares sense. If only two probes are used the solution reduces to that of Goda and Suzuki. Mansard and Funke derived a solution for three probes, and later the method has been derived for an arbitrary number of probes by Zelt and Skjelbreia (1992).

In the case of oblique waves, i.e. 2D-waves travelling along a line not perpendicular to the reflecting structure, the previous methods can be applied by assuming that the waves can be decomposed into two vectorial components, being respectively perpendicular and parallel to the structure.

$$
\begin{aligned}
\eta(x,t) &= \sum_{n=1}^{N} a_{I,n}\cos(k_n x - \omega_n t + \Phi_{I,n}) \\
&\quad + \sum_{n=1}^{N} a_{R,n}\cos(k_n x + \omega_n t + \Phi_{R,n})
\end{aligned}
\tag{2.4}
$$

Omitting index n and rewriting (2.4) in cartesian coordinates leads to (2.5).

$$
\begin{aligned}
\eta(x,y,t) &= a_I \cos(kx\cos(\theta_I) + ky\sin(\theta_I) - \omega t + \Phi_I) \\
&\quad + a_R \cos(kx\cos(\theta_R) + ky\sin(\theta_R) + \omega t + \Phi_R)
\end{aligned}
\tag{2.5}
$$
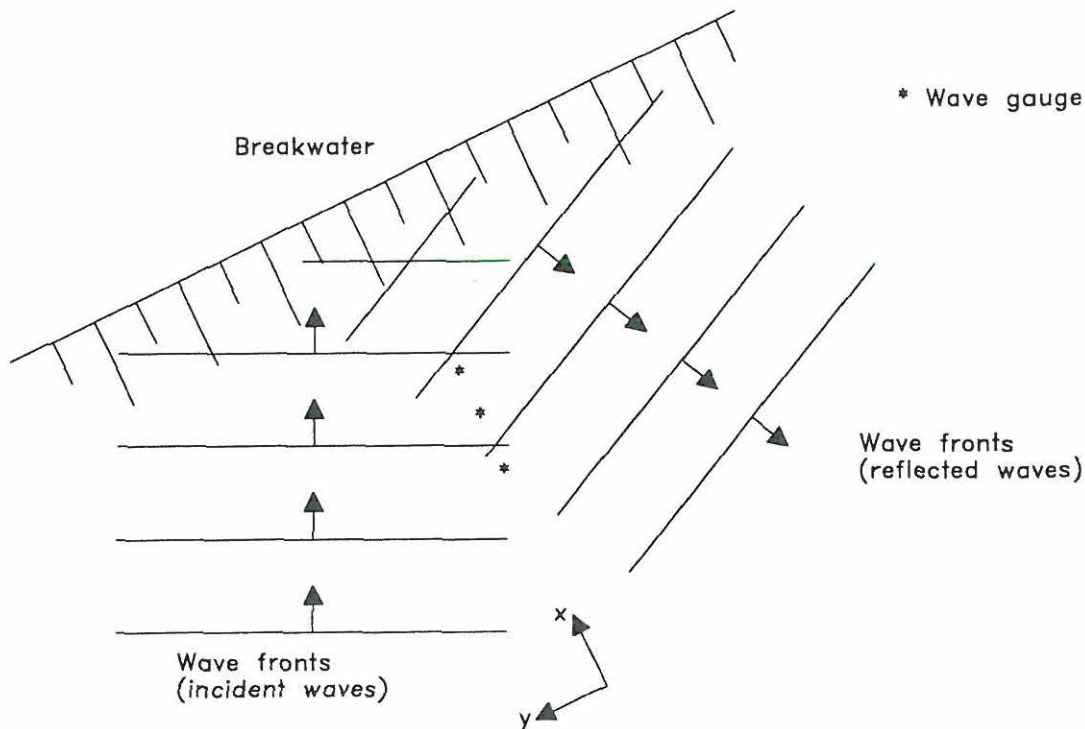
Figure 2.1: *Position of wave gauges in front of a structure.*

One example of solving the problem is to place all wave gauges on a line with y-coordinate $\equiv 0$ as shown in Figure 2.1. Equation (2.5) will then reduce to (2.6).

$$
\begin{aligned}
\eta(x,0,t) \;=\; & a_I \cos(kx \cos(\theta_I) - \omega t + \Phi_I) \\
& + a_R \cos(kx \cos(\theta_R) + \omega t + \Phi_R)
\end{aligned} \tag{2.6}
$$

It is seen, that if the angle of the incident wave is known, and the angle of the reflected wave is calculated using Snells law, i.e. incident angle equals reflected angle, (2.6) is very similar to the original expression, (2.1), for the wave elevation.

2.3   Directional Wave Spectra

Along with the increased number of 3D wave tanks it has become essential to be able to describe short-crested seas. The directional wave spectrum was introduced as an extension to the one dimensional wave spectrum, accounting for the distribution of wave energy on both frequency and direction. Whereas it is easy to characterise a short-crested sea state by the directional wave spectrum, it is much more difficult and tedious to actually estimate the directional wave spectrum of a measured sea state.

With strong reference to methods used in geophysics and communication engineering a number of methods have been proposed through the years. Among those most often used are the Maximum Likelihood Method, Capon (1969), and the Maximum Entropy Method, Burg (1967). Since then several authors have modified and improved these methods, whereas only a few new methods have been proposed. The basic problem, however, remains, namely to estimate a complete directional wave spectrum based on a limited number of measurements.

A complete directional wave spectrum is capable of describing a reflected sea state, and reflection coefficients can be derived. Some methods are, however, not capable of dealing with a reflected sea state. The reason is either, that the method simply does not allow the presence of reflected waves, or the method fail to treat phase-locked waves properly. Not allowing for the presence of reflected waves is often advantageous when analysing ocean waves, where reflection rarely appears. Phase-locking occurs, when a reflected wave interacts with the original incident wave propagating with the same frequency. This phenomenon may result in standing waves, which introduce inhomogeneous wave conditions. In a short-crested sea this effect is, however, not as prevalent as in a 2D case. The problem may be overcome by including an interaction term in the existing methods, although making the methods even more complex, see e.g. Isobe and Kondo (1984).

2.3.1 Basic Relation

Estimation of directional wave spectra may be based on any kind of wave measurements. Most common are recordings of particle velocities, wave elevations and heave-pitch-roll data. For simplicity only wave elevations will be considered in the following.

The relationship between cross spectral values of two measured elevation time series and the directional wave spectrum, in terms of the full directional spreading function, can be expressed as in (2.7).

$$\frac{S_{\eta_1\eta_2}(f)}{S_\eta(f)} = \int_{-\pi}^{\pi} H(f,\theta)\exp(-ikr_{12}\cos(\theta-\beta_{12}))d\theta \qquad (2.7)$$

where the directional wave spectrum has been decomposed into the auto spectrum and a directional spreading function, $H(f,\theta)$, as expressed in (2.8).

$$S(f,\theta) = S(f)H(f,\theta) \qquad (2.8)$$

The geometric variables are defined as shown in Figure 2.2.

The cross spectrum of η_1 and η_2, $S_{\eta_1\eta_2}(f)$, is defined as the Fourier transform
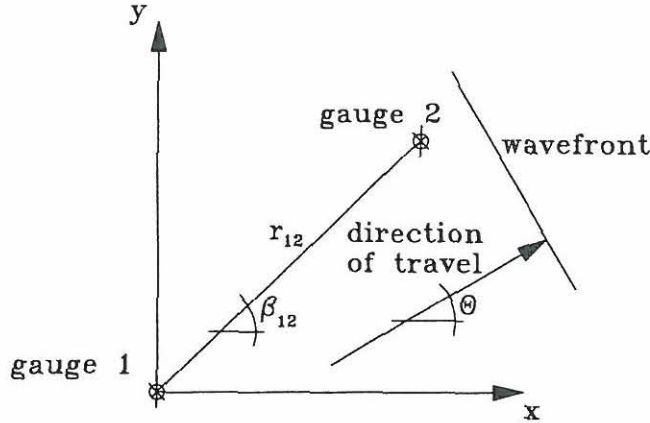
Figure 2.2: Definition of geometric parameters.

of the cross-correlation function, $R_{\eta_1 \eta_2}(\tau)$, as shown in (2.9).

$$S_{\eta_1 \eta_2}(f) \quad = \quad \int_{-\infty}^{\infty} R_{\eta_1 \eta_2}(\tau) \exp(-i 2\pi f \tau) d\tau \qquad (2.9)$$

Based on measurements estimates of the cross spectra can easily be obtained by use of e.g. FFT analysis. What remains, is then to solve (2.7) with respect to the directional wave spectrum. This is not a straight forward procedure, as the shape of the spreading function is not known, and an explicit expression cannot be derived from (2.7). Hence the numerous methods for directional wave spectrum estimation basically differ in selecting a model to discribe the spreading function term in (2.7). Having assumed a model the methods may further differ in how to fit the data to the model.

Since the purpose of a 3D wave spectrum estimation method is to describe the distribution of wave energy on frequency and direction, a higher resolution, of both frequency and direction, implies a better description. This problem of improving the frequency resolution is well known from ordinary spectral analysis of a plain time series, Newland (1993). A lower frequency resolution leads to larger confidence bands on the spectral estimates. This problem applies to all methods based on cross-spectral estimates of simultaneous recorded time series.

2.3.2   Comparison of Methods

Out of the large number of methods for estimating a directional wave spectrum none can be said to be significantly superior. Thus the selection of a particular method is not straight forward, which is also reflected in numerous papers comparing the performance of various methods, see e.g. Davis and Regier (1977),

Benoit (1992), Benoit (1993), Kim et al. (1993), Chadwick et al. (1995) or Hawkes et al. (1997).

Comparing the various methods is, however, a very difficult task, as the individual performances will depend strongly on the input data. If a short-crested sea state is generated e.g. by numerical simulation using a Mitsuyasu-type directional spreading function, Mitsuyasu et al. (1975), $\alpha \cos^{2s}(\frac{\theta-\theta_m}{2})$, good result will be obtained for methods fitting to such a function, whereas other methods may not get as close to the target distribution. Likewise it will not make sense to fit a bi-modal spreading function, as if reflection occurs, to a single-modal spreading function. The same can be said about noise on signals, non-linearity of waves, and phase-locking of waves etc.

Among the methods being most widely used today are, as mentioned earlier, various implementations of the Maximum Likelihood Method, and the Maximum Entropy Method. In general such methods define a likelihood function or an entropy function, which is to be maximised in order to obtain the most probable estimate of the wave spectrum.

For the present work, the Bayesian Directional Wave Spectrum Estimation Method, described in the following Section 2.5, has been used. The method is one of the latest proposed methods, and makes use of a Bayesian approach. It has the advantage of being less sensitive to the available input data. That is, it does not assume a specific shape of directional spreading functions, it is very stable with respect to noise, and it is fairly capable of resolving incident and reflected waves. The price is a need for a larger number of simultaneous measurements and a relatively long processing time.

2.4 The MLM Method

Time series of elevations are assumed to be random processes being joint Gaussian distributed. Thus,

$$\eta_i(x, t) = \sum_{j=1}^{\infty} (a_{i_j}^c \cos \omega_j t + a_{i_j}^s \sin \omega_j t) \tag{2.10}$$

where $i = 1, 2, ..., M$, and M is the number of time series.

The Fourier coefficients are considered as random integrals

$$a_{i_j}^c = \frac{2}{T} \int_0^T \eta_i \cos \omega_j t \, dt \tag{2.11}$$

$$a_{i_j}^s = \frac{2}{T} \int_0^T \eta_i \sin \omega_j t \, dt \tag{2.12}$$

Hence $a_{i_j}^c$ and $a_{i_j}^s$ are joint Gaussian distributed.

In the following only one frequency is considered. Further let

$$\boldsymbol{A}^T \;\; = \;\; [a_1^c \; a_2^c \; \cdots \; a_M^c \; a_1^s \; a_2^s \; \cdots \; a_M^s] \tag{2.13}$$

In order to establish the joint distribution of the Fourier coefficients, the expected value of $\boldsymbol{A}$ and the cross covariance matrix need to be defined.

$$E[\boldsymbol{A}] \;\; = \;\; \boldsymbol{0} \tag{2.14}$$

$$\kappa = \kappa_A \;\; = \;\; \frac{1}{\Delta f} E[\boldsymbol{A}\boldsymbol{A}^T] \;\; = \;\; \begin{bmatrix} \boldsymbol{C} & \boldsymbol{Q} \\ -\boldsymbol{Q} & \boldsymbol{C} \end{bmatrix} \tag{2.15}$$

where $\boldsymbol{C}$ and $\boldsymbol{Q}$ are the co– and quad–spectrum respectively.

The joint probability then reads as follows.

$$p_{\boldsymbol{A}} \;\; = \;\; \frac{1}{(\sqrt{2\pi})^{2M}|\kappa|^{1/2}} \exp\left(-\frac{1}{2}\boldsymbol{a}^T\kappa\,\boldsymbol{a}\right) \tag{2.16}$$

where $\boldsymbol{a}$ is a realization of $\boldsymbol{A}$.

Having determined the probability of observing the realization $\boldsymbol{a}$, the probability of observing a number of observations can be calculated by multiplying the individual probabilities. Taking the P'th root, where P is the number of realizations, the value is defined as the likelihood of the realizations.

$$L(\boldsymbol{a}_1, \boldsymbol{a}_2, ..., \boldsymbol{a}_P, S) \;\; = \;\; (p_{\boldsymbol{A}}(\boldsymbol{a}_1)p_{\boldsymbol{A}}(\boldsymbol{a}_2)\cdots p_{\boldsymbol{A}}(\boldsymbol{a}_P))^{1/P} \tag{2.17}$$

$$= \;\; \prod_{p=1}^{P} \left(\frac{1}{(\sqrt{2\pi})^{2M}|\kappa|^{1/2}} \exp\left(-\frac{1}{2}\boldsymbol{a}_p^T\kappa^{-1}\boldsymbol{a}_p\right)\right)^{1/P} \tag{2.18}$$

$$= \;\; \frac{1}{(\sqrt{2\pi})^{2M}|\kappa|^{1/2}} \exp\left(-\frac{1}{2P}\sum_{p=1}^{P}\boldsymbol{a}_p^T\kappa^{-1}\boldsymbol{a}_p\right) \tag{2.19}$$

$$= \;\; \frac{1}{(\sqrt{2\pi})^{2M}|\kappa|^{1/2}} \exp\left(-\frac{1}{2P}\sum_{p=1}^{P}\sum_{i=1}^{2M}\sum_{j=1}^{2M} a_{p_i}\kappa_{ij}^{-1}a_{p_j}\right) \tag{2.20}$$

$$= \;\; \frac{1}{(\sqrt{2\pi})^{2M}|\kappa|^{1/2}} \exp\left(-\frac{1}{2}\sum_{i=1}^{2M}\sum_{j=1}^{2M}\kappa_{ij}^{-1}\frac{1}{P}\sum_{p=1}^{P} a_{p_i}a_{p_j}\right) \tag{2.21}$$

$$= \;\; \frac{1}{(\sqrt{2\pi})^{2M}|\kappa|^{1/2}} \exp\left(-\frac{1}{2}\sum_{i=1}^{2M}\sum_{j=1}^{2M}\kappa_{ij}^{-1}\overline{a_i a_j}\right) \tag{2.22}$$

where $\overline{a_i a_j}$ is the average product of the Fourier coefficients.

The aim of the MLM analysis is to maximize the probability, i.e. the likelihood, of observing the measured cross spectrum. In practice a number of directional wave spectra can be computed, and used to calculate the cross covariance matrix determining the probability function in (2.16).

Refer to e.g. Isobe and Kondo (1984) and Yokoki et al. (1992) for further description.

2.5 The BDM Method

An alternative to classical statistical approaches is found in the Bayesian approach, which systematically combines subjective judgements with observed data. Especially when new information is limited, inclusion of any additional information can be an advantage.

Considering a directional spreading function which is discretized into a number of discrete values, the number of unknowns will often be large compared to the number of cross-spectra, which can be calculated from measurements. Hence use of the Bayesian approach appears reasonable if any prior information can be made available.

The principle in the Bayesian approach is to express the prior information in terms of an initial probability distribution function of the unknown parameters. This distribution function is referred to as the prior distribution. The prior information is then combined with a suitable likelihood function, expressing the likelihood of an observed event. The relation is described in (2.23).

$$p_{post}(\theta) \quad = \quad K' \cdot L(\theta) p_{prior}(\theta) \tag{2.23}$$

where

$$K' \quad = \quad \left[\int_{-\infty}^{\infty} L(\theta) p_{prior}(\theta) d\theta \right]^{-1}$$

and where θ symbolises the input parameter(s).

The BDM method implies the Bayesian approach by first to assume a prior probability distribution function of the directional spreading function.

The chosen prior probability function may be regarded as a smoothness criterion, since the probability increases with increased smoothness of the directional spreading function. It is important to stress, that it is in fact the smoothness

criterion, which is the prior information the method makes use of. The prior probability distribution assumed is given in (2.24). The distribution corresponds to a singular multivariate Gaussian distribution, each component being Gaussian distributed with zero mean and standard deviation σ/u.

$$p_{prior}(x|u,\sigma^2) = \left(\frac{u}{\sqrt{2\pi}\sigma}\right)^K \exp\left(\frac{-u^2}{2\sigma^2}\sum_{k=1}^K (x_{k-1} - 2x_k + x_{k+1})^2\right) \quad (2.24)$$

where x is a vector, which elements are the logarithm to each discrete value of the directional spreading function, i.e. $x_k(f) = \ln H(f,\theta_k)$, $k = 1,2,...,K$. u is a hyperparameter, which can be used to alter the influence of the smoothness criteria by changing the standard deviation. Further discussion on (2.24) is postponed to appendix.

By taking the logarithm of $H(f,\theta_k)$ it is assumed, that the directional spreading function is always larger than zero. Hence the estimated directional wave spectrum cannot become negative, which physically does not make sense.

Second a likelihood function is defined, by considering the error on the normalised cross-spectra, which are estimated from wave measurements. The errors on cross-spectral estimates are defined as in (2.25).

$$\varepsilon_n = \phi_n - \sum_{k=1}^K \exp(x_k)\alpha_{nk} \quad (2.25)$$

where the following notation has been introduced.

$$\phi_n = \frac{\text{Real}(S_{\eta_i\eta_j})}{\sqrt{S_{\eta_i}S_{\eta_j}}} \quad , \quad n \leq N \quad (2.26)$$

$$\phi_n = \frac{\text{Imag}(S_{\eta_i\eta_j})}{\sqrt{S_{\eta_i}S_{\eta_j}}} \quad , \quad n > N \quad (2.27)$$

$$\alpha_{nk} = \frac{\text{Real}(\exp(-ikr_{ij}\cos(\theta_k - \beta_{ij})))}{\sqrt{S_{\eta_i}S_{\eta_j}}} \quad , \quad n \leq N \quad (2.28)$$

$$\alpha_{nk} = \frac{\text{Imag}(\exp(-ikr_{ij}\cos(\theta_k - \beta_{ij})))}{\sqrt{S_{\eta_i}S_{\eta_j}}} \quad , \quad n > N \quad (2.29)$$

$$N = \frac{M(M-1)}{2}$$

$$n \in \{1,2,...,2N\}$$

That is, each combination of indices i and j correspond to one value of index n. M is the number of gauges.

The above notation is introduced to avoid complex variables and may be rather confusing, but as it will appear later, it simplifies the solution procedure.

The errors are assumed to be outcomes of a Gaussian distribution with zero mean and an unknown standard deviation, σ, being the same parameter as in (2.24). Thus, as each individual error has the probability as in (2.30), the likelihood function is defined as (2.31), which is simply the joint probability.

$$p(\varepsilon_n) = \frac{1}{\sqrt{2\pi}\sigma} \exp\left(-\frac{\varepsilon_n^2}{2\sigma^2}\right) \tag{2.30}$$

$$L(\boldsymbol{x}, \sigma^2|\overline{\varepsilon}) = \prod_{n=1}^{2N} \frac{1}{\sqrt{2\pi}\sigma} \exp\left(-\frac{\varepsilon_n^2}{2\sigma^2}\right) \tag{2.31}$$

It is seen, that small errors lead to a large likelihood.

By substituting the definition (2.25) in (2.30) and the likelihood function (2.31) these can be rewritten as in (2.32) and (2.33).

$$p(\varepsilon_n) = \frac{1}{\sqrt{2\pi}\sigma} \exp\left(-\frac{1}{\sigma^2}\left(\phi_n - \sum_{k=1}^{K} \exp(x_k)\alpha_{nk}\right)^2\right) \tag{2.32}$$

$$L(\boldsymbol{x}, \sigma^2|\overline{\varepsilon}) = \frac{1}{(\sqrt{2\pi}\sigma)^N} \exp\left(-\frac{1}{2\sigma^2}\sum_{n=1}^{N}\left(\phi_n - \sum_{k=1}^{K} \exp(x_k)\alpha_{nk}\right)^2\right) \tag{2.33}$$

Having assumed the prior distribution function of $\boldsymbol{x}$, as in (2.24), and the likelihood function of $\boldsymbol{x}$, as in (2.33), these may be multiplied according to the Bayesian approach, (2.23), yielding the posterior distribution of $\boldsymbol{x}$. This is formulated in (2.34) and (2.35), where a convenient matrix notation has been introduced.

$$p_{post}(\boldsymbol{x}|u, \sigma^2) \propto L(\boldsymbol{x}, \sigma^2)p_{prior}(\boldsymbol{x}|u, \sigma^2) \tag{2.34}$$

$$\propto \exp\left(-\frac{1}{2\sigma^2}|\overline{\phi} - \boldsymbol{A}\exp(\boldsymbol{x})|^2\right) \exp\left(-\frac{u^2}{2\sigma^2}|\boldsymbol{Dx}|^2\right) \tag{2.35}$$

where $\boldsymbol{D}$ is defined in (C.4), and

$$\boldsymbol{A} = \{\overline{\alpha}_1, \overline{\alpha}_2, ..., \overline{\alpha}_{2N}\}^T \tag{2.36}$$

$$\overline{\alpha}_n = \{\alpha_{n,1}, \alpha_{n,2}, ..., \alpha_{n,K}\}^T \tag{2.37}$$

The complete posterior distribution of $\boldsymbol{x}$ is obtained by calculating (2.35) for all combination of $\boldsymbol{x}$. This will, however, be very time consuming, due to the large dimension of $\boldsymbol{x}$. Instead the estimate of the directional spreading function will be taken as the estimate, which yields the highest probability in the posterior distribution, namely the mode. Subsequently finding $\boldsymbol{x}$ involves an optimisation of (2.35) with respect to $\boldsymbol{x}$, u and σ.

Hashimoto, Kobune, and Kameyama (1987) suggest to apply a Householder transformation in the optimisation procedure. This procedure has been shown in Appendix C.

An estimate of x is achieved for each chosen value of u, hence it remains to select one of these estimates. For this purpose Hashimoto, Kobune, and Kameyama (1987) suggested to calculate the ABIC value, Akaike's Bayesian Information Criterion, which is based on the marginal likelihood and is defined as in (2.38).

$$\text{ABIC} = -2 \ln \int_{-\infty}^{\infty} \cdots \int_{-\infty}^{\infty} L(x, \sigma^2) p(x|u^2, \sigma^2) dx \qquad (2.38)$$

This is seen to correspond to $-2\ln(K')$, where K' is the normalising factor in (2.23).

The estimate to be chosen is the one with the lowest ABIC value, i.e. the largest value of K'.

A note on the performance analysis of the BDM method is given in Appendix F.

3

Physical Experiments

3.1 Introduction

The reflection performance of two types of structures has been investigated by physical modelling in 3D wave tanks. The first to be considered is a porous structure with vertical front. The second is a caisson with either a plain vertical front or a perforated vertical front.

The main purposes of the tests have been the following.

- To obtain reflection coefficients in short-crested seas for the selected structures as function of incident main direction in particular.

- To provide suitable data material for evaluating the performance of partially reflective boundaries in a numerical model given the same conditions as the physical models.

Since the models are established for purely scientific reasons, the scaling is not specified. The models are designed to be as large as possible considering the conditions in the wave tanks. However, suitable scales would be in the range of 1:10 to 1:50, thus covering waterdepths from 3 metres to 30 metres.

3.2   Scale Effects

In work with physical scale models proper scaling laws must be applied. Here the Froude scaling law is used, but in some cases this may cause scale effects due to dissimilar viscous effects. This may be of importance, mainly if the flow through a porous media is turbulent. Using Froude scaling the Reynolds number will be reduced significantly, and the flow may change from turbulent to laminar.

Considering the porous structure and the perforated caisson the results may be affected by scale effects, but for the caisson with plain front this is not the case. This is assumed, that the waves will not break at the structure, since this may also cause scale effects.

The scale effects on the reflection performance have not been investigated in this study, but it is presumed that scale effects, if present, will increase the measured reflection, as a change from turbulent flow to laminar flow will reduce the loss of energy.

The subject has been discussed briefly in Hydraulics and Coastal Engineering Laboratory, AAU (1993), where some comparisons have been made. Figures 3.1 and 3.2 show the tested structures in prototype scale and the estimated reflection. From the first graph it appears, that a smaller scaling causes the reflection coefficients to increase. In the second case, the change is opposite, but the difference is much smaller and within the uncertainty of the reflection estimation method. Further it is believed that less turbulence takes place in the second case, thus reducing the scale effects.
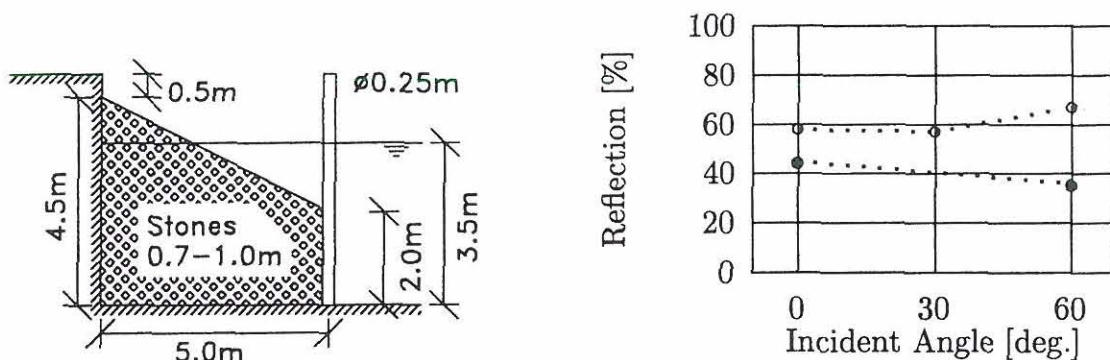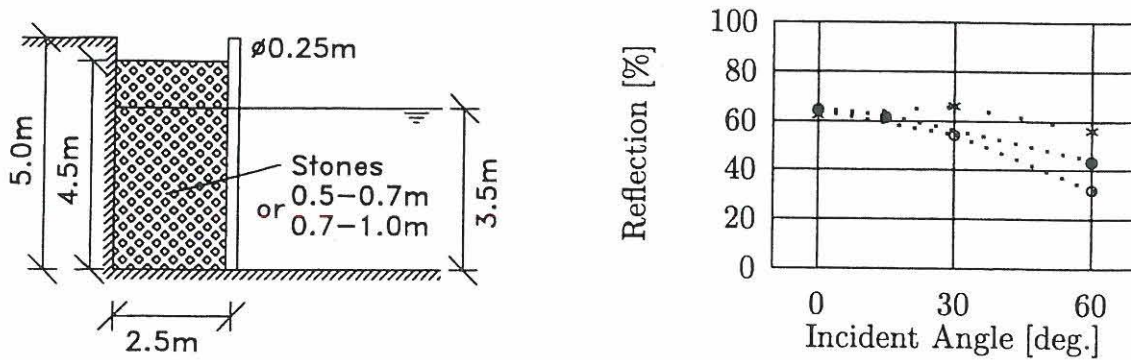

Figure 3.1: Cross-section (prototype) and measured reflection. • denotes scale 1:10 and ○ scale 1:50. 0° is the head–on direction.

Figure 3.2: *Cross-section (prototype) and measured reflection. • denotes scale 1:10, ∘ scale 1:50, and * scale 1:50 with larger stones.*

3.3 Experiments with Vertical Porous Structure

3.3.1 Experimental Set-Up

The structure considered is a vertical face porous structure. The structure consists of a number of baskets made out of a wire mesh (grid size $15 \times 15mm$). The baskets were filled up with rubble, having a porosity of 0.34 (defined as V_{void}/V_{total}). A cross-section of the structure is seen in Figure 3.3, also showing the dimensions.
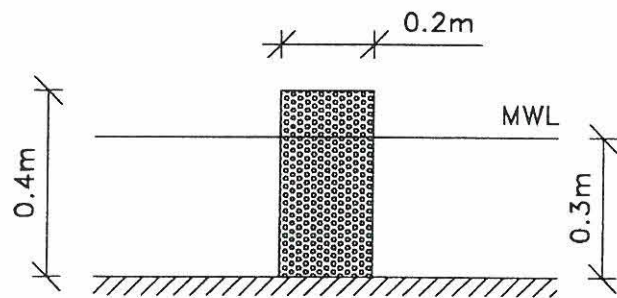
Figure 3.3: *Cross-section of porous structure.*

The model was tested in the 3D wave tank at the Hydraulics and Coastal Engineering Laboratory, Aalborg University. The dimensions of the wave tank and the position of the model are shown in Figure 3.4.

An array of 10 linear resistance wave gauges was placed in front of the structure. The array of wave gauges was placed as shown in Figure 3.5.

Target specifications for the incident waves are listed in Table 3.1.
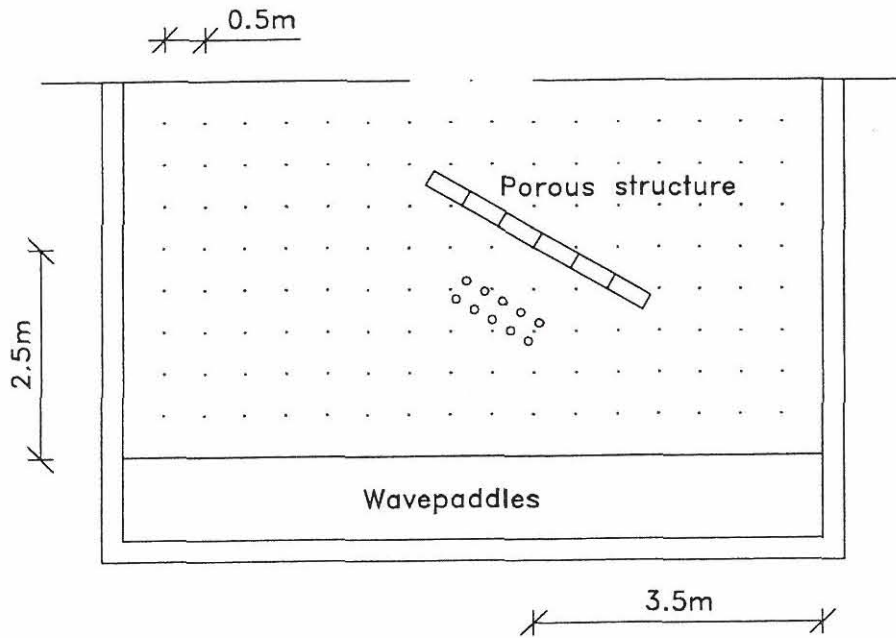
Figure 3.4: Position of model in 3D wave tank.
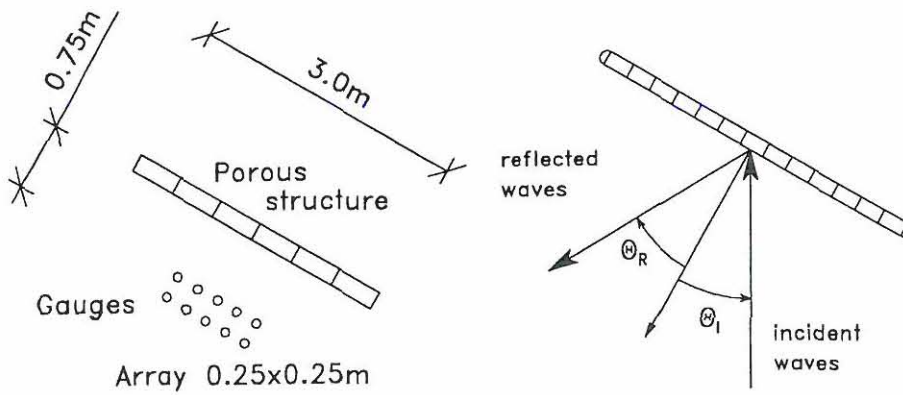
Figure 3.5: Positioning of wave gauges and definition of directions.

Wave spectrum	JONSWAP, $\gamma = 3.3$
Peak period, T_p	$0.9s - 1.3s$
Significant wave height, $H_{s,I}$	$0.06m, 0.04m$
Wave steepness H_{s0}/L_{0p}	$0.023 - 0.047$
Main direction, $\theta_{m,I}$	$0°, 10°, 20°$, or $30°$
Type of spreading	Mitsuyasu, $\cos^{2s}(\cdot)$
Standard deviation of spreading	$\sigma_{\theta,I} = 25°$, $(s = 10)$

Table 3.1: Incident wave conditions.

The test programme is listed in Table 3.2. Angles are measured in degrees, where $0°$ is head on, and positive is measured clockwise.

T_p	L_{0p}	L_p	H_s	H_s/L_{0p}	$\theta_{m,I}$	$\sigma_{\theta,I}$
0.9s	1.27m	1.15m	0.06m	0.047	0,10,20,30°	25°
1.0s	1.56m	1.36m	0.06m	0.038	0,10,20,30°	25°
1.1s	1.89m	1.56m	0.06m	0.032	0,10,20,30°	25°
1.2s	2.25m	1.76m	0.06m	0.027	0,10,20,30°	25°
1.3s	2.64m	2.00m	0.06m	0.023	0,10,20,30°	25°
0.9s	1.27m	1.15m	0.04m	0.035	10,30°	25°
1.1s	1.89m	1.56m	0.04m	0.026	10,30°	25°
1.3s	2.64m	2.00m	0.04m	0.020	10,30°	25°

Table 3.2: Test programme.

3.3.2 Results

The total reflection coefficient may be defined as an energy weighted average of the frequency dependent reflection coefficient as in (3.1).

$$C_{R,T} = \sum \frac{S_T(f)\Delta f}{m_0} C_R(f) \tag{3.1}$$

where m_0 is the zero'th order moment of the resulting autospectrum, i.e. $m_0 = \sum S_T(f)\Delta f$ and $S_T(f)$ is the total spectral density, i.e. the sum of the incident and reflected spectral density.

In Figure 3.6 and Figure 3.7 the total reflection for the porous structure has been plotted as a function of the incident angle of wave attack and peak frequency, respectively. The reflection as a function of incident angle appeared to be almost constant, at least the small amount of tests did not reveal any other tendency.

The Bayesian Directional Spectrum Estimation Method, described in Section 2.5, has been used for the analysis.
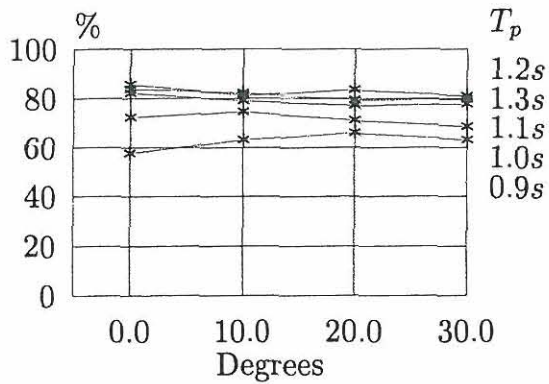
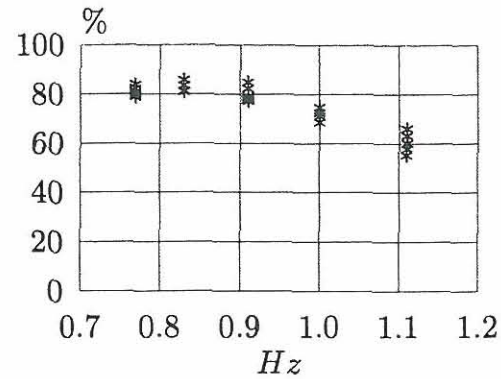**Figure 3.6:** *Total reflection as function of incident angle.*

Figure 3.7: *Total reflection as function of peak frequency.*

3.3.3 Conclusions

The results have been presented as total reflection with respect to the peak frequency. The reflection varies from 85% to 55% peaking at a peak frequency of approximately $0.85 Hz$.

The reflection with respect to the incident main direction appeared to be constant.

3.4 Experiments with Caissons

These experiments have been carried out as a combined LIP–MAST–TAW project during May to July, 1994, in the Vinje–Basin at Delft Hydraulics. The experiments were carried out in order to investigate the hydraulic performance of caisson breakwaters exposed to irregular multidirectional seas. In the following attention is paid only to the reflection of waves from the caissons as a function of frequency and direction of the incident waves.

3.4.1 Experimental Set-Up

A scale model of a caisson breakwater was designed and constructed in plywood. The model consisted of thirteen individual caissons, each having a width of $0.9\ m$ and two roundheads covered with a thin steel shell, see Figure 3.11. The model was placed on a permeable two layer berm. Other relevant dimensions are shown in Figure 3.8, which shows a cross–section of the model.
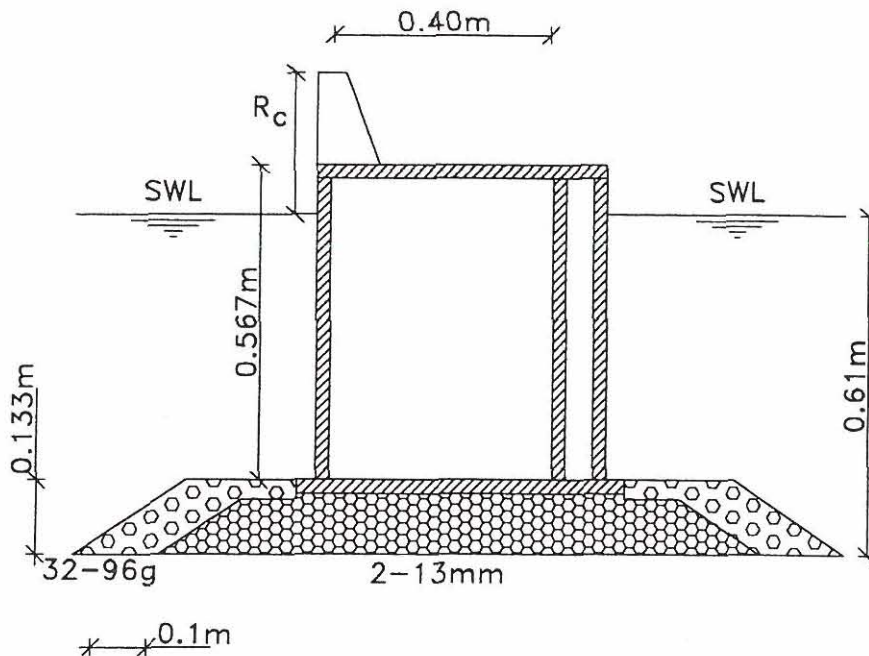
Figure 3.8: Cross-section of caisson and foundation berm.

As indicated on Figure 3.8 the caissons were constructed with a crest. The crest was replaceable in order to vary the crest height R_c. Further it was the idea to use two different crest heights simultaneously, i.e. the first 7 caissons having one crest height and the remaining 6 caissons another crest height. The various types of crests will influence on the reflection characteristics, mainly due to changes in overtopping. However, it is assumed that the influence in these cases is very small, and the various types of crests will not be considered further.

Three different types of caissons were constructed. These are listed below.

- Caissons with plain vertical front.

- Caissons with impermeable mound.

- Caissons with perforated vertical front.

The impermeable mounds were constructed with a concrete surface. Two mounds were investigated, see Figure 3.9. The first was constructed so that the slope reached the caissons just below SWL. The second had a horizontal berm with a width of $1\ m$. The sloping ratio of the mound was in both cases 1:3.

Two permeable fronts were prepared for the caissons. The design of the permeable fronts are shown in Figure 3.10. The porosity of each type were approximately 25%.
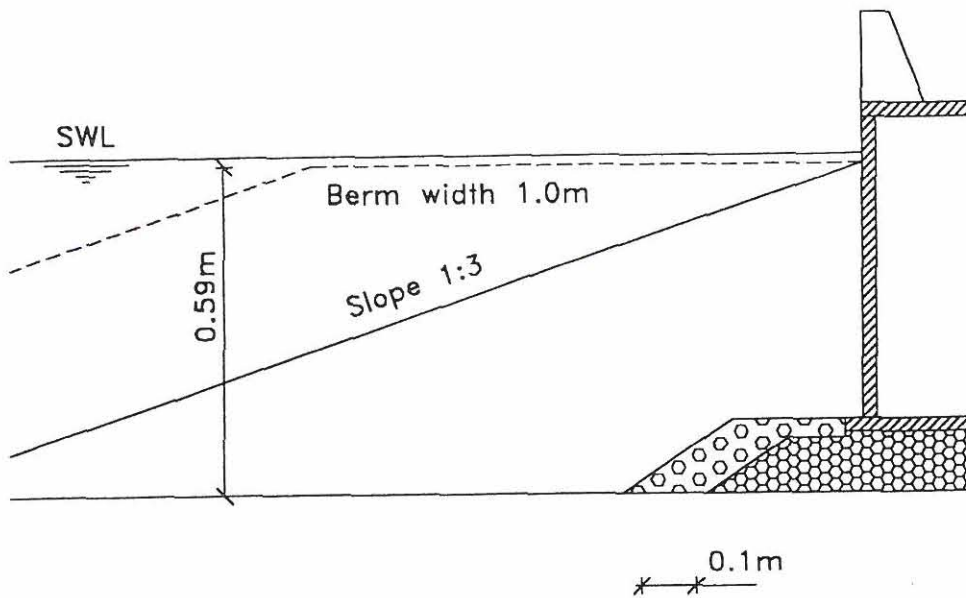
Figure 3.9: *Cross-section of caisson with mounds.*
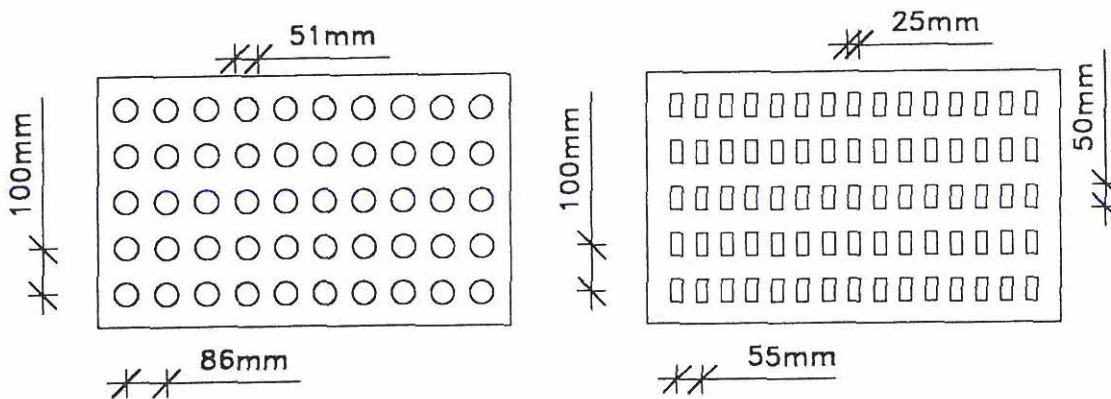
Figure 3.10: *The two types of permeable fronts.*

The model was prepared for experiments in the Vinje–Basin at Delft Hydraulics, The Netherlands. The basin is a multidirectional wave basin capable of generating irregular multidirectional waves with a significant wave height up to about 0.14 m at a waterlevel of 0.61 m. The wave basin dimensions and lay–out of the model is shown in Figure 3.11.

In order to provide an acceptable absorption of the waves at the rear boundary the basin has been equipped with a straight sloping foreshore.

Due to the high reflection from the caissons, especially for those with a plain front, various absorbing material were placed in the basin during the tests in order to avoid an unacceptable amount of re–reflection at the solid boundaries and at the wavepaddles. Absorbing material were placed at side boundaries and
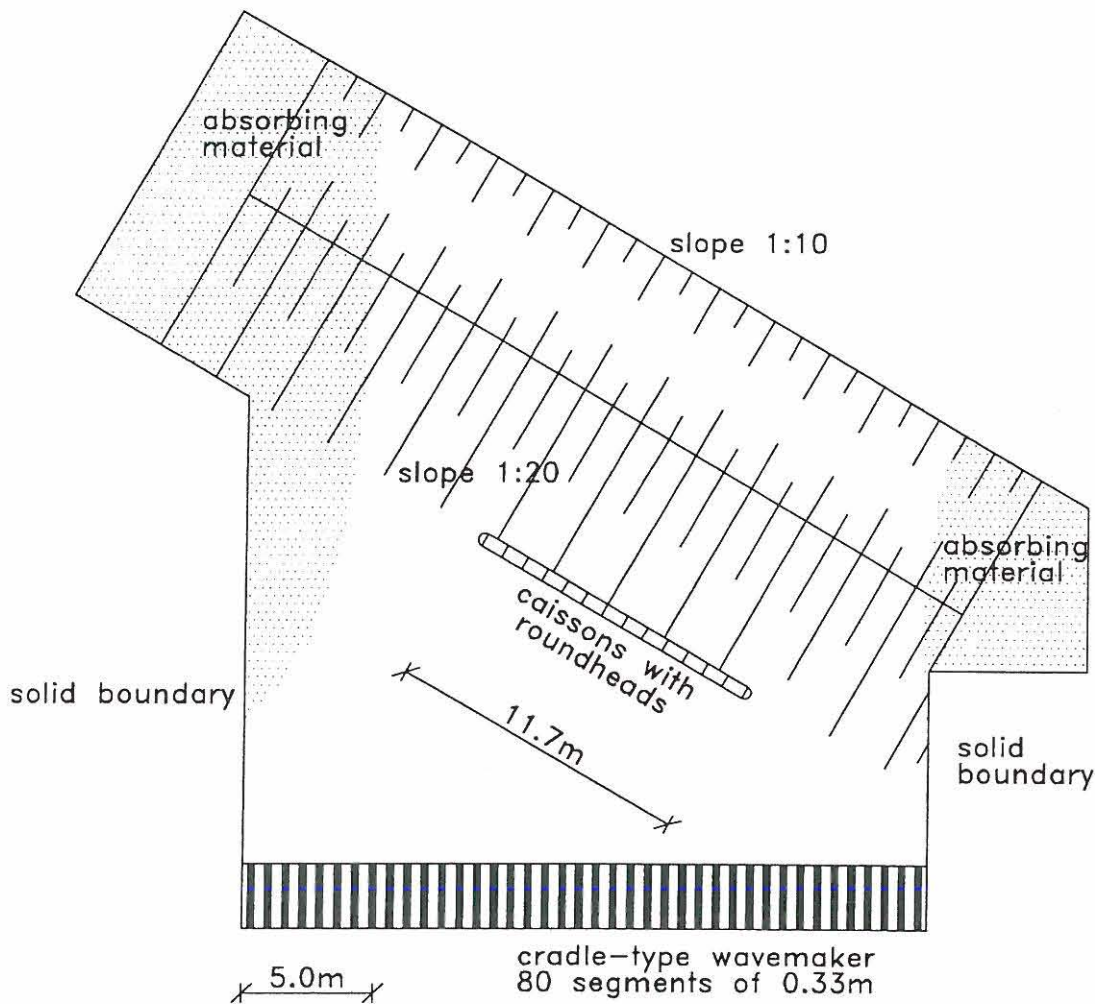
Figure 3.11: *Position of model in the Vinje-Basin at Delft Hydraulics.*

at roundheads. The damping was changed for the most oblique waves.

The water depth during all tests was 0.61 m in the area between the caissons and the wavepaddles.

The model was equipped, such that it was possible to measure the total forces on the centre caisson, accumulated overtopping at two distinct positions, number of overtopping waves at the same two positions, pressure distribution on the fronts (vertical and horizontal) and pressure distribution below caissons. Further an array of 20 linear resistance wave gauges were placed in front of the caissons.

The wave gauges were placed in a 0.5×0.5 m grid. Two lines with 10 gauges were placed on a beam supported at each end on two legs having a diameter of approx. 15 mm. The stability of the beams appeared to be satisfactory during the tests. The choice of positioning of the gauges was based on another purpose and

is not considered as the best choice for estimation of the reflection characteristics. A number of 10 gauges were used in the reflection analysis, and this large number of gauges was expected to compensate for not having optimised the positions. The array of wave gauges was placed as shown on Figure 3.12.
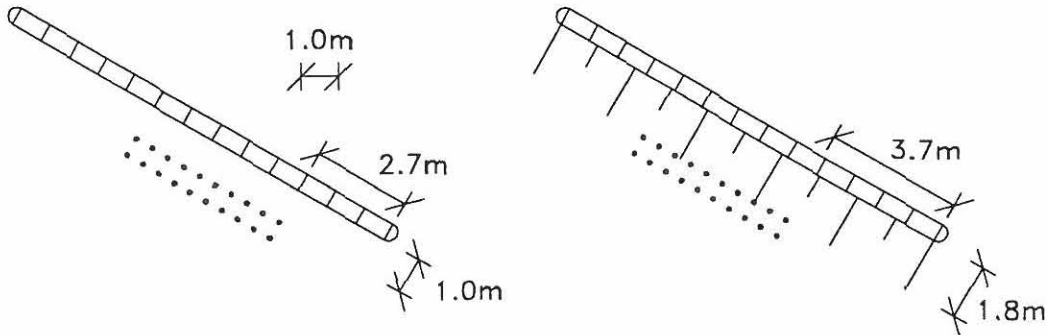
Figure 3.12: *Positioning of wave gauges. For caissons with a mound the array was placed with the first line of gauges (closest to the caissons) just above the toe of the mound.*

3.4.2   Wave Conditions

Target specifications for the incident waves are listed in Table 3.3.

Wave spectrum	JONSWAP
Peak period, T_p	$1.5s$
Significant wave height, $H_{s,I}$	$0.14m$
Wave steepness H_{s0}/L_{0p}	0.04
Main direction, $\theta_{m,I}$	$0°, 10°, 20°, 40°$ or $60°$
Type of spreading	Gaussian
Standard deviation of spreading, $\sigma_{\theta,I}$	$0°, 15°$ or $30°$

Table 3.3: *Incident wave conditions.*

Each test was assigned a test-number referring to the test programme listed in Table 3.4. As it appears from the table, 7 test series were carried out. The conditions for each test series are listed in Table 3.5. Thus the first digit in a test-number specifies the test series. The remainder is a serial number referring to the test-programme.

| Test $\theta_{m,I}$ deg.	$\sigma_{\theta,I}$ deg.	Vertical plain front			Berm 0 m	1 m	Vertical perf. front	
0	0	002	203	302	402	502	602	702
0	15		204					
0	30	005	205	305	405	505	605	705
10	15		213					
20	0	009		309	409	509	609	709
20	15	007	202	307	407	507	607	707
20	30	010		310	410	510	610	710
40	15		201					
40	30	015		315	415	515	615	715
60	0		210					
60	15	017					618	718

Table 3.4: Test-programme. Angles are measured in degrees, where 0° is head on, and positive is measured clockwise, see Figure 3.13a.

Test series	Front type	$R_c/H_{s,I}$ a	b
0	Vertical plain	1.18	1.63
2	Vertical plain	1.18*	1.18
3	Vertical plain	1.18*	1.5
4	Mound, no berm	1.18	1.5
5	Mound, berm width 1m	1.18	1.5
6	Circular perforated	1.18	1.5
7	Rectangular perforated	1.18	1.5
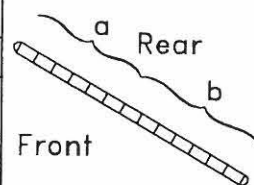
*Table 3.5: Conditions in the 7 test series. Suffix a is the left half of caissons and b is the right half. * indicates, that the crests were supplied with a nose.*

3.4.3   Results and Discussions

In each test the directional spectra have been estimated by use of the Bayesian Directional Spectrum Estimation Method – BDM, cf. Hashimoto and Kobune (1988). In the applied implementation of the method 10 elevation timeseries have been analysed.

The frequency range has been truncated to $0.5\ Hz < f < 1.3\ Hz$ as most energy is represented within this range. The directional spreading functions has been discretized into 72 directions corresponding to a directional resolution of $5°$.

The frequency analysis has been done with subtimeseries containing 256 elements sampled at $5\ Hz$. This leads to a step in frequency of $0.02\ Hz$. No overlapping of subtimeseries has been applied, but the subtimeseries has been tapered over a length of 10% at each end using a cosine tapering function. Each timeseries, having a duration of 24 minutes, thus consist of 28 subtimeseries.

Having estimated the directional spectrum, waves can be separated into incident waves and reflected waves. Following the definition in Figure 3.13b energy in the range from $0°$ to $180°$ must represent the incident waves and energy from $180°$ to $360°$ must represent the reflected waves.

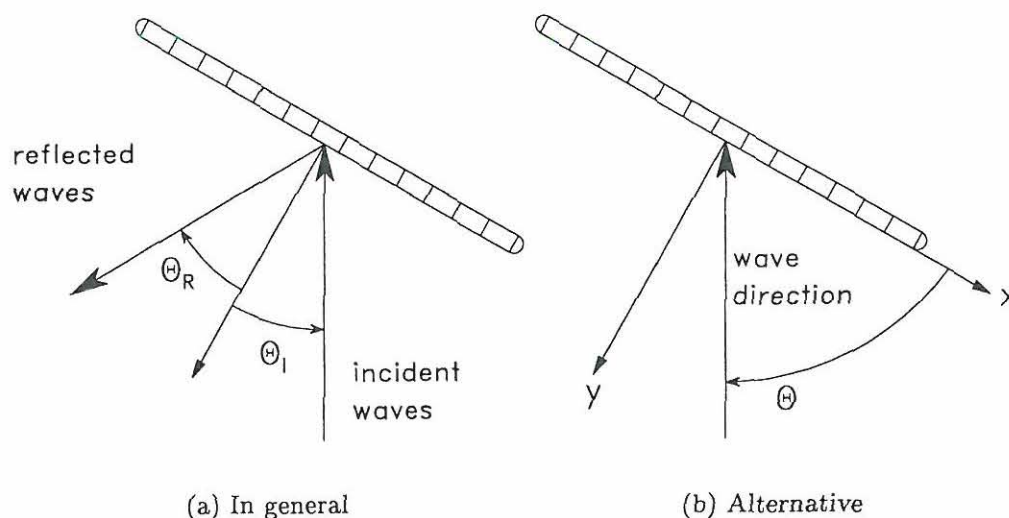(a) In general   (b) Alternative

Figure 3.13: Definitions of wave directions.

Considering the directional spreading functions it is seen, that they may be regarded as probability density functions. Thus the main direction is defined as the expected value of stochastic variables $\Theta(f)$ having a probability density function determined by the corresponding spreading functions. This is formulated in (3.2) and (3.3).

$$\theta_{m,I}(f) \;=\; \mathrm{E}[\Theta_I(f)] = \sum_{k=1}^{K/2} \theta_k H(f,\theta_k)\Delta\theta \qquad (3.2)$$

$$\theta_{m,R}(f) \;=\; \mathrm{E}[\Theta_R(f)] = \sum_{k=K/2+1}^{K} \theta_k H(f,\theta_k)\Delta\theta \qquad (3.3)$$

In (3.2) and (3.3) $H(f,\theta_k)$ is the spreading function at the frequency f. θ_k are discrete values of the directions, $\theta_k = \frac{k-0.5}{K}360°$. K is the total number of discrete directions. Further it is presumed, that angles from θ_1 to $\theta_{K/2}$ are incident waves.

The standard deviation of the directional spreading functions $\sigma_\theta(f)$ is defined in (3.4) and (3.5).

$$\sigma_{\theta,I}^2(f) \;=\; \mathrm{Var}[\theta_{m,I}(f)] = \sum_{k=1}^{K/2} (\theta_k - \theta_{m,I}(f))^2 H(f,\theta_k)\Delta\theta \qquad (3.4)$$

$$\sigma_{\theta,R}^2(f) \;=\; \mathrm{Var}[\theta_{m,R}(f)] = \sum_{k=K/2+1}^{K} (\theta_k - \theta_{m,R}(f))^2 H(f,\theta_k)\Delta\theta \qquad (3.5)$$

In Figure 3.14 some results from the analysis of test 609, 607 and 610 are shown as examples. In these examples, which are fairly representative, the incident main directions are estimated within a range of $\pm 5°$. Slightly more scatter is observed in the estimation of the reflected main directions. These are varying from $\pm 5°$ for long crested waves to $\pm 15°$ for waves with a directional spreading of $30°$.
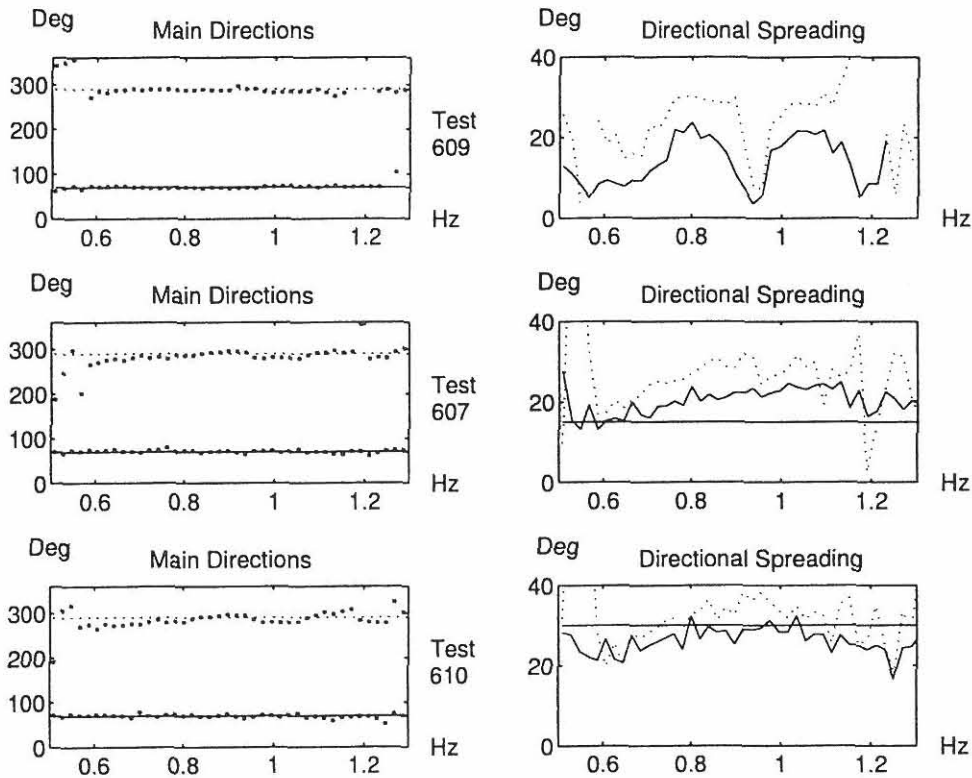
Figure 3.14: *Estimated main directions and directional spreading. Solid lines represent incident waves. Dotted lines represent the reflected waves. Straight lines are target values. In the upper right graph the target value is 0°. No target values of the spreading of the reflected waves are defined.*

The standard deviation of the spreading functions, also referred to as the directional spreading, is for long crested oblique waves poorly estimated. The reason is that the BDM method cannot handle a directional spreading function with a value at just one discrete direction. The method will instead distribute the energy at some, although few, neighbouring directions, which leads to a standard deviation larger than zero.

In all tests with short crested waves the spreading of the incident waves are estimated fairly well.

In the examples shown in Figure 3.14 the spreading of the reflected waves is higher than the spreading of the incident waves. This is observed in all tests with perforated fronts and must be due to diffraction effects at the holes in the front.

In tests with plain fronts the spreading of the reflected waves is estimated to be of the same value as for the incident waves.

In tests with mounds the spreading of the reflected waves does not show any clear trend compared to the spreading of the incident waves. In general, however, the spreading of the reflected waves appears slightly higher than for the incident waves.

In Figure 3.15 the total reflection for the caissons with vertical plain front is plotted with solid dots. The graph shows very clearly, that the reflection for these caissons is nearly constant with respect to the angle of wave attack; at least within the range $0° \pm 40°$ ($0°$ is head on). The total reflection is estimated to 95%.

Figure 3.15 also shows the total reflection for the caissons with perforated fronts. There is no significant difference between circular and rectangular perforation, for which reason they will be regarded as the same structure. Regarding the reflection there is a clear decrease in the reflection coefficient with an increased obliquity. The graph shows a reflection of 50% at head on wave attack decreasing to 30% at an angle of wave attack $60°$ off the head on direction. There seems to be no clear trend with respect to the spreading of the waves.
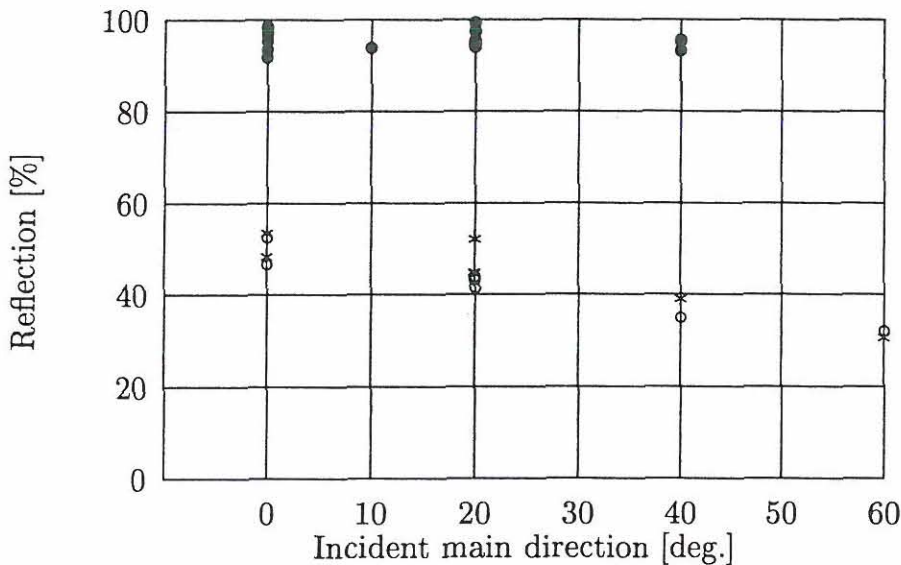
Figure 3.15: *Reflection coefficients for vertical caissons with plain front (test series 0, 2 & 3) and perforated front (test series 6 & 7).* • *is representing test series 0, 1 and 2,* * *test series 6 and* ○ *test series 7.*

The total reflection for the caissons with a mound is shown in Figure 3.16. As expected there is less reflection when the mound is supplied with a berm width, see Figure 3.9. Due to the few number of tests in these cases it is not possible to observe any trend, if any, in the reflection with respect to the angle of wave attack. Thus the reflection may be regarded as, however unlikely, to be

independent of the angle of wave attack. This gives reflection coefficients of 60% and 35% for the two different mounds respectively.
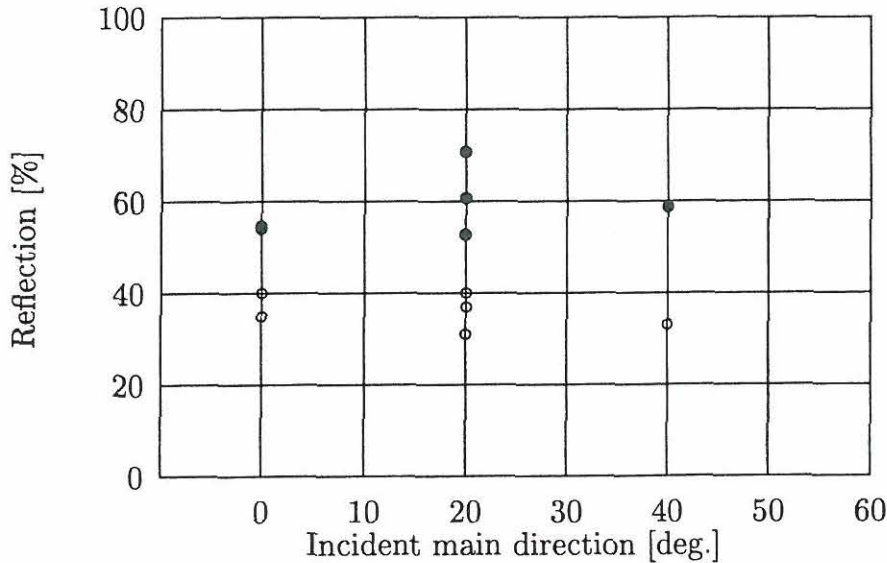
Figure 3.16: *Reflection coefficients for caissons with berm.* • *is representing test series 4 and* ∘ *test series 5.*

The frequency dependent reflection coefficient may be defined as the wave height ratio as shown in (3.6).

$$C_R(f) \quad = \quad \sqrt{\frac{S_{\eta,R}(f)}{S_{\eta,I}(f)}} \tag{3.6}$$

In Figure 3.17 the frequency dependent reflection coefficient for caissons with plain front is shown. The graph has been calculated as an average of all tests from test series 0, 2 and 3. This can be done since, as stated in the previous sections, the angle of wave attack and the spreading of the incident waves have almost no influence on the reflection.

Figure 3.18 shows the frequency dependent reflection coefficient for the caissons with perforated fronts. The labels refer to incident main directions according to Figure 3.13a.

The same procedure has been applied to the results from the test series with mounds. The corresponding curves are shown in Figure 3.19 and Figure 3.20.
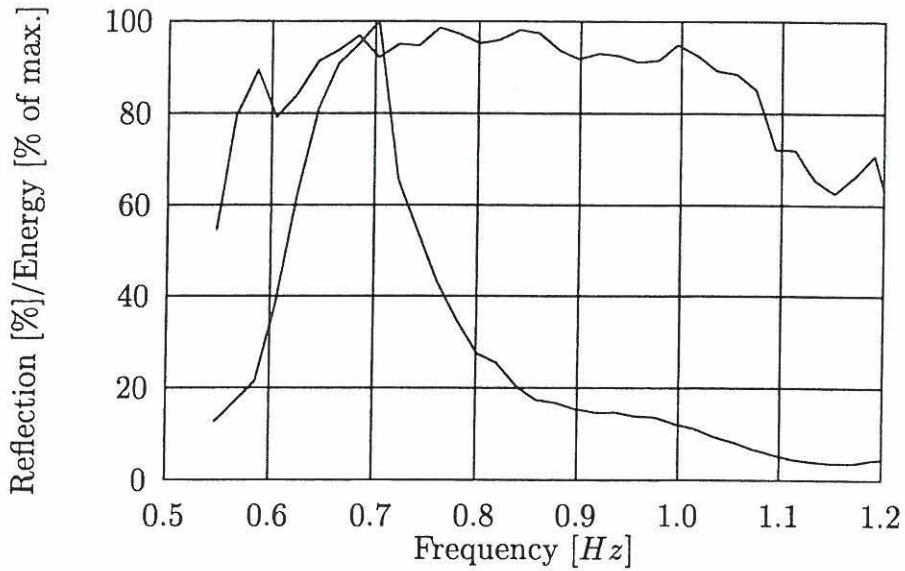
Figure 3.17: *Average frequency dependent reflection coefficient for test series 0, 2 and 3. (Caisson with vertical plain front.)*
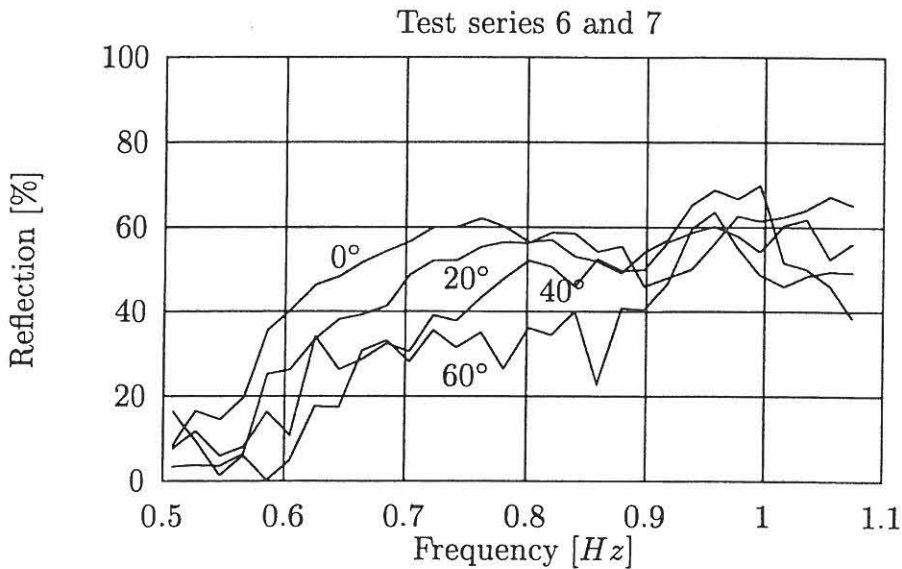
Figure 3.18: *Frequency dependent reflection coefficients for caissons with perforated fronts. The curves are representing various incident main directions.*
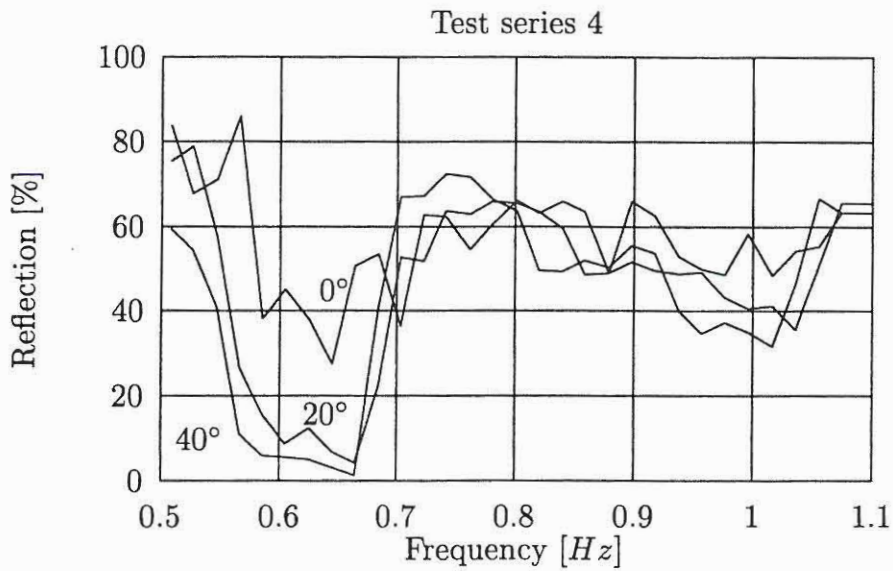
Figure 3.19: *Frequency dependent reflection coefficients for caissons with a mound (no berm). The curves are representing various incident main directions.*
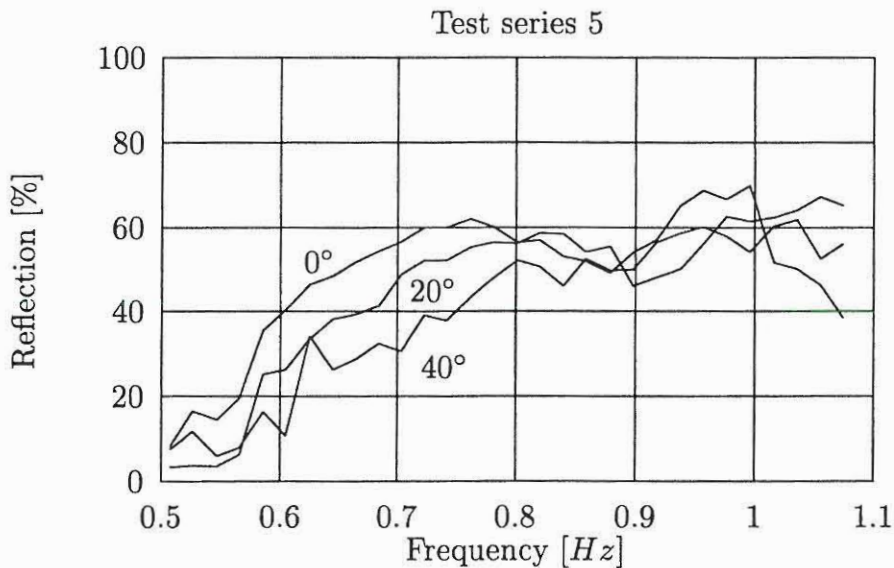
Figure 3.20: *Frequency dependent reflection coefficients for caissons with a mound and a berm (width 1 m). The curves are representing various incident main directions.*

3.4.4 Conclusions

The results presented in the present report are based on the *Caisson Investigations* carried out at Delft Hydraulics as a combined LIP–MAST–TAW project, see MAST (1994). The results concern the reflection performance of the caissons under study exposed to directional waves. It was the primary aim of the analysis to investigate the influence of the incident main direction and the directional spreading on the reflection. Further the variation of the reflection in the frequency domain was studied.

Vertical Plain Caissons

The reflection for vertical plain caissons has been shown to be independent on both the incident main direction and the directional spreading. As an average the total reflection was estimated to 95%. The variation of the reflection coefficient in the frequency domain is seen in Figure 3.17. The figure shows a maximum at a frequency of approximately 0.8 Hz. The variation in the reflection coefficient is probably due to inaccuracies in the applied method.

Vertical Perforated Caissons

Two types of perforated fronts were tested. The porosity was in both cases 25%. With respect to reflection the results show no significant difference, and thus the caissons with perforated fronts have been treated as the same type of structure. The reflection has been shown to decrease with increased obliquity. No consistent influence of the directional spreading was observed, whereas it is believed not to have any influence on the reflection. The reflection varies from 50% at head on wave attack to 30% at an angle of 60° off the head on direction. In the frequency domain the reflection coefficient varies as shown in Figure 3.18.

Vertical Caissons with Mounds

The results from these experiments are less significant as fewer tests were performed. It was not possible to show any decrease in the reflection with an increased obliquity, which was expected. Thus the reflection was estimated to approximately 60% for a mound with no berm and approximately 35% for a mound with a berm of 1.0 m. The reflection in the frequency domain is seen in Figure 3.19 and Figure 3.20.

Directional Spreading

In the results it is observed that, in case of a perforated front or a mound, the spreading of the reflected waves is larger than of the incident waves. Since the reflection line is not a straight line, the waves will be reflected in many directions, and diffraction will also take place, when waves are propagating through the perforated front. For *caissons* with a plain front this is not observed, as the reflection line is well defined.

The above conclusions are believed to be valid only within the limits of the experiments. In general this implies incident main directions in the range $0° \pm 60°$, where $0°$ is head on, and directional spreading up to $30°$.

4

Field Measurements

4.1 Introduction

In most situations the best way of getting information of the effect of a certain occurrence is to investigate the occurrence itself. This may be possible in many cases, but in civil engineering it is often practically impossible due to the large costs involved. As a compensation scale models are being used although scale effects are being introduced. The value of any investigation of a prototype is therefore considerable, as it in addition to the main results also provides a mean of assessing results from scale experiments. Further it has, during recent years, also been important to evaluate numerical models by comparisons to prototype measurements.

To achieve such prototype information it is often chosen to carry out field measurements to investigate the behaviour of existing structures or other existing environments. An investigation can be initiated because of problems with an existing layout, or it can be initiated purely due to a scientific interest. In any case field measurements can provide researchers and engineers with useful information, without having to construct an expensive prototype.

While field measurements can lead to unique information, such measurements are subjected to a large number of environmental conditions, which cannot be manipulated. Hence it is often a difficult task to interpret results based on field measurements. Furthermore, equipment can easily be destroyed or lost during deployment.

During the present study, possibility to analyse field measurements were given through a collaboration with the School of Civil and Structural Engineering, University of Plymouth, United Kingdom. While the measurements will remain property of the School, permission has been granted to present results achieved within the present study based on selected measurements.

4.2   The Alderney Admiralty Breakwater

4.2.1   Site, Structure and Equipment

The School of Civil and Structural Engineering has done a great amount of work to be able to carry out field measurements in the coastal zone. Wave recording systems have been developed and subsequently deployed at a number of sites, see e.g. Bird et al. (1994), Bird et al. (1995) or Davidson et al. (1994).

At Alderney Harbour, the Channel Islands, field measurements were initiated in 1993 and are still in progress. The overall aim of these measurements is to improve information on the effect of aeration on impact pressures on a rigid structure. The structure considered is the Admiralty Breakwater, which consists of a wall constructed on a rubble mound. The mound is sloping approximately 1:6 ($\cot \alpha = 6$). A cross–section of the original design of the breakwater wall is seen in Figure 4.1, and anestimated cross–section of the mound is seen in Figure 4.2.
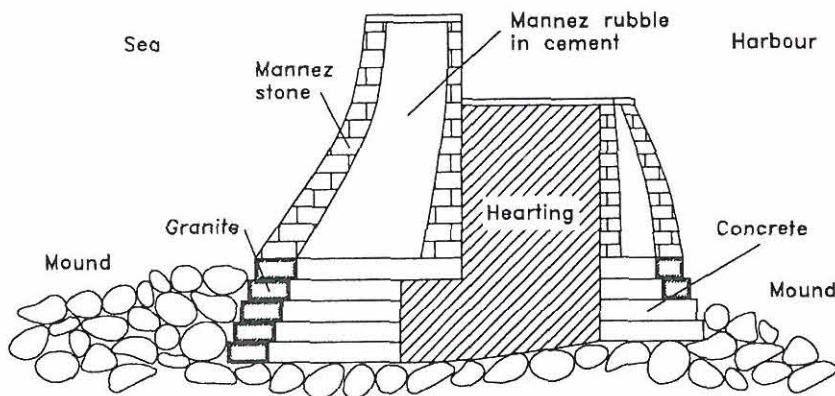
Figure 4.1: Cross–section through breakwater wall.   After Bray and Tatham (1992).

The harbour is located on the north coast of Alderney, facing the English Channel. The breakwater is subjected to severe damage every year and is rather expensive to maintain, see e.g. Allsop et al. (1991). It is, however, the severe wave conditions, which makes the breakwater suitable for studying wave impacts.

An outline of the harbour is seen in Figure 4.3.
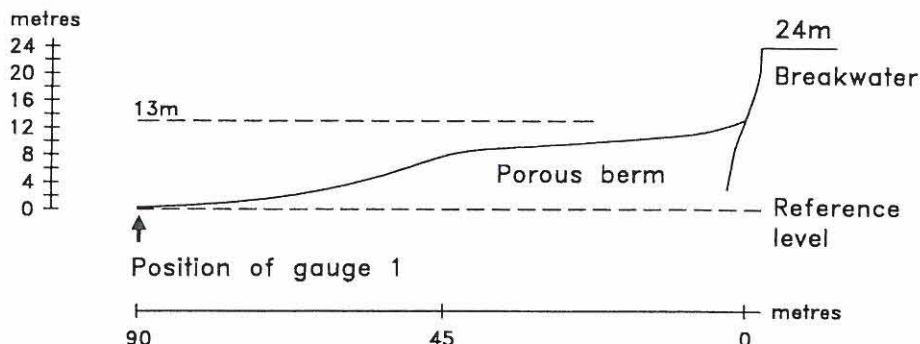
Figure 4.2: Cross-section through breakwater.

Besides the equipment mounted on the breakwater, the School's wave recording system, Bird et al. (1994), has been deployed some 100 to 150 metres seawards to the breakwater wall. In this case the system consisted of six pressure transducers mounted on the seabed, see Figure 4.4. As the figure shows, five of the transducers are positioned on a line with exponential increased spacing, and the last gauge some distance off the line.
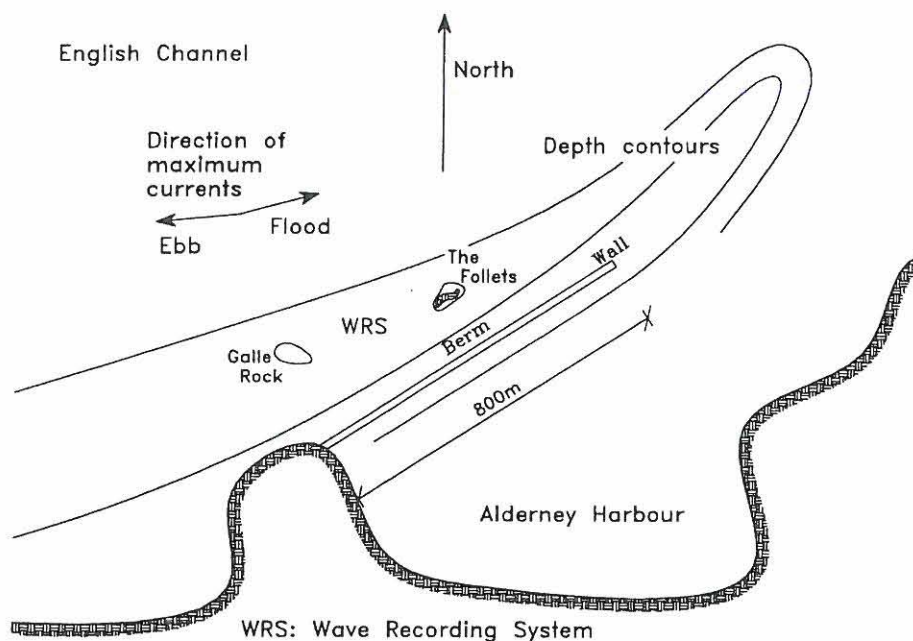
Figure 4.3: Schematic outline of Alderney Harbour.

The seabed can be considered almost uniform over a distance of ±50 metres relative to the transducers. Towards the head of the breakwater this section is broken by The Follets, which is a group of rocks reaching a level of four metres above lowest tide. In the other direction Gallé Rock breaks the continuity. This rock is smaller in size and only reaches a level of 1.8 metres below lowest tide.
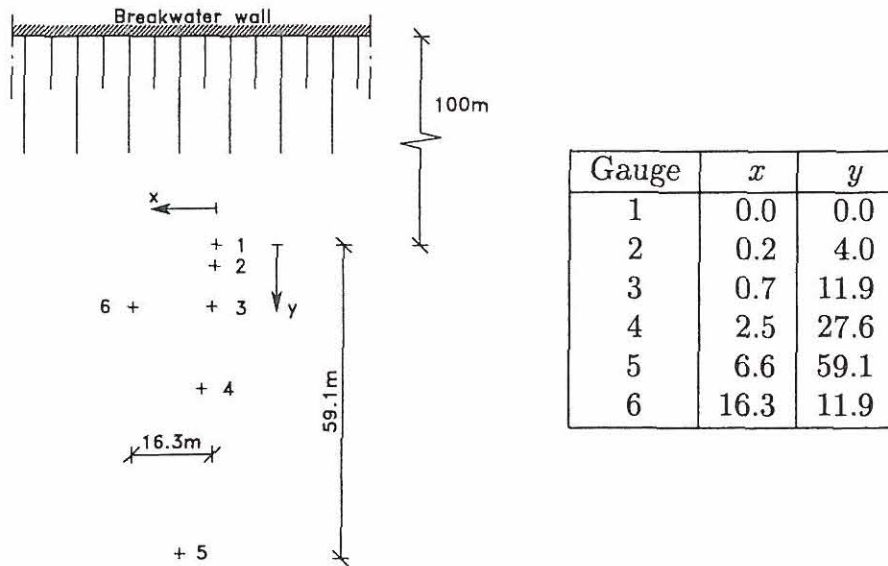
Figure 4.4: *Array of pressure transducers. Measures in metres.*

Under these conditions the seabed can be considered uniform for nearly head–on waves. It is seen from the results, that outgoing reflected waves sometimes appears without the corresponding incident waves. Hence some diffraction presumably takes place for waves with a certain oblique incidence.

The tidal range is around $7m$. During ebb and flood tide strong currents, up to 3.4 knots, are present. The current has not been measured, for which reason it has not been accounted for in the analysis.

4.2.2 Measurements

In the present study only the measurements of the wave conditions are of any relevance. A number of 140 data files containing recorded pressure time series has been analysed with permission from the School. The files have been recorded during November and December 1994, and has been selected on the basis of the energy content to ensure a satisfactory amount of activity. During a pre-processing procedure the pressure time series are transformed to wave elevation time series according to the linear wave theory. The atmospheric pressure has been accounted for in the transformation, based on recordings from Jersey Airport. At the time of processing there was a lack of atmospheric pressure recordings towards the end of the period, but this hardly plays any role in the reflection analysis.

Each measurement has been sampled with $2Hz$ during 11 minutes. Thus each measurement consists of 1320 samples from each of the six transducers.

4.3 Analysis

4.3.1 Wave Analysis

It is impossible completely to describe a real sea state in a compressed form. This arises naturally from the complex nature of the waves. All measurements have, however, been analysed with respect to a number of parameters often used to describe a standard sea state. Such an analysis gives an indication of the actual sea state, which is useful despite the shortcomings.

Results of this initial analysis are listed in Appendix D. As the time series only contain something like 100-200 waves, the parameters are relatively uncertain, although averaged for all six transducers. To improve results overlapping and tapering of sub time series have been applied.

4.3.2 Directional Analysis

As it has been described in Chapter 2, numerous methods exist for estimating the amount of reflection in a wave field containing both incident and reflected waves. Here the BDM method has been used. It has the advantage of not presuming a certain shape of the directional spreading function, which is useful when dealing with field measurements. The raw results of the analyses are listed in Appendix D.

Errors will be introduced in the analysis by not considering current and diffraction effects. The current changes the wavenumber, which will have an effect on estimating directions. Diffraction effects are considered less significant, but a more thorough analysis could have been carried out.

Overall values are weighted with the energy content within the specific frequency band.

4.4 Results

Due to the tide the hydraulic performance of the considered breakwater will change continuously. Based on results and available information on the breakwater cross-section the structure will be considered as a solid wall for water levels higher than $14m$, and for a sloping porous structure for water levels lower than $13m$. The transition zone has not been considered particularly.

4.4.1   Plain Vertical Structure

Figure 4.5 and 4.6 show the estimated overall reflection for the breakwater wall
as a function of water level (depth of water) and main direction of incident waves
respectively.
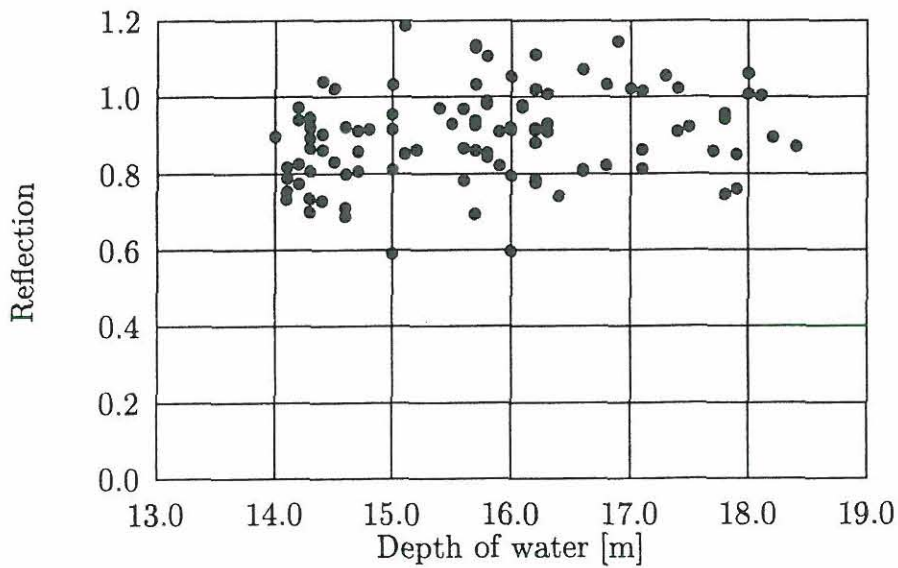
Figure 4.5: Reflection for breakwater wall.
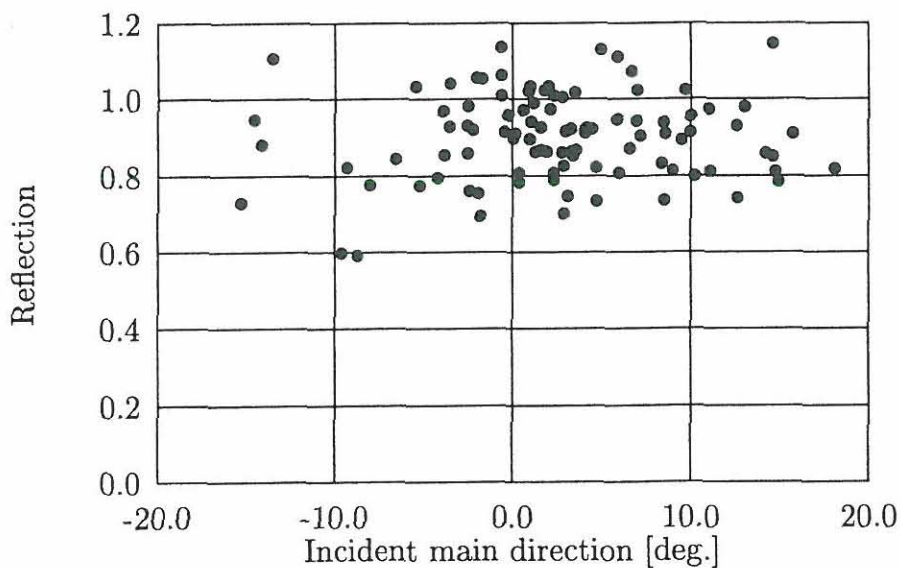
Figure 4.6: Reflection for breakwater wall.

The average overall reflection for selected estimates is $C_R = 0.90$, $\sigma_{C_R} = 0.12$.
A total of 90-100 estimates are included.

4.4.2 Sloping Porous Structure

Figure 4.7 and 4.8 show the estimated overall reflection for the slope as a function of depth of water and main direction of incident waves respectively.
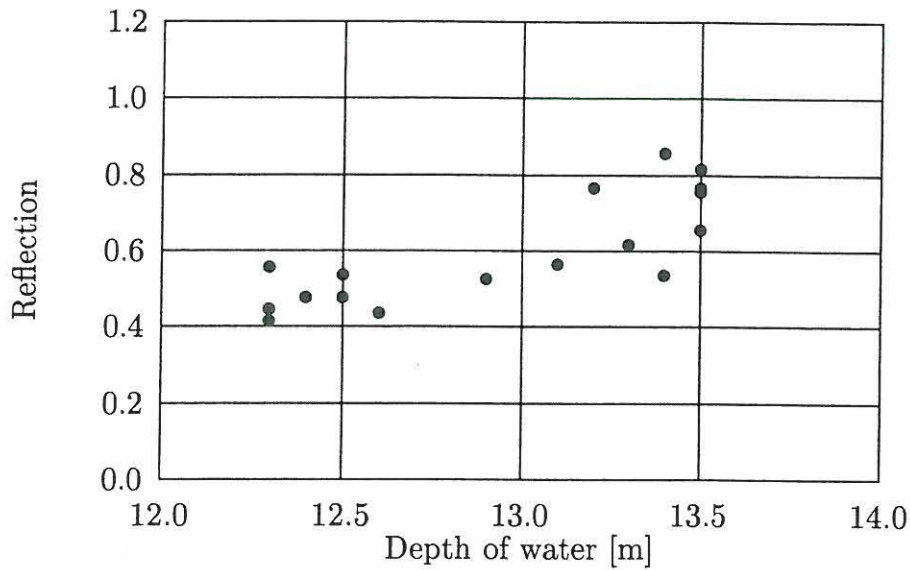
Figure 4.7: Reflection for porous slope.
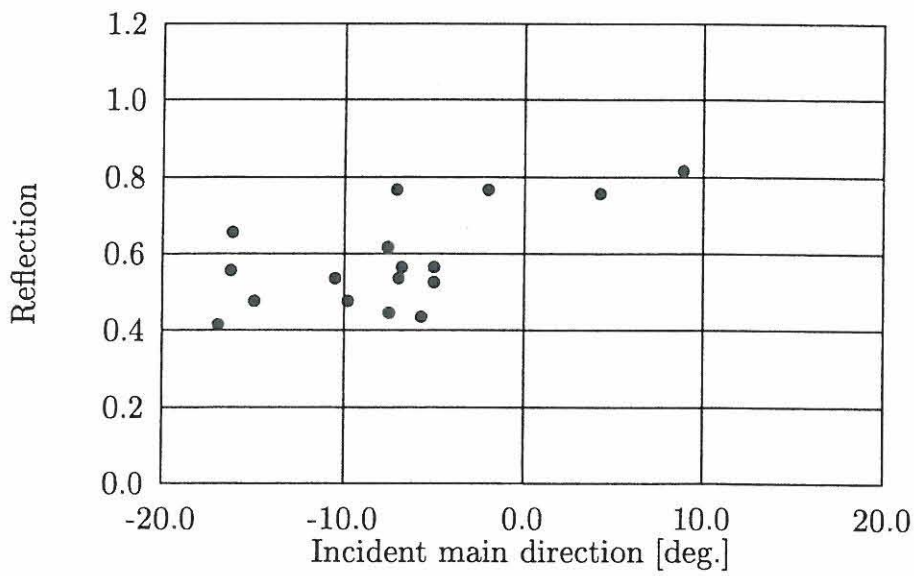
Figure 4.8: Reflection for porous slope.

For the sloping structure the reflection is also shown as a function of the surf similarity parameter, also referred to as the Iribarren number, defined as

$$\xi_p = \frac{\tan \alpha}{\sqrt{H_s/L_p}} \qquad (4.1)$$

where the parameters are for deep water conditions.

The lowest recorded waterdepths were around $12.4m$, with significant incident wave heights ranging up to $1.5m$.

The gradient of the slope at the considered level (between $12.4m$ and $13.1m$) is difficult to assess based on the available survey data. However, a slope angle of 35 degrees has been estimated. Further, in order to calculate the Iribarren number, the incident wave conditions must be known. As is usually the case with field experiments, these must be estimated from the measurements.

Approximately 10 recordings falls within the considered range of waterdepths, and the overall reflection for these are seen in Figure 4.9.
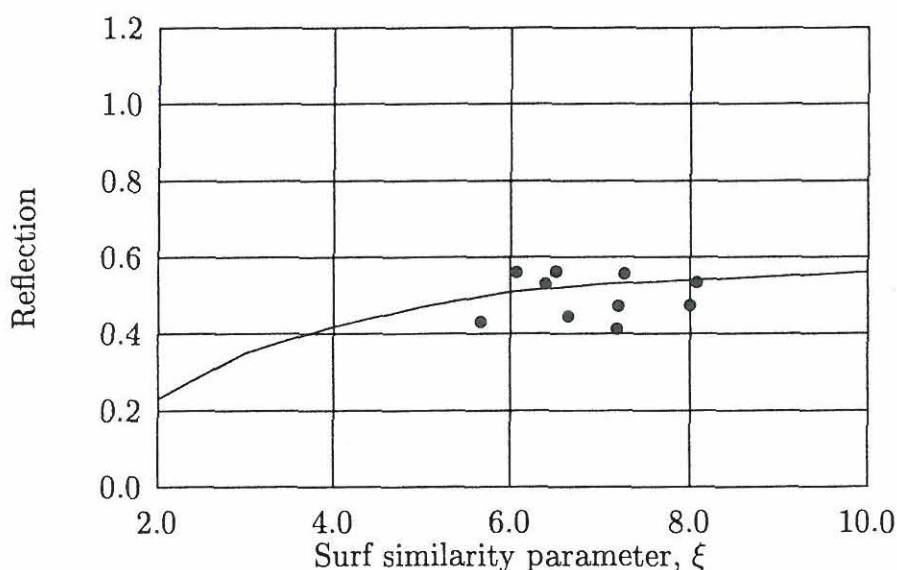
Figure 4.9: Reflection for porous slope.

Also shown in the figure, are the prediction formula by Seelig (1983), which is valid for head on long-crested waves, cf. Appendix A. Due to the few recordings and rough estimate of slope angle the prediction formula cannot be said to be verified. However, the estimated reflection coefficients are within a reasonable range of the predicted values.

5

Numerical Simulations

5.1 Introduction

As an alternative or supplement to physical small scale experiments it may be convenient to use numerical simulations to estimate the wave disturbance inside a harbour. The major advantage in doing this is the option of easily changing the layout of the harbour enabling the design engineer to choose the most appropriate layout for the actual purpose. The present level of numerical wave propagation models makes the models useful for comparison purposes, i.e. they contribute mainly with a qualitative description of the wave conditions for a given layout. The models do, however, also provide a quantitative description of the wave conditions, but the accuracy is still to be improved. This, naturally, depends on how complex the model domain need be.

Among the methods being most widely used are those based on the Boussinesq equations and recently in addition those based on the mild–slope equation. The Boussinesq models are developed to a relative high level by inclusion of e.g. wave breaking, but the models are difficult to implement and often lack in stability. Mild–slope models are easier to implement, but ways of implementing physical processes like wave breaking have not yet been presented thoroughly. Hence, the mild–slope models are not developed to the same level as are the Boussinesq

models.

In principle a numerical wave propagation model consists of a wave generation point or line and boundaries representing the domain to be considered. The boundaries must represent the seabed, the involved structures, if any, and artificial boundaries to absorb waves travelling out of the calculation domain. How to model the various boundaries is not straight forward, since it, generally speaking, must be expressed in terms of the governing equations for the actual model.

The purpose of the numerical simulations to be discussed in this chapter is mainly to evaluate the modelling of reflection from harbour structures with various reflection characteristics. Especially the performance with respect to reflection of short-crested waves attacking the structure with normal or oblique incidence.

The model to be considered is based on the mild–slope equation. Simulations have been carried out both without reflecting structure and with vertical face structures having different reflection characteristics. This covers the physical experiments with caissons and porous structures described in chapter 3.

In the considered model a partially reflecting structure is modelled by a number of absorbing layers, which gradually reduce the wave height. Hence, while some energy is being absorbed, the remaining energy will transform to reflected waves. This method is known from 2D simulations, and has been implemented without further considerations in the mild–slope model used here.

The following sections describe the theory of the mild–slope equation, preliminary simulations without structure, simulations with high reflective structure and simulations with low reflective structure. In the case of a high reflective structure, the simulations are intended to match the physical experiments with the caissons, see Section 3.4, and the low reflective structure is intended to match the physical experiments with the vertical face porous structure, see Section 3.3.

5.2 Mild–Slope Wave Propagation Model

A superficial description of the theory leading to the mild–slope equation will be presented within this section. The implementation of the equation actually forming the model will be discussed only very briefly.

5.2.1 Theoretical Background

Although derived earlier, it was Berkhoff (1972) who initially proposed the mild–slope equation. The derivation was an extension of a refraction model proposed

by Battjes (1968) and applied only to regular waves.

It is, however, possible to derive an expression similar to the original mild-slope equation, which does not assume regular waves. The derivation is based on Hamiltons principle and calculus of variation. A complete derivation is given in Dingemans (1997), whereas only a superficial derivation will be given here. Within this section indices of x, y, z and t denotes partially derivaties, e.g. $\phi_t = \frac{\partial \phi}{\partial t}$.

The difference in kinetic and potential energy of a physical system may be expressed by Lagranges function, given in (5.1).

$$F = E_{kin} - E_{pot} \tag{5.1}$$

If the system, during the time Δt, is moving from one point to another, it will move in a way, so that the value of $\int_0^{\Delta t} F dt$ will be stationary for small time step. By calculus of variation this is expressed as in (5.2), which is referred to as Hamiltons principle.

$$\delta \int_0^{\Delta t} F dt = 0 \tag{5.2}$$

where δ is the variational derivative.

The potential and kinetic energy of a wave motion in a sub-area dA is given in (5.3) and (5.4) respectively.

$$E_{pot} = \int_A \frac{1}{2} \rho g \eta^2 dA \tag{5.3}$$

$$E_{kin} = \int_A \left(\int_{-h}^{\eta} \frac{1}{2} \rho v^2 dz \right) dA \tag{5.4}$$

Presuming ρ and g to be constants, it is seen, that the potential energy varies only with η, whereas the kinetic energy varies with η and v.

Assuming potential flow the square velocity is determined by (5.5).

$$v^2 = \phi_x^2 + \phi_y^2 + \phi_z^2 \tag{5.5}$$

where $\phi = \phi(x, y, z, t)$ is the velocity potential.

By expressing the variation of ϕ with respect to z in a separate function the potential can be expressed as in (5.6).

$$\phi(x, y, z, t) \quad = \quad f(z, d)\varphi(x, y, t) \tag{5.6}$$

where

$$f(z, h) \quad = \quad \frac{\cosh k(z + h)}{\cosh kh} \tag{5.7}$$

h is the depth of water and φ is the velocity potential at $z = 0$.

Using (5.6) the square velocity can now be written as in (5.9).

$$v^2 \quad = \quad (\nabla\phi)^2 + \left(\frac{\partial\phi}{\partial z}\right)^2 \tag{5.8}$$

$$= \quad f^2(\nabla\varphi)^2 + \varphi^2(\nabla f)^2 + 2f\varphi(\nabla\varphi \cdot \nabla f) + \varphi^2\left(\frac{\partial f}{\partial z}\right)^2 \tag{5.9}$$

where $\nabla = \left(\frac{\partial}{\partial x}, \frac{\partial}{\partial y}\right)$.

Assuming small variations in the seabed topography (mild slopes), $\frac{h}{L^*} \ll 1$, where L^* is a typical length of the seabed topography, and $1st$ order wave theory, $\frac{H}{h} \ll 1$, E_{kin} can be approximated to (5.10).

$$E_{kin} \quad = \quad \int_A \frac{1}{2}\rho\left((\nabla\varphi)^2 A(kh) + \varphi^2 B(kh)\right) dA \tag{5.10}$$

where

$$A(kh) \quad = \quad \frac{1}{2k}\left(1 + \frac{2kh}{\sinh 2kh}\right)\tanh(kh) \tag{5.11}$$

$$B(kh) \quad = \quad \frac{k}{2}\left(1 - \frac{2kh}{\sinh 2kh}\right)\tanh(kh) \tag{5.12}$$

The wave elevation η is approximated by the linearised Bernoulli equation in (5.13).

$$\eta \quad = \quad -\frac{1}{g}\varphi_t \ , \text{ for } z = 0 \tag{5.13}$$

Having approximated v and η Hamiltons principle, as in (5.2), can be modified to (5.14).

$$\delta \int_0^{\Delta t} \left(A(\nabla\varphi)^2 + B\varphi^2 - \frac{1}{g}\varphi_t^2 \right) dt \;=\; 0 \tag{5.14}$$

Thus the Lagrange function has been modified to (5.15).

$$G \;=\; A(\nabla\varphi)^2 + B\varphi^2 - \frac{1}{g}\varphi_t^2 \tag{5.15}$$

(5.15) is seen to depend only on φ and its derivatives.

From calculus of variation it is known, that (5.14) is fulfilled if G is a solution to the corresponding Euler equation in (5.16).

$$G_\varphi - \frac{\partial}{\partial x}(G_{\varphi_x}) - \frac{\partial}{\partial y}(G_{\varphi_y}) - \frac{\partial}{\partial t}(G_{\varphi_t}) \;=\; 0 \tag{5.16}$$

Inserting G in (5.16) leads to (5.17), which is a time-dependent mild–slope equation.

$$B\varphi - \frac{\partial}{\partial x}(A\varphi_x) - \frac{\partial}{\partial y}(A\varphi_y) + \frac{1}{g}\varphi_{tt} \;=\; 0 \tag{5.17}$$

φ_{tt} may be expressed by the linearised Bernoulli equation in (5.13). Hence (5.17) may be written as in (5.18).

$$\eta_t + \frac{\partial}{\partial x}(A\varphi_x) + \frac{\partial}{\partial y}(A\varphi_y) - B\varphi \;=\; 0 \tag{5.18}$$

The equations are valid for irregular waves, if the wavenumber k is calculated for the carrier frequency f_c and $|f - f_c|$ is small, i.e. the wave energy spectrum is narrow. If the spectrum is broad, it can be divided into several bands each being modelled with a representative carrier frequency, as also suggested in e.g. Suh, Lee, and Park (1997). Quantitative measures of how narrow the spectrum need be has not been found.

5.2.2   Numerical Scheme

Equations (5.13) and (5.18) are the governing differential equations and may be rewritten as

$$\varphi_t = -g\,\eta \tag{5.19}$$

$$\eta_t = B\varphi - A_x\varphi_x - A\varphi_{xx} - A_y\varphi_y - A\varphi_{yy} \tag{5.20}$$

These differential equations may be discretized by calculating φ for each timestep n, i.e. φ^n, and η in the middle of two timesteps, i.e. $\eta^{n+\frac{1}{2}}$.

Thus $\eta_{i,j}^{n+\frac{1}{2}}$ can be determined from $\eta^{n-\frac{1}{2}}$ and φ^n, as in (5.22).

$$
\begin{aligned}
\frac{\eta_{i,j}^{n+\frac{1}{2}} - \eta_{i,j}^{n-\frac{1}{2}}}{\Delta t} \simeq\; & B_{i,j}\varphi_{i,j}^n \\
& - \frac{A_{i+1,j} - A_{i-1,j}}{2\Delta x} \cdot \frac{\varphi_{i+1,j}^n - \varphi_{i-1,j}^n}{2\Delta x} \\
& - A_{i,j}\frac{\varphi_{i-1,j}^n - 2\varphi_{i,j}^n + \varphi_{i+1,j}^n}{(\Delta x)^2} \\
& - \frac{A_{i,j+1} - A_{i,j-1}}{2\Delta y} \cdot \frac{\varphi_{i,j+1}^n - \varphi_{i,j-1}^n}{2\Delta y} \\
& - A_{i,j}\frac{\varphi_{i,j-1}^n - 2\varphi_{i,j}^n + \varphi_{i,j+1}^n}{(\Delta y)^2}
\end{aligned}
\tag{5.21}
$$

$$
\begin{aligned}
\eta_{i,j}^{n+\frac{1}{2}} =\; & \eta_{i,j}^{n-\frac{1}{2}} + B_{i,j}^*\varphi_{i,j}^n \\
& - 0.25(A_{i+1,j}^* - A_{i-1,j}^*)(\varphi_{i+1,j}^n - \varphi_{i-1,j}^n) \\
& - A_{i,j}^*(\varphi_{i-1,j}^n - 2\varphi_{i,j}^n + \varphi_{i+1,j}^n) \\
& - 0.25(A_{i,j+1}^* - A_{i,j-1}^*)(\varphi_{i,j+1}^n - \varphi_{i,j-1}^n) \\
& - A_{i,j}^*(\varphi_{i,j-1}^n - 2\varphi_{i,j}^n + \varphi_{i,j+1}^n)
\end{aligned}
\tag{5.22}
$$

where

$$A_{i,j}^* = \frac{A_{i,j}\Delta t}{(\Delta x)^2} = \frac{A_{i,j}\Delta t}{(\Delta y)^2}, \text{ when } \Delta x = \Delta y \tag{5.23}$$

$$B_{i,j}^* = B_{i,j}\Delta t \tag{5.24}$$

New values of φ can then be determined from $\eta^{n+\frac{1}{2}}$ and φ^n, as in (5.26).

$$\eta_{i,j}^{n+\frac{1}{2}} = -\frac{1}{g}(\varphi_t)_{i,j}^{n+\frac{1}{2}} \simeq -\frac{1}{g}\frac{\varphi_{i,j}^{n+1} - \varphi_{i,j}^n}{\Delta t} \qquad (5.25)$$

$$\varphi_{i,j}^{n+1} = \varphi_{i,j}^n - g\,\Delta t\,\eta_{i,j}^{n+\frac{1}{2}} \qquad (5.26)$$

5.2.3   Boundary Conditions

In order to provide the mild–slope model with information about the domain on which it should operate, the domain need be defined mathematically. The domain is discretized into a number of boxes in the horizontal plane. The boxes may be defined as being one of the following types.

- Impermeable box.

- Fully permeable box.

- Partially permeable box.

- Wave generation box.

The impermeable box is used to symbolise a fixed boundary like a structure or land. A fully permeable box is simply water, and a partially permeable box is used to describe an absorbing boundary such as a porous structure. Partially permeable boxes are also combined in layers, so-called sponge layers, to provide partial absorption of waves. Finally wave generation boxes, usually combined as aline, are used to generate incident waves. Depth of water must be specified in all boxes.

In sponge layers a reduction coefficient, μ, must be assigned to each box. This is described in Brorsen and Helm-Petersen (1998) and will not be addressed further here.

Figure 5.1 shows the principles in constructing a domain for a numerical model. Notice, that the domain need to be much larger than the area of interest, in order to generate waves and absorb seawards travelling waves.
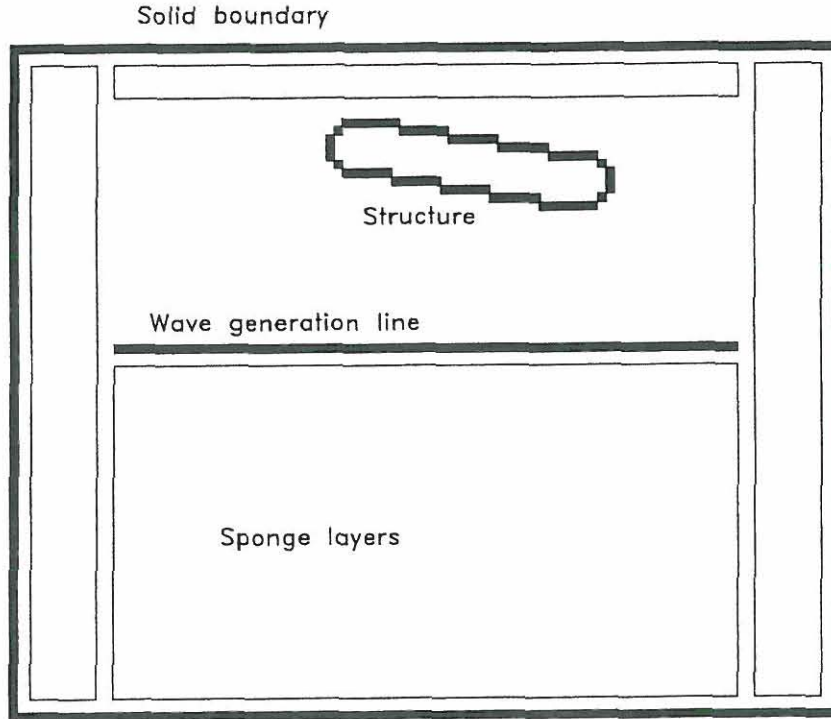
Figure 5.1: Numerical model domain in principles.

5.2.4 Wave Generation

The problems in synthetic reproduction of waves have been acknowledged for decades. In a numerical 3D model most problems can be avoided by an infinite fine discretisation of frequency and direction. This is, however, not applicable as it will imply an infinite large number of wave components, which is practically inconvenient and unnecessary.

In the present simulations a single summation wave generation model has been applied. Hence each wave component has a unique frequency, whereas several wave components are travelling in the same direction. This can be expressed as in (5.27).

$$\eta(x, y, t) \quad = \quad \sum_{l=1}^{L} \sum_{m=1}^{M} a_{lm} \cos(\omega_{lm} t - k_{lm}(x \cos\theta_m + y \sin\theta_m) + \phi_{lm}) \quad (5.27)$$

where

$$\omega_{lm} \quad = \quad 2\pi f_{lm} \quad\quad\quad\quad\quad\quad\quad\quad\quad\quad\quad (5.28)$$
$$= \quad 2\pi(M(l-1) + m)\Delta f + 2\pi f_{min} \quad\quad (5.29)$$

$$a_{lm} = \sqrt{2S_\eta(f_{lm})H(f_{lm},\theta_m)M\Delta f\Delta\theta} \tag{5.30}$$

$$\theta_m = (m-1)\Delta\theta - \theta_{max} \tag{5.31}$$

$S_\eta(f)$ and $H(f,\theta)$ are the wave energy spectrum and the directional spreading function respectively.

The waves are being generated in the numerical model by forcing the elevation along a gridline, referred to as the wave generation line. The elevation at the generation line, may be determined by considering the necessary change of volumes. For this purpose the definitions in Figure 5.2 are introduced.
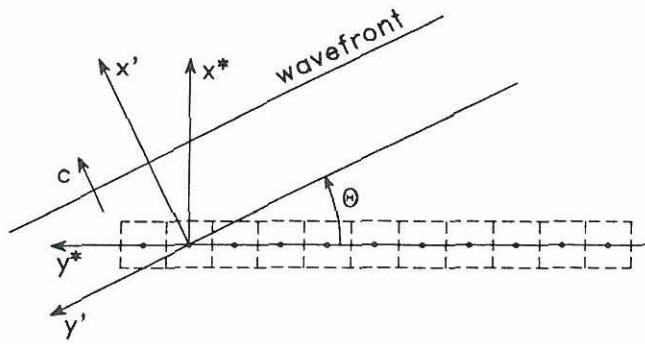
Figure 5.2: Definition of parameters.

Similar to (5.27) a wave component can be expressed as follows.

$$\eta_I = a\sin(kx' - \omega t + \varphi) \tag{5.32}$$

$$= a\sin(k\cos\theta x^* + k\sin\theta x^* - \omega t + \varphi) \tag{5.33}$$

Assuming the wave does not change shape, the flow is then given by

$$q' = c\eta_I \tag{5.34}$$

which must be calibrated in order to achieve the correct amplitude for waves with $f \neq f_c$ [1].

Hence

$$q^* = q'\cos\theta \tag{5.35}$$

In order to account for the wave travelling opposite the actual wave direction, the volume must be doubled.

$$q = 2q^* = 2q'\cos\theta = 2c\eta_I\cos\theta \tag{5.36}$$

---

[1] In a more recent paper, Lee and Suh (1998), this problem has been solved by considering energy transport rather than mass transport.

A box with dimensions $\Delta x^* \times \Delta y^*$ must during the timestep Δt be added a volume of $\Delta \eta \Delta x^* \Delta y^*$, that is,

$$\Delta \eta \Delta x^* \Delta y^* = q \Delta y^* \Delta t = 2c\eta_I \cos \theta \Delta y^* \Delta t \qquad (5.37)$$

$$\Delta \eta = \frac{2c\eta_I \cos \theta \Delta t}{\Delta x^*} \qquad (5.38)$$

Inserting the surface elevation η_I into (5.38) will then give the actual change in the elevation within the considered box.

5.3   Model Set-Up

5.3.1   In General

The set-up of the models correspond roughly to the set-up of the physical experiments with caissons, described earlier in Section 3.4. The model domain has, however, been reduced in order to reduce processing time.

A number of 5 principal model set-up have been applied in the simulations to be considered in this chapter. These will be referred to as model-1 to 5. Further the structure in model-2 is modelled either as a full, high or low reflective structure, and in model-3 to 5 the structure is modelled either as full or low reflective. These variations are indicated by adding a **f**, **h** or **l** to the model name. Thus a total number of 10 model set-up have been applied.

All models are based on a grid size of $0.125 \times 0.125m$, and have a width of 208 elements, i.e. a width of $26m$. The depth of water is $0.61m$.

In the following each principal model will be described by a graphical presentation and relevant data. Variations with respect to the structure will also be specified.

5.3.2   No Structure

Model-1, see Figure 5.3, only contains a rigid boundary and two large sponge layers. The model does not contain any structure and is intended for testing the characteristics of the incident waves. The two sponge layers in the model are alike, and have a depth of 35 boxes.
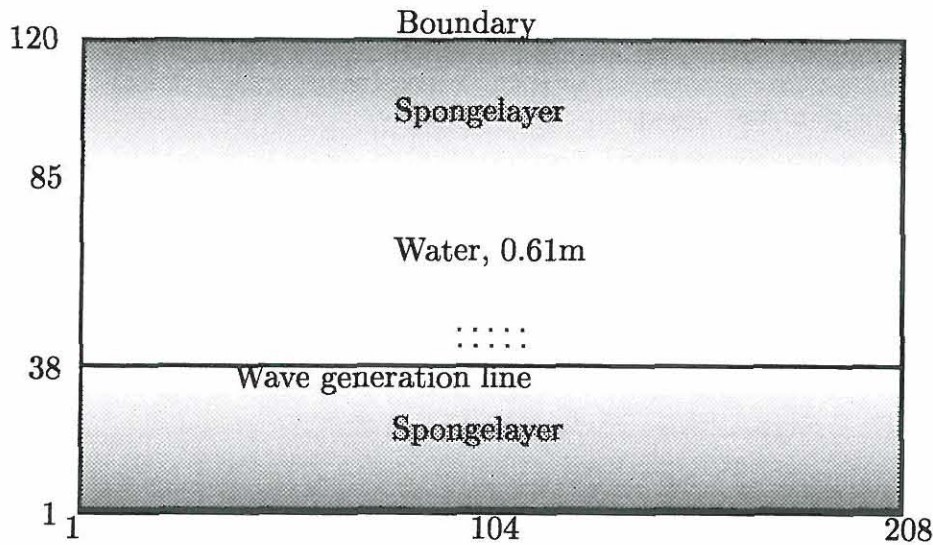
Figure 5.3: Model-1. No structure.

5.3.3 Regular Structure

Model-2, see Figure 5.4, contains a rigid boundary, a large sponge layer, and a structure (modelled as a rigid boundary). The structure is fully reflective and is positioned along a grid line. Hence the face of the model will be regular. The model is reduced in size, since the structure, having the full width of the model, replaces one of the sponge layers. The large sponge layer is similar to the one in the previous model, and has the only function of absorbing waves leaving the model domain.
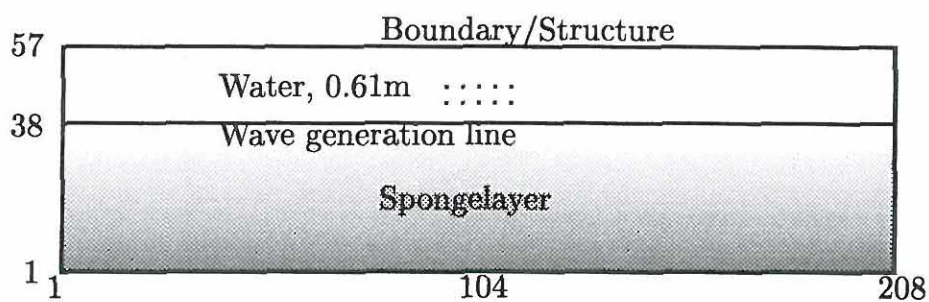
Figure 5.4: Model-2f. Regular structure, full reflection.

Variations of the structure are created by adding absorbing layers in front of the structure. The high reflective structure, model-2h, is modelled by a 1 box sponge layer, whereas the low reflective structure, model-2l, is modelled by a 3 box sponge layer.

(a) High reflective structure   (b) Low reflective structure
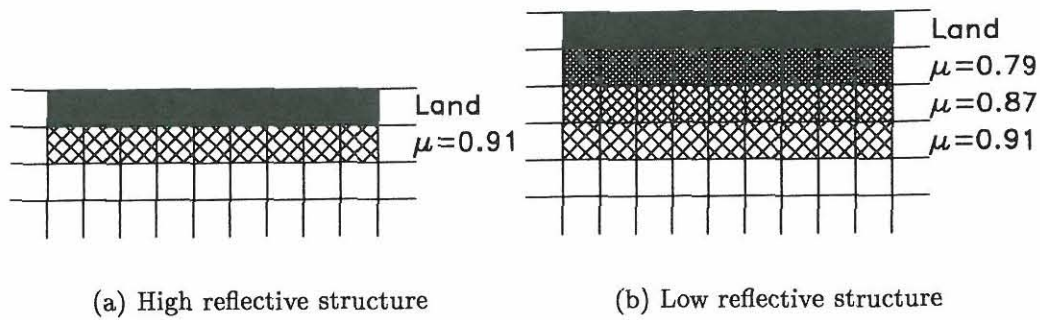
Figure 5.5: Variations of structure in model-2.

5.3.4   Irregular Structure

Model-3, 4 and 5 contain a rigid boundary, three sponge layers, and a structure. The structure is either full or low reflective and is positioned oblique in an angle of 9.5°(1:6), 18.4°(1:3) or 26.6°(1:2) respectively. Hence the face of the model will be somewhat saw-tooth shaped. Model-4l is shown in Figure 5.6.

The two large sponge layers for the open boundaries are similar to the previous ones, but an additional sponge layer has been placed along the left boundary to absorb oblique waves reflected off the structure.
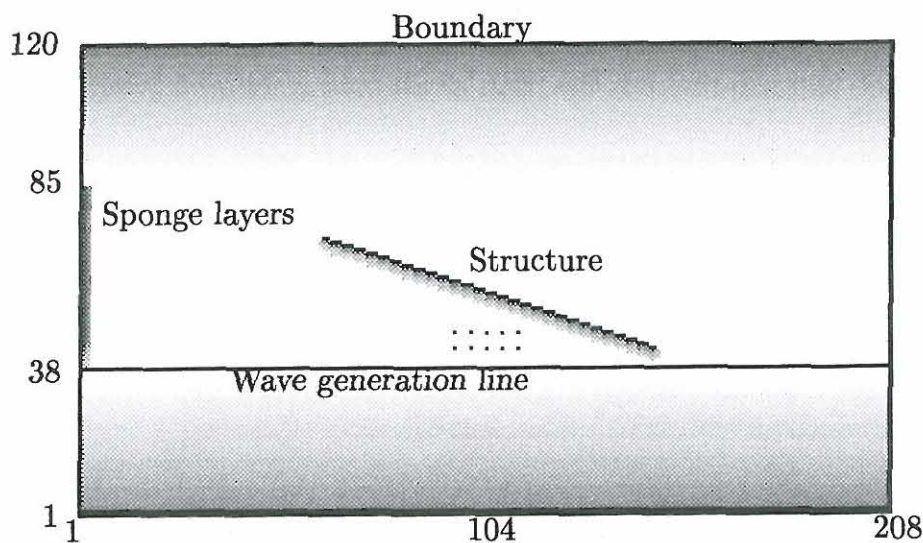
Figure 5.6: Model-4l. Irregular structure, low reflection.
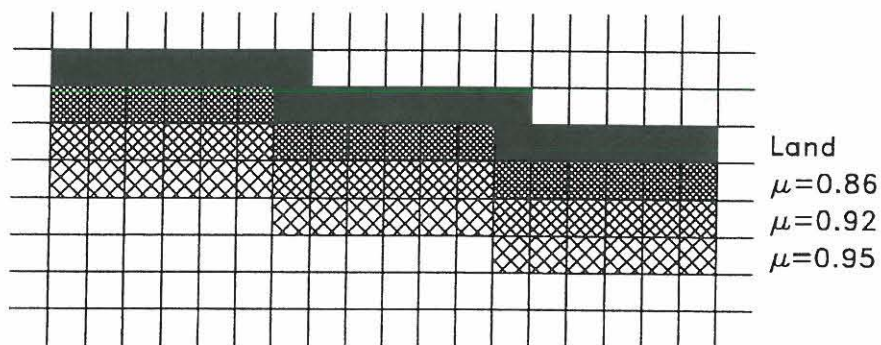
Figure 5.7: Model-3l. Irregular structure, low reflection.

(a) Model-4l   (b) Model-5l
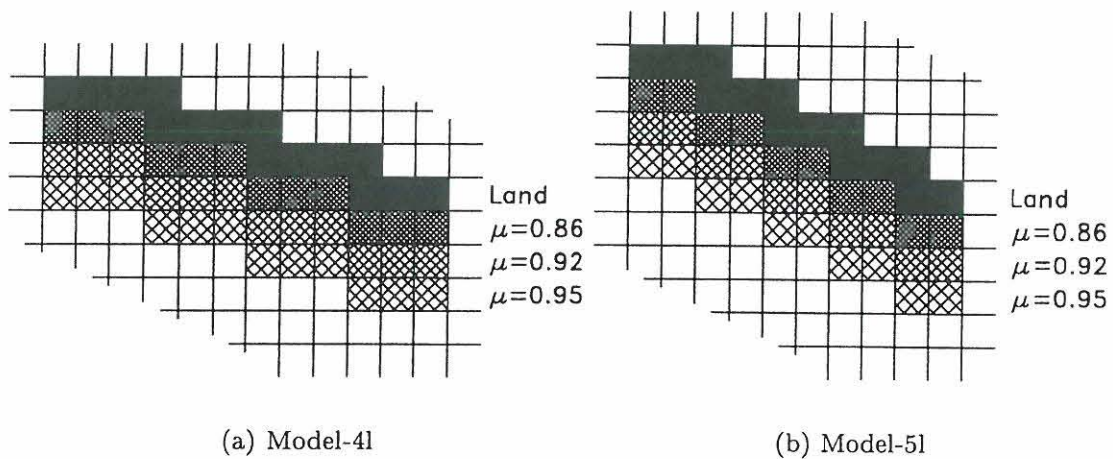
Figure 5.8: Irregular structures, low reflection.

5.4   Wave Conditions

Experiments have been performed with the target specifications for the incident waves as listed in Table 5.1. The wave conditions are similar to those used in the physical experiments with caissons, described in Section 3.4. Main direction and directional spreading of incident waves are specified in the test programme, to appear in the following section.

Wave spectrum	JONSWAP
Peak period, T_p	$1.5s$
Significant wave height, $H_{s,I}$	$0.10m$
Wave steepness H_{s0}/L_{0p}	0.028
Wave steepness H_{s0}/L_p	0.033
Type of spreading	$\cos^{2s}\left(\frac{\theta-\theta_m}{2}\right)$

Table 5.1: Incident wave conditions.

5.5   Test Programme

Table 5.2 shows the test programme for preliminary simulations with the definitions of directions as shown in Figure 5.9.
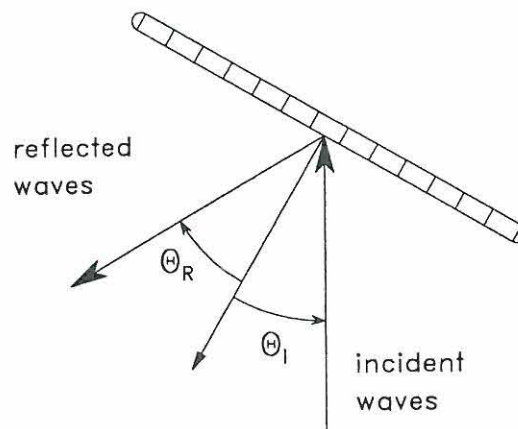
Figure 5.9: Definition of incident and reflected directions.

Model	$\theta_{m,I}$	s	Label	Test of
Model-1*	0°	15	01	Original spreading algorithm
	0°	15	02	New spreading algorithm
	10°	15	03	Oblique incidence
Model-2*	0°	15	01	Full reflection
	10°	15	02	Full reflection, oblique incidence

Table 5.2: Target wave conditions for preliminary simulations.

Table 5.3 shows the primary test programme. The main parameter, which has been changed, is the incident main direction. For the structures which are aligned obliquely in the model a larger range of directions can be considered. For the regular structure, different variations of directional spreading have been included in the test programme.

Model	$\theta_{m,I}$ [deg.]	s	Label
Model-2f	0,10,20,30	15	Test 5-8
	0,10,20,30	60	Test 9-12
Model-2h	0,10,20,30	15	Test 23-26
Model-2l	0,10,20,30	15	Test 30-33
	0,10,20,30,40	200	Test 34-38
Model-3f	0,20	15	Test 7,10
Model-3l	10,0,-10,-20,-30	15	Test 91-95
Model-4f	0	15	Test 8
Model-4l	20,10,0,-10,-20,-30	15	Test 61-66
Model-5f	0	15	Test 9
Model-5l	30,20,10,0,-10,-20,-30	15	Test 81-87

Table 5.3: List of target specifications.

5.6 Acquisition

During a simulation the mild–slope model will measure the variance in each box symbolising water. Subsequently plots of the overall wave disturbance can be presented. In order for the model to remain stable a sample frequency of $20Hz$ has been applied.

It is possible, in addition, to record elevation time series in specified points. Such recordings will form the basis for the succeeding 3D reflection analysis. Elevation time series have being recorded in an array corresponding to the array used in the physical experiments with caissons, see Section 3.4. The array was a 5×2 array with a grid dimension of $0.5 \times 0.5m$. In the physical experiments the first

row of gauges was placed $1.0m$ off the caissons. Figure 5.10 shows the variance infront of a fully reflective structure, and gives an indication of the phase-locking effect. More reliable results were obtained, if the first row of gauges was placed in a distance of $1.25m$ off the structure.
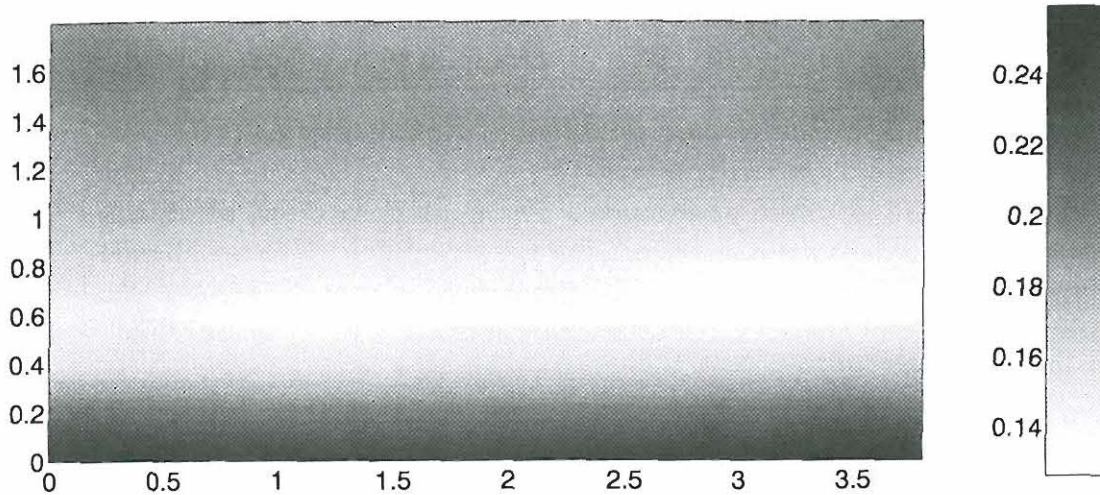
Figure 5.10: *Relative variance in front of a fully reflective structure. Wave conditions: $\theta_{m,I} = 0°$, $s = 15$ $(\cos^{2s})$, depth=0.61m.*

The elevation time series were recorded with a sample frequency of $10Hz$ during a simulation period of 18 minutes.

5.7 Analysis of Simulations

5.7.1 Wave Generation

For the purpose of verifying the numerical model's capability to generate the specified incident wave field a number of preliminary simulations were carried out. This, in particular, concerns the following properties of the numerical model.

- Spectral distribution of wave energy.

- Main direction of wave propagation.

- Directional spreading of short-crested waves.

- Ability of absorbing boundaries.

Based on the preliminary simulations minor modifications of the model were done to improve the performance. This included adjustment of carrying frequency,

wave generation, and directional spreading. The simulations to be presented here are only those carried out using the modified version of the numerical model. Target wave specifications for the simulations are seen in Table 5.2.

In the analysis of the simulations the BDM method, as described in Section 2.5, has been applied. Results from the analysis are shown in Table 5.4. Comparing the specified wave field and the estimated wave field a satisfactory agreement is found. Hence it can be verified that the numerical model is capable of simulating a specified wave field satisfactory.

Type	#	#	Δf Hz	$H_{s,I}$ m	$\theta_{m,I}$ deg.	$\sigma_{\theta,I}$ deg.
Model-1*	1	a	0.020	0.097	−0.8	17.5
		b	0.039	0.100	−0.5	21.3
	2	a	0.020	0.097	−0.1	16.4
		b	0.039	0.097	−0.4	20.3
	3	a	0.020	0.096	8.6	15.9
		b	0.039	0.098	7.8	19.5

Table 5.4: Results from preliminary simulations.

5.7.2 Reflection Performance

Regular Structure

The results based on the preliminary tests with reflection show that the model is capable of modelling the reflection of short-crested waves with a head on main direction. Results are seen in Table 5.5. The time series were analysed using two different frequency resolutions, but no significant differences were obtained in the results.

Type	#	#	Δf Hz	$H_{s,I}$ m	$\theta_{m,I}$ deg.	$\sigma_{\theta,I}$ deg.	$\theta_{m,R}$ deg.	$\sigma_{\theta,R}$ deg.	C_R %
Model-2*	1	a	0.020	0.093	0.0	24.3	−1.0	24.5	100.2
		b	0.039	0.094	−1.1	23.8	−0.5	24.6	101.4
	2	a	0.020	0.091	9.1	24.0	9.0	23.1	102.3
		b	0.039	0.093	7.8	23.3	9.9	23.5	103.4

Table 5.5: Results from preliminary simulations.

A graphical presentation of the results from test Model-2*.1 is given in Figure 5.11.
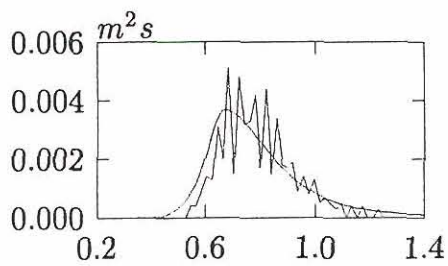
(a) Total spectral density
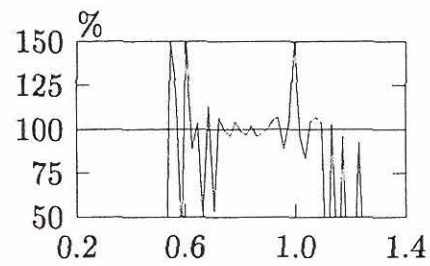
(b) Reflection performance
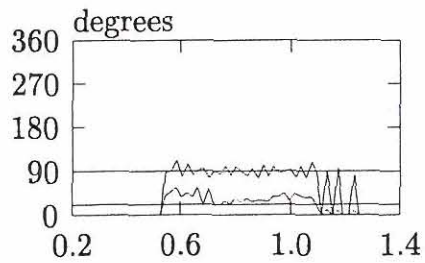
(c) Incident main direction and spreading
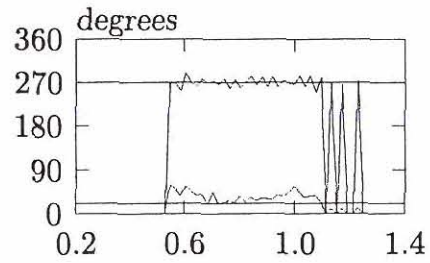
(d) Reflected main direction and spreading

Figure 5.11: Results of Model-2*.1. Abscissa is frequency in Hz. (Notice that here directions are defined according to Figure 3.13b.)

The overall reflection coefficients obtained during analysis of all tests with a fully reflective structure are shown in Figure 5.12. The reflection is seen to be independent of the incident main direction and also of the directional spreading.
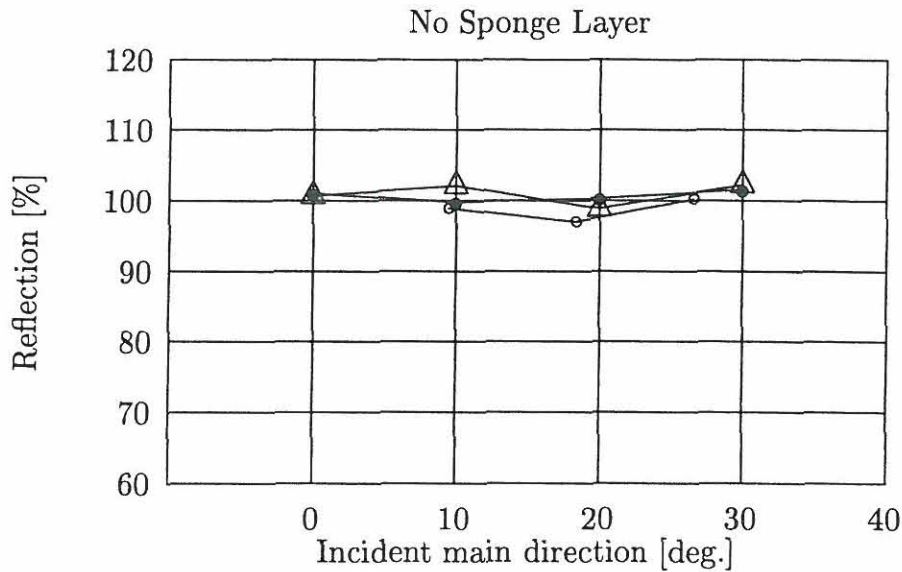
Figure 5.12: Analysis of fully reflective structure.

For the partially reflective structures overall reflection coefficients are shown in Figure 5.13. It is seen, that the reflection is decreasing with increased obliquity of the incident waves. For the nearly long-crested waves, the reflection do, however, peak at approximately 25° off the head on direction.

Irregular Structure

No significant difference between the reflection performance of the fully reflective irregular and regular structures can be seen.

Overall reflection coefficients of the partially reflective irregular structures are shown in Figure 5.14 altogether. Increased irregularity of the structure is seen to slightly lower the reflection of the structure. The effect of decreased reflection with increased obliquity of incident waves is still clear.
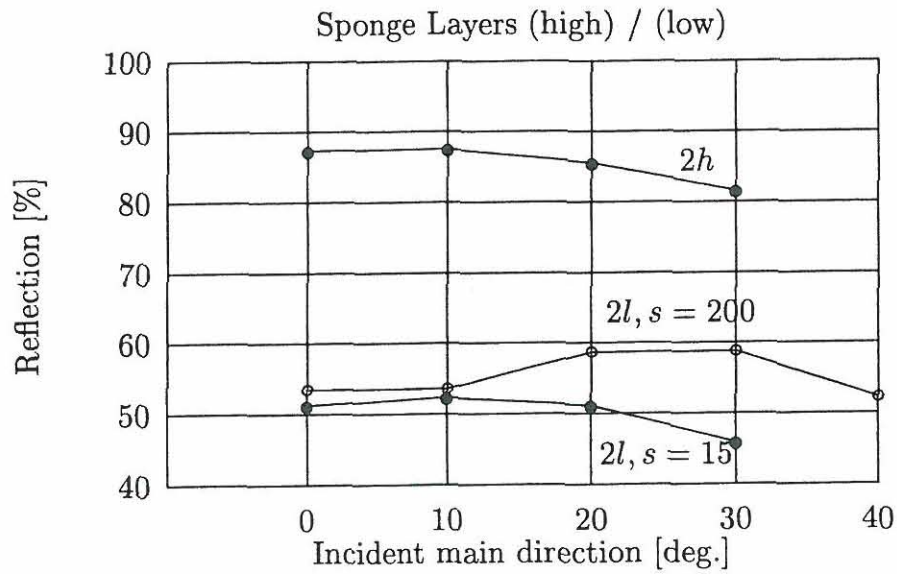
Figure 5.13: *Analysis of partially reflective regular structures.*
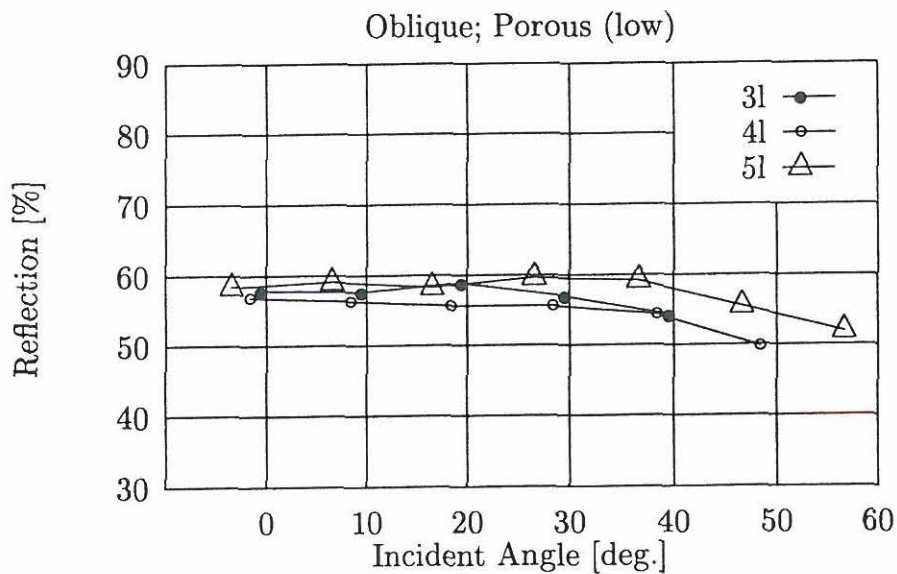
Figure 5.14: *Analysis of oblique partially reflective structures.*

5.7.3 Main Directions

For the full and high reflective regular structure the relation between main direction of incident and reflected waves is very satisfactory, see Figure 5.15 and Figure 5.16. That is, waves are reflected according to Snell's law. For the more oblique waves, the main direction of the generated incident waves do, however, deviate slightly from the expected values.
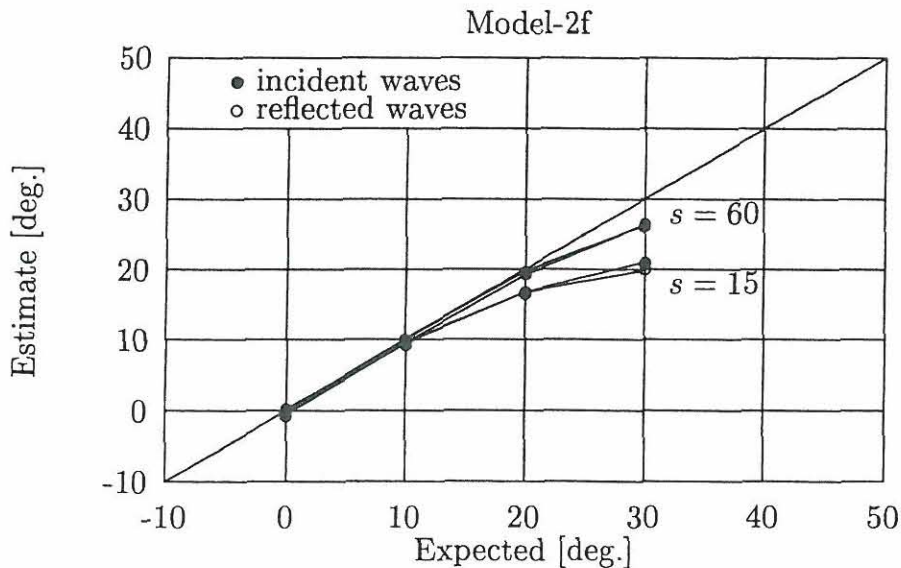
Figure 5.15: *Comparison of main directions.*

For the low reflective regular structure the effect is similar, but it appears more confused, see Figure 5.17. In particular, for narrow spreaded waves the reflected waves are bending more than they should, when they are being reflected.

For the irregular structures the relation between main directions for incident and reflected waves also appears to be very satisfactory. For very oblique directions larger deviation from expected values are found, but a proper relation between incident and reflected waves remains. The results are shown if Figures 5.18, 5.19, and 5.20.

The deviation from expected values are likely to be due to the generation of incident waves, as the most oblique waves are being truncated.
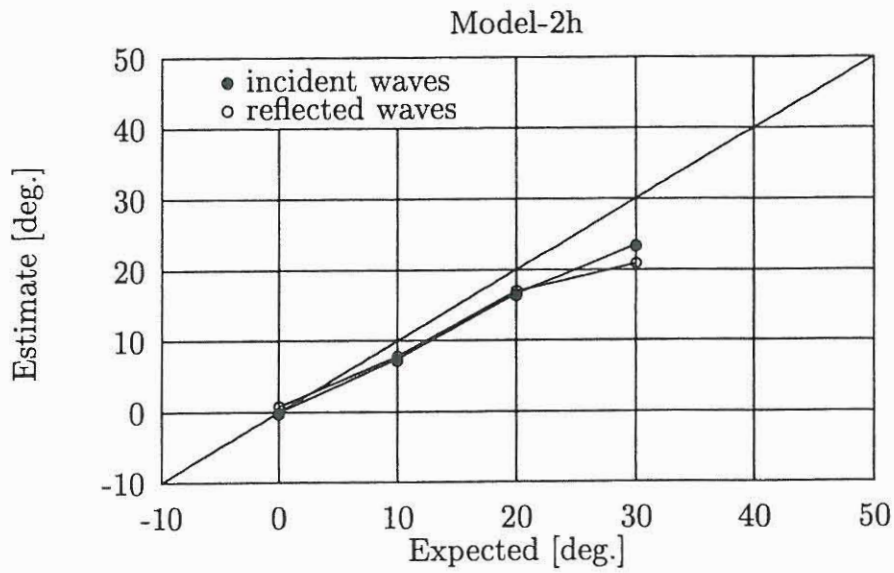
Figure 5.16: Comparison of main directions.
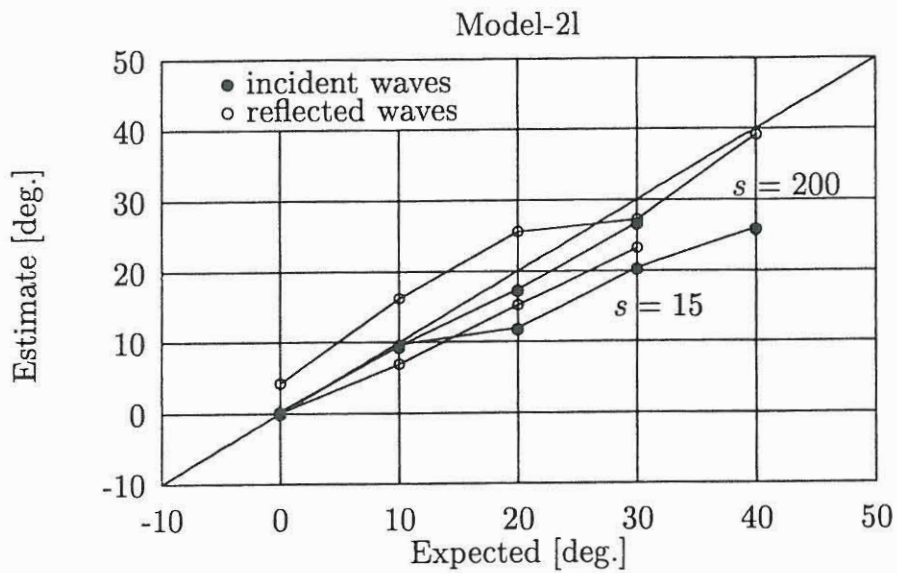
Figure 5.17: Comparison of main directions.
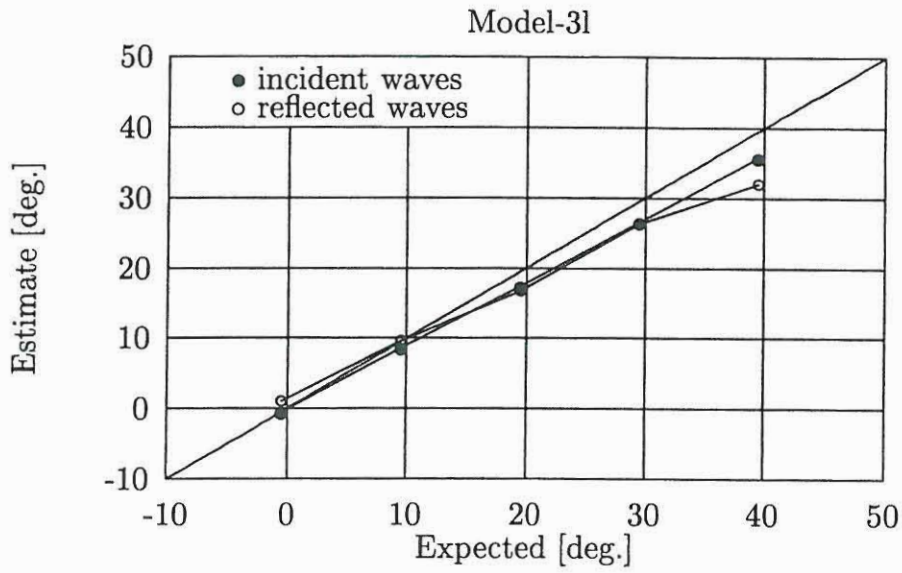
Figure 5.18: *Comparison of main directions.*
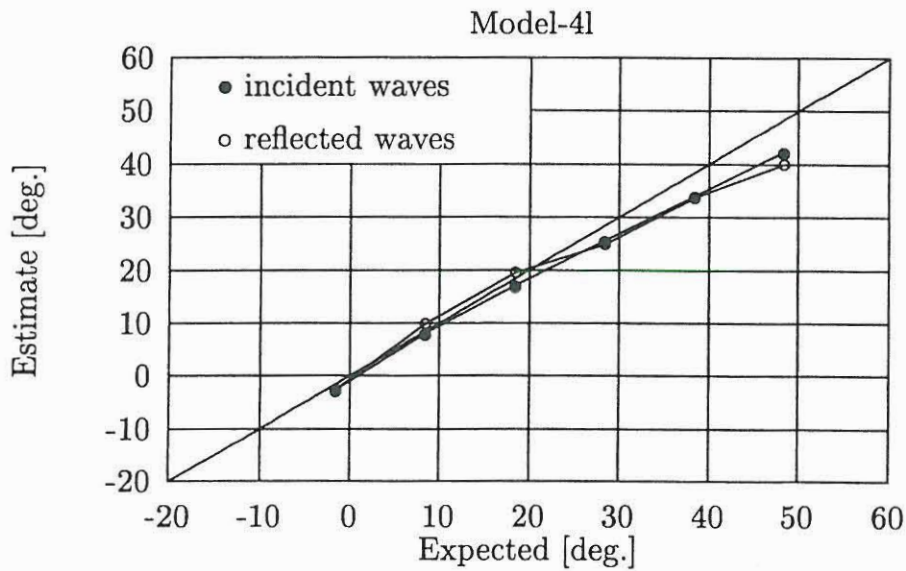
Figure 5.19: *Comparison of main directions.*
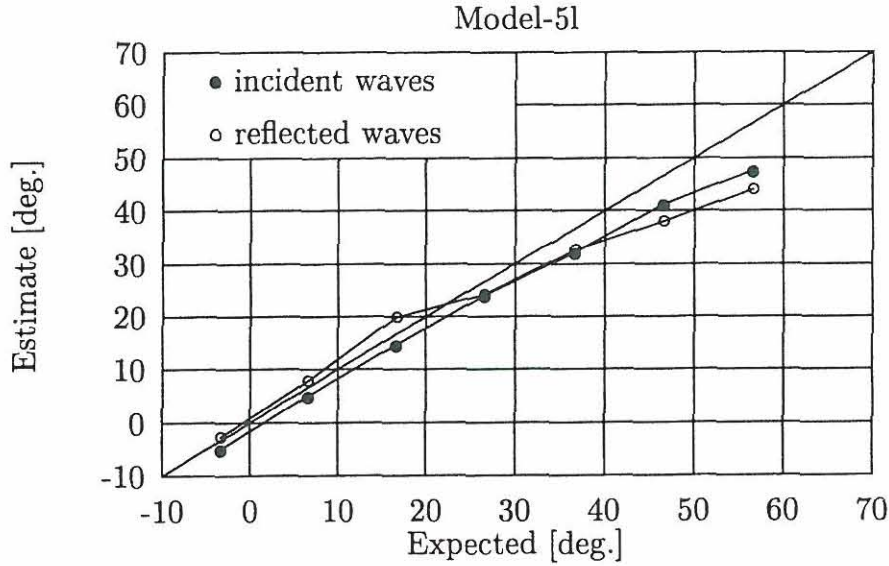
Figure 5.20: *Comparison of main directions.*

5.7.4 Directional Spreading

Considering the generated (incident) waves the directional spreading appears to be satisfactory and will not be discussed further.

The ratio between the directional spreading of incident and reflected waves are shown in Table 5.6. For the full and high reflective structures the ratio is close to unity, whereas it increases for low reflective and very irregular structures. The highest value is obtained for the almost long-crested waves, but the high value may be due to the method of analysis (i.e. the BDM method), since it is designed for short-crested waves in particular.

Reference	Average	Std. Dev.	Comments
Model-2f	1.00	0.03	$s = 15$ and $s = 60$
Model-2h	1.05	0.03	
Model-2l	1.33	0.04	$s = 15$
Model-2l	1.59	0.20	$s = 200$
Model-3l	1.18	0.10	
Model-4l	1.24	0.16	$s = 15$
Model-5l	1.19	0.19	

Table 5.6: *Relative directional spreading, $(\sigma_{\theta,R}/\sigma_{\theta,I})$, and standard deviation.*

6

Wave Disturbance
in Grenaa Harbour

6.1 Introduction

During previous chapters the reflection performance in long- and short-crested waves of selected coastal structures has been considered in terms of physical experiments, field measurements, and numerical modelling. In this chapter the results of these consideration will be taken into account in an application of a numerical model for estimating the overall wave disturbance in a selected harbour. The numerical model to be used is the Mild-Slope model previously used and described in Chapter 5.

The harbour to be taken as an example is Grenaa Harbour positioned on the East coast of Jutland in Denmark. Physical experiments were carried out during 1991 by the Hydraulics and Coastal Engineering Laboratory, Aalborg University, due to a planned extension of the harbour. Hence data were available prior to the present work, enabling a valuable comparison of results from physical experiments and the numerical simulations carried out during the present work and described in this chapter.

The numerical simulations were performed with various reflection characteristics for the involved structures. Thus it will be possible to assess which influence a

correct modelling of reflection in the numerical model will have on the overall wave disturbance, which will often be a design criterion.

In principle the reflection depends on a large number of parameters, describing both the structure and the incident waves. Since it is not possible in the used numerical model to vary the reflection coefficients during simulation, it is not possible to take any such parameters into account. Thus, a fully correct modelling of reflection cannot be implemented. Despite of this, the term is used herein, as it can be expected that the true reflection performance will result in a wave disturbance somewhere within the range obtained from the applied reflection conditions.

When defining the model domain the expected conditions at specific locations may, however, be considered when determining the desired reflection coefficients. This may involve an iterative procedure.

6.2   Description of the Harbour

Views of Grenaa Harbour during and after the extension are seen in Figures 6.1 and 6.2. After the extension the harbour consists of two rubble-mound breakwaters forming the outer boundaries of the harbour. A *detached rubble-mound* breakwater shelters the inner harbour.

The quay walls of the new harbour area, the central area seen in Figure 6.2, are constructed as backfilled sheet pile walls.

The model domain considered in both the physical experiments and the numerical model is outlined in Figure 6.3. The main area of interest prior to the extension is the new harbour basin behind the northern breakwater. In order to limit the model domains, the inner sections of the harbour have been omitted in the analysis. This is believed to have only small effect on the estimated wave disturbance. Some reflection do occur, as the applied sponge layer is only nearly fully absorbing.
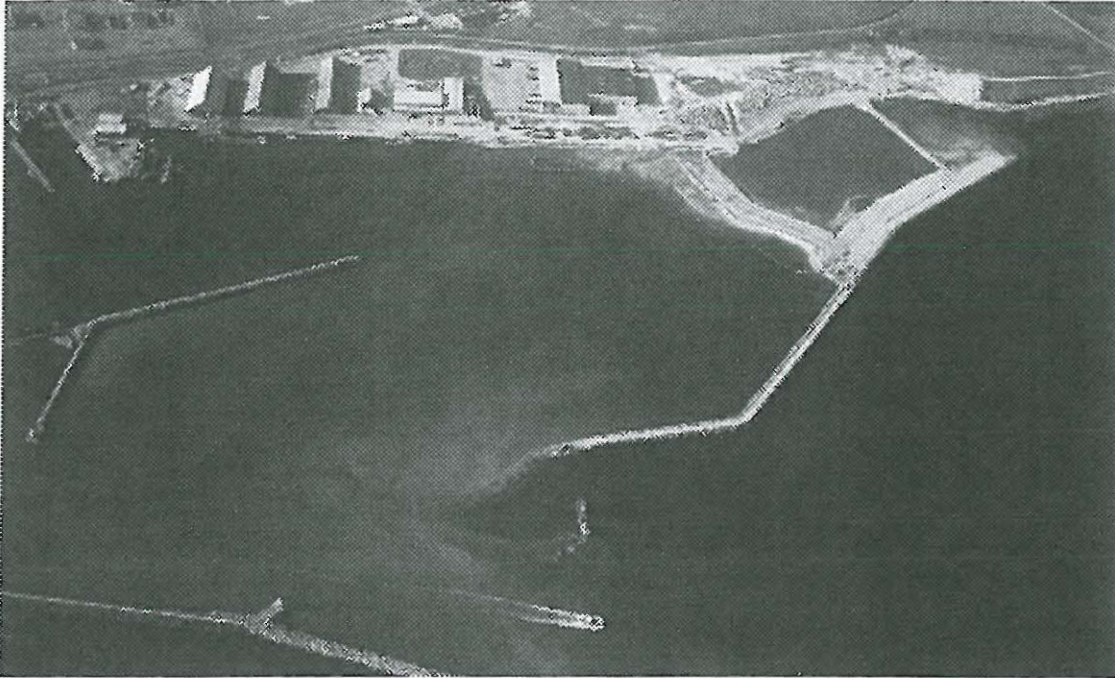
Figure 6.1: *Photo from Grenaa Harbour during construction of new northern breakwater (C.G. Jensen).*

Figure 6.2: *Photo from Grenaa Harbour after construction of new northern harbour (C.G. Jensen).*
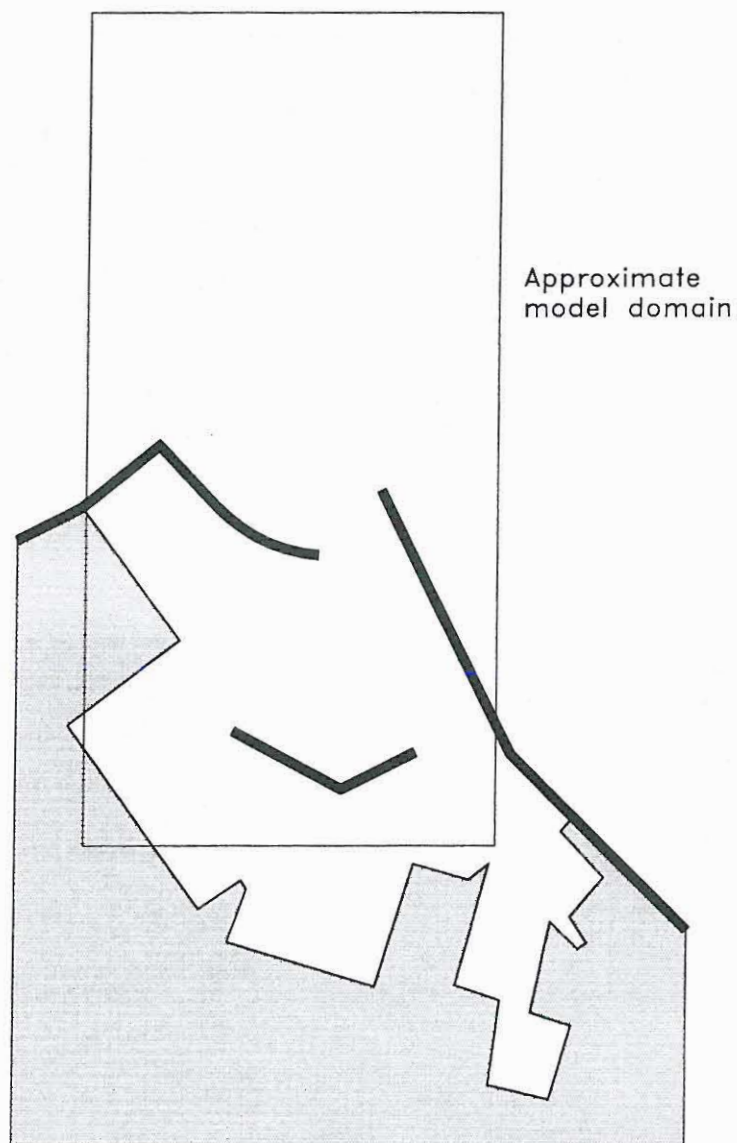
Figure 6.3: Domain of the model of Grenaa Harbour.

6.3 Physical Experiments

Figure 6.4 shows the set-up of the physical model, which was constructed at 1:100 scale. Long-crested waves were generated from a direction of 60° azimuth, with a significant wave height of $H_s = 2.7m$ and a peak period of $T_p = 9.5s$. A JONSWAP wave energy spectrum with a peak enhancement factor of 3.3 was applied.

Angular stones were used to model the quarry stones of the rubble mound breakwaters. The reflection of the rubble mounds was not measured. However, based on later experiments carried out with the same type of stones, it appeared reasonable to use reflection coefficients given by Equation (6.2).

During testing, surface elevations were measured in a $50\times50m$ grid in the outer part of the harbour, and results were stored as H_{m_0}-values $(= 4\sigma_\eta)$.

A wave disturbance plot based on the physical experiments is shown in Figure 6.5. During the experiments wave breaking was observed in the area around L3 and L9, cf. Figure 6.4.
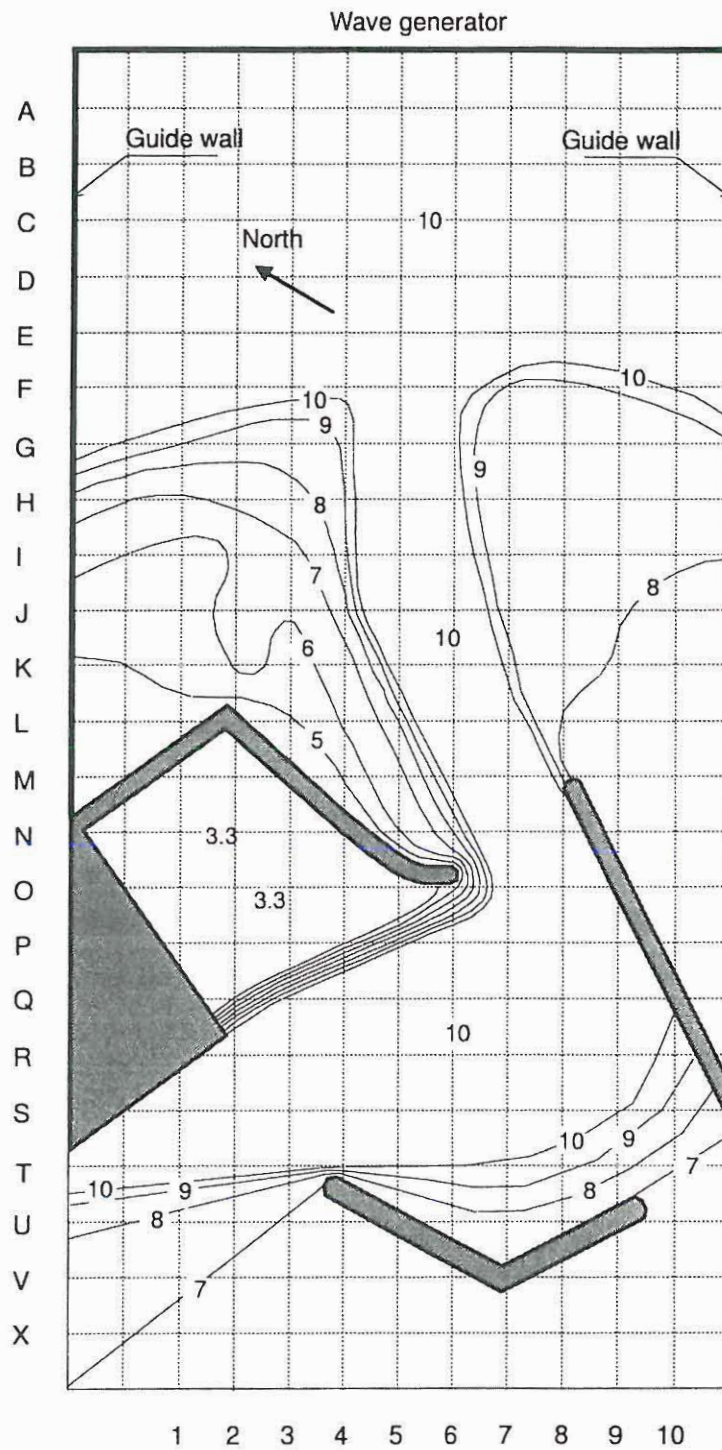
Figure 6.4: *Bottom topography and harbour layout of physical model. Water depths in metres. The distance between grid lines is 50m.*
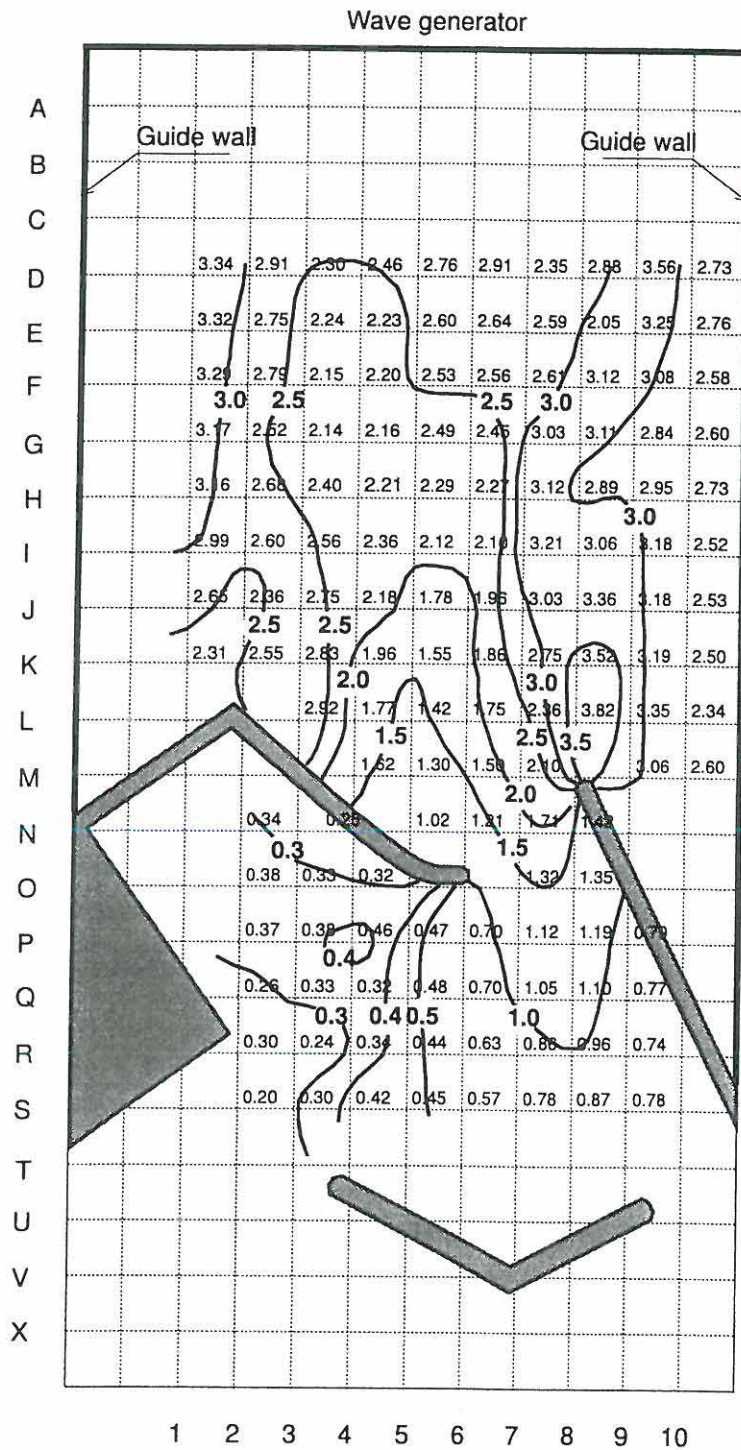
Figure 6.5: *Wave disturbance. Physical model. Wave heights (H_{m_0}) and contour levels in metres.*

6.4   Numerical Simulations

6.4.1   Reflection Coefficients

When initializing the model domain for the numerical model, it is necessary to have an idea about the amount of reflection which will take place at the various structures/boundaries. As mentioned earlier this may be based on published results of previous measurements or theoretical considerations. Information on reflection is usually available for long-crested head-on waves, whereas less information is available regarding reflection of oblique and short-crested waves.

Reflection of long-crested waves

Reflection from slopes armoured with stones, rocks or artificial blocks has traditionally been quantified as a function of the surf similarity parameter defined here as

$$\xi_p \;\; = \;\; \frac{\tan \alpha}{\sqrt{s_p}} \quad \text{where} \quad s_p \;\; = \;\; \frac{H_s}{L_p} \tag{6.1}$$

and α is the angle of the slope, s_p is the wave steepness, H_s is the significant wave height, and L_p is the wavelength calculated for the peak period.

A number of prediction formulae have been proposed for different structures under various conditions. Postma (1989) analysed data for a rock armoured slope from van der Meer (1988), and Allsop and Channell (1989). The results are cited in CUR (1995). Postma arrived at the following relations respectively.

$$C_R \;\; = \;\; 0.14\xi_p^{0.73} \quad \text{with} \quad \sigma_{C_R} = 0.055 \quad \text{(van der Meer)} \tag{6.2}$$
$$C_R \;\; = \;\; 0.125\xi_p^{0.73} \quad \text{with} \quad \sigma_{C_R} = 0.060 \quad \text{(Allsop et al.)} \tag{6.3}$$

where C_R is defined as the ratio of the reflected wave height to the incident wave height, i.e. $C_R = H_R/H_I$, and σ_{C_R} is the standard deviation of C_R.

Considering that more prediction formulae may exist, it is clear, that the choice of prediction formula is not straight forward.

Also considering the uncertainty in predicting the parameters included in the Equations (6.2) and (6.3) emphasizes the overall uncertainty in predicting the reflection coefficient for a certain structure. As an example the variation of the
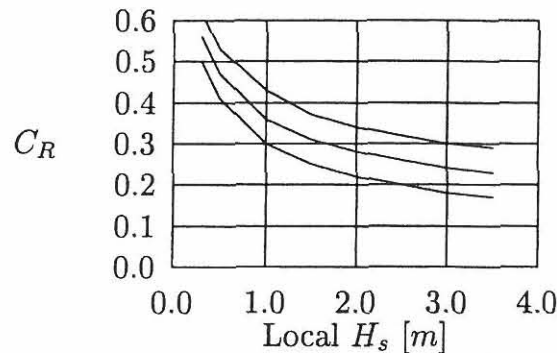
Figure 6.6: *Example of variation in reflection coefficient, $C_R \pm \sigma_{C_R}$. $T_p = 9.5s$ and $h = 3.5m$.*

reflection coefficient with respect to significant wave height is shown in Figure 6.6 for Equation (6.2).

Reflection of oblique and short-crested waves

Information on the reflection of oblique and short-crested waves from rubble mound structures have been presented by e.g. Benoit and Teisson (1994). The results, based on physical scale measurements with irregular long-crested waves, reveal an almost constant level of reflection coefficient for waves deviating up to 20-25 degrees from the normal to the structure. At 45 degrees off the normal the reflection has its maximum and hereafter decreases to a lower level. The maximum difference in reflection coefficient is approximately 0.15.

In Helm-Petersen and Frigaard (1996) the reflection of an upright perforated structure has been measured for irregular long- and short-crested waves with oblique incidence. The reflection was found to have a maximum for head-on waves, and then decreased with increased obliquity of the incident waves. This is shown in Figure 3.15.

Any published results on the effect of the degree of short-crestedness of the waves on the reflection performance for rubble mounds have not been found. However, it has been proposed that porous structures are likely to increase the directional spreading of the reflected waves relative to the incident waves, see e.g. Isaacson, Papps, and Mansard (1996) or Helm-Petersen and Frigaard (1996).

6.4.2 Model Domain

According to Postma (1989) reflection coefficients estimated by Equation (6.2) have a standard deviation of approximately 0.06. This standard deviation applies in cases, where the incident wave field is well known. It is possible, but in practice

probably not worth the effort, to estimate the size of the incident wave height near all the boundaries inside a harbour. In most cases the incident wave height will be lower than $H_{m_0} = 4\sigma_\eta$, but not always. If the local value of H_{m_0} is used to estimate the local reflection coefficient, this leads to an additional uncertainty. It is therefore proposed, that an overall uncertainty of ± 0.10 applies to reflection coefficients calculated from e.g. Equation (6.2), but it should be emphasized that this figure is only a guess.

Three combinations of reflection performance have been investigated, representing the most probable value, a reduced value and an increased value, which represents the range of uncertainty. The combinations are shown in the table in Figure 6.7.

To distinguish the various breakwaters (or part of) reference numbers have been allocated as shown in Figure 6.8.

Model	min.	medium	max.
Section I	0.23	0.33	0.43
Section II	0.37	0.47	0.57
Section III		1.00	
Section IV	0.30	0.40	0.50
Section V	0.30	0.40	0.50
Roundhead	0.17	0.27	0.37

Figure 6.7: *Combinations of reflection coefficients.*
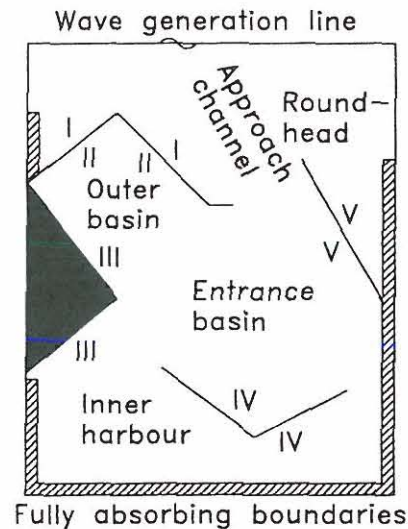
Figure 6.8: *References to breakwaters (or part of).*

The choice of reflection coefficients are based on Equation (6.2). Considering, for example, the leeward side of the northern breakwater yields the following reflection coefficient, when a wave height of $H_s = 0.5m$ is assumed:

$$\xi_p \simeq \frac{0.5}{\sqrt{0.5m/54.2m}} = 5.2 \tag{6.4}$$

$$C_R \simeq 0.14 \cdot 5.2^{0.73} = 0.47 \tag{6.5}$$

This value is valid for long-crested head-on waves. Benoit and Teisson (1994)

show that for rubble mounds, the reflection will increase to a maximum at approximately 45 degrees off the head-on direction.

The partially reflective structures are all modelled by a sponge layer, which is one grid deep ($\mu = 0.91$), corresponding to the sketch in Figure 5.5(a).

The bottom topography and harbour layout of the numerical model correspond to the physical model, except that the above mentioned part of the inner harbour has not been included in the numerical model. Due to very low wave heights in the inner harbour, wave energy radiated from the inner harbour is considered insignificant justifying the modification. Hence, reducing the model domain by using an almost fully absorbing sponge layer instead reduces computational time significantly.

6.4.3 Results

The results of the numerical simulations may be given in terms of contour plots showing the wave disturbance in the horizontal plane, see Figures 6.9, 6.10, and 6.11.
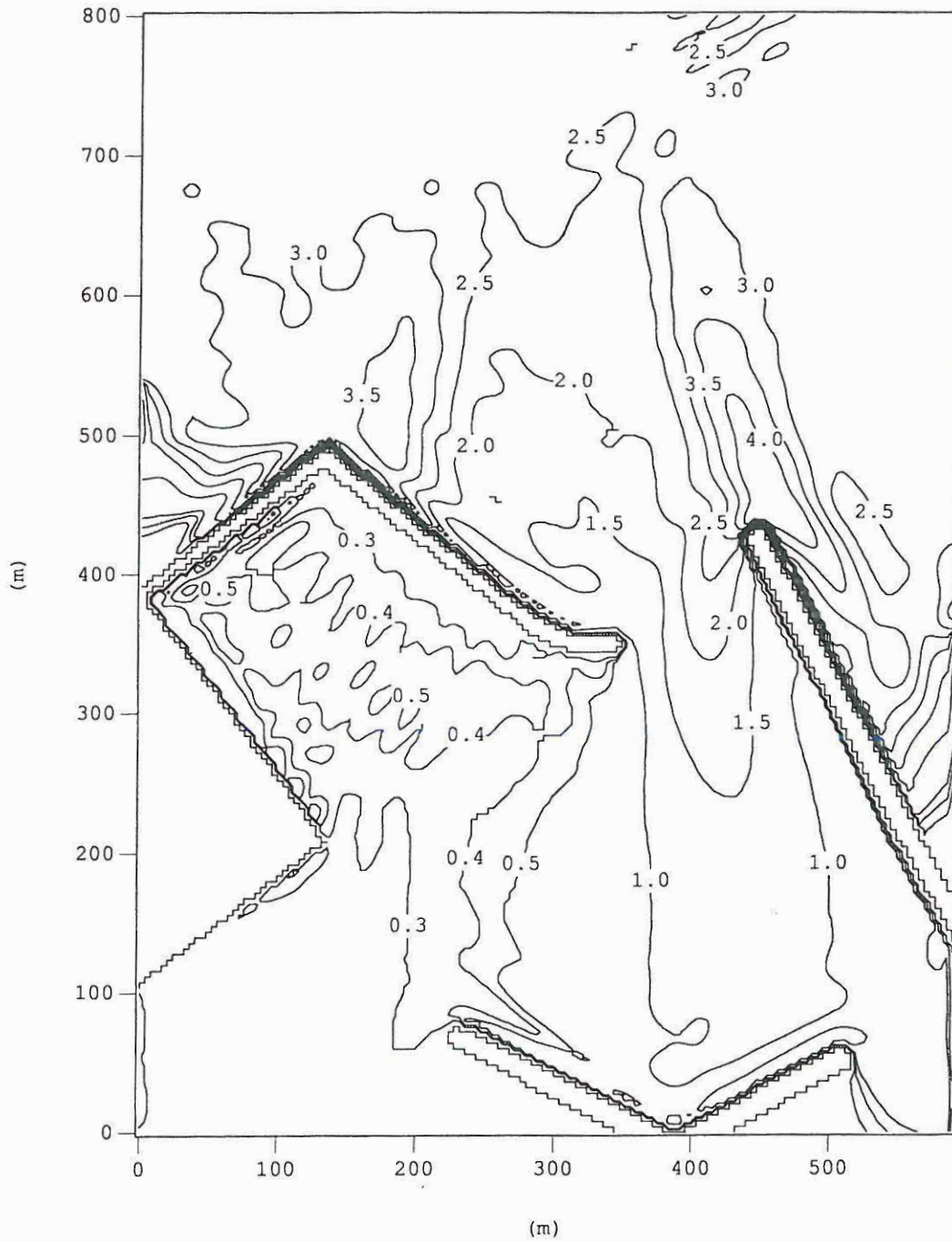
Figure 6.9: *Wave disturbance. Numerical model, low reflection. Only part of the model domain is shown. Wave heights (H_{m_0}) in metres.*
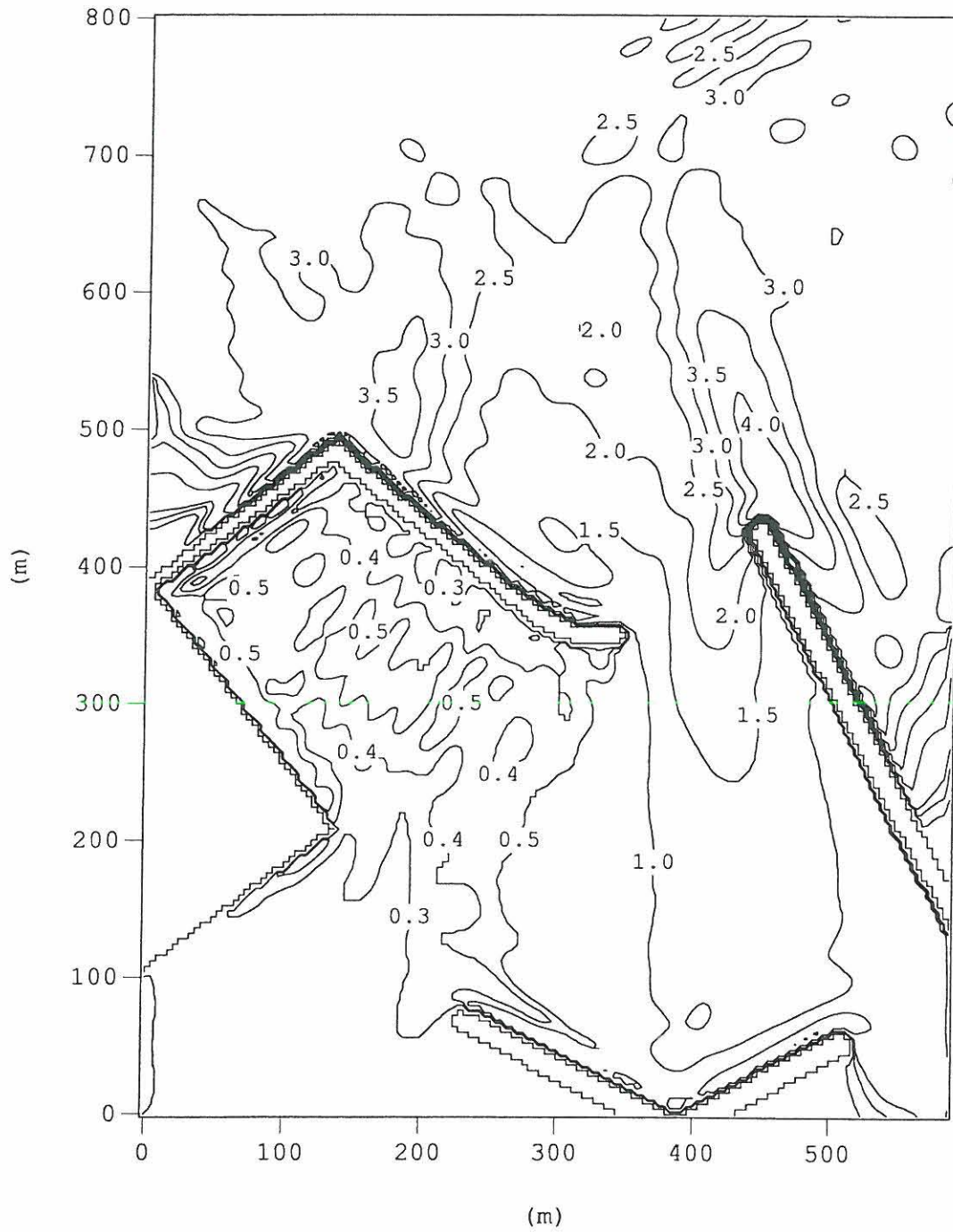
Figure 6.10: *Wave disturbance. Numerical model, medium reflection. Only part of the model domain is shown. Wave heights (H_{m_0}) in metres.*
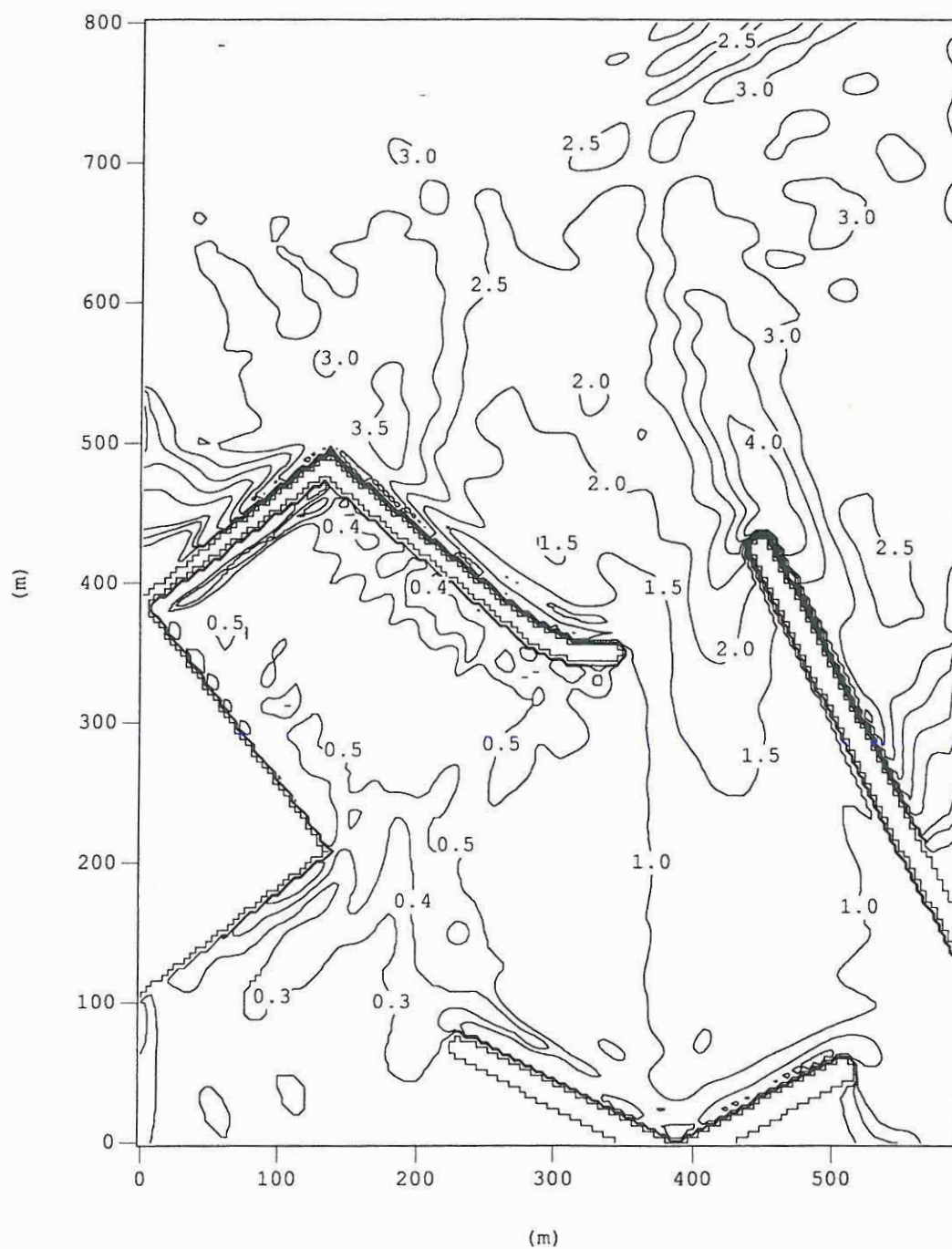
Figure 6.11: *Wave disturbance. Numerical model, high reflection. Only part of the model domain is shown. Wave heights (H_{m_0}) in metres.*

6.5 Comparison of Results

In the present study results from physical experiments have been used to verify the numerical model. Hereafter the numerical model has been used to estimate the level of wave disturbance inside the harbour for three degrees of reflection from the rubble mound structures. Thus, the discussion will first concern the verification of the numerical model, and then the effect that the change of wave reflection has on the wave disturbance in the outer basin.

As the physical experiments include the approach channel, reaching some 300 metres seawards, the numerical model had to include this area too. This was in order to provide similar refraction of the waves. Looking at Figure 6.5, 6.10, and 6.12 a reasonable agreement is found for the area outside the entrance.

It is seen from Figure 6.12 that along this line (line L, cf. Figure 6.4) there is almost no difference in wave activity for different levels of reflection. However, this is because the waves are not being reflected back towards the considered reference line.
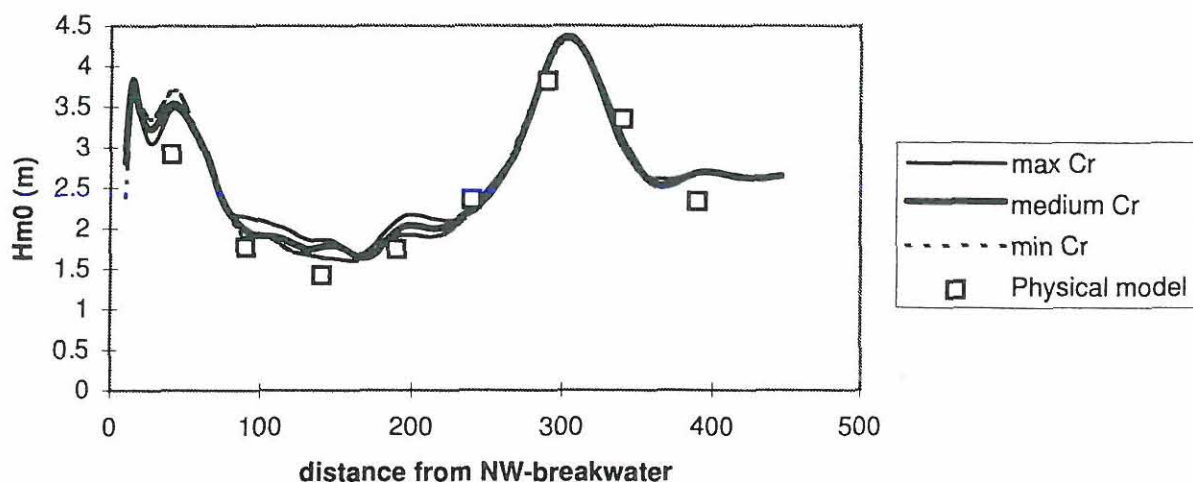
Figure 6.12: Wave disturbance. Cross-section in approach channel (line L).

From Figures 6.5, 6.10, and 6.12 it is also seen that due to refraction, large gradients in the wave height are present in sections perpendicular to the approach channel. In all 3 numerical simulations the wave height in the approach channel is approximately 0.3-0.5 metres higher (20-30%) than observed in the physical model. This is probably due to differences in the refraction in the physical and numerical model. The difference can be caused by the assumption of a mild bed slope in the numerical model, different bathymetry of the approach channel in the numerical and physical model or nonlinear effects not described by the linear model. The result is some overestimation of the wave heights inside the harbour

in the numerical model. However, Figure 6.13 shows that the effect is largest near the harbour entrance. Figure 6.13 also shows, that the overestimation of the wave height near the entrance is not caused by a bad estimation of the reflection coefficient along section V, cf. Figure 6.8, as changes in reflection coefficient only has a local effect close to the breakwater. It was also tried to increase the dissipation of energy due to wave breaking in the numerical model, but only very local effects outside the approach channel were seen.

All in all, it is assessed that, even though the numerical model is assuming mild bed slopes and small values of H/h, the wave disturbance is modelled with an acceptable accuracy.

Inside the harbour the major changes can be seen in Figure 6.13 and 6.14, showing cross-sections in the wave field.
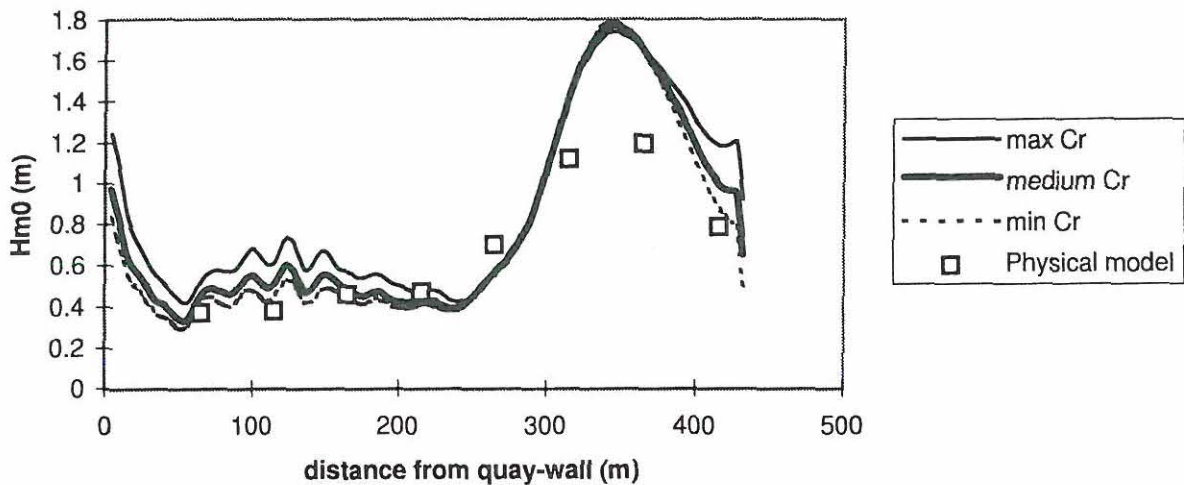
Figure 6.13: *Wave disturbance. Cross-section in entrance basin (line P).*

The wave disturbance in the entire outer basin is seen to depend much on the actual level of reflection from the breakwater (section II, cf. Figure 6.8). Along the quay-wall the average wave height was found to be $0.68m$, $0.78m$, and $0.98m$ corresponding to minimum, medium, and maximum reflection conditions, respectively. Similar changes in the wave height were seen in most of the outer basin. In the rest of the modelled area changes in reflection level only cause very local changes of the wave field.

Note that the 9 peaks in the wave height along the quay-wall, as seen in Figure 6.14, are due to the 9 major steps present in the discretized wall boundary, see Figure 6.10.
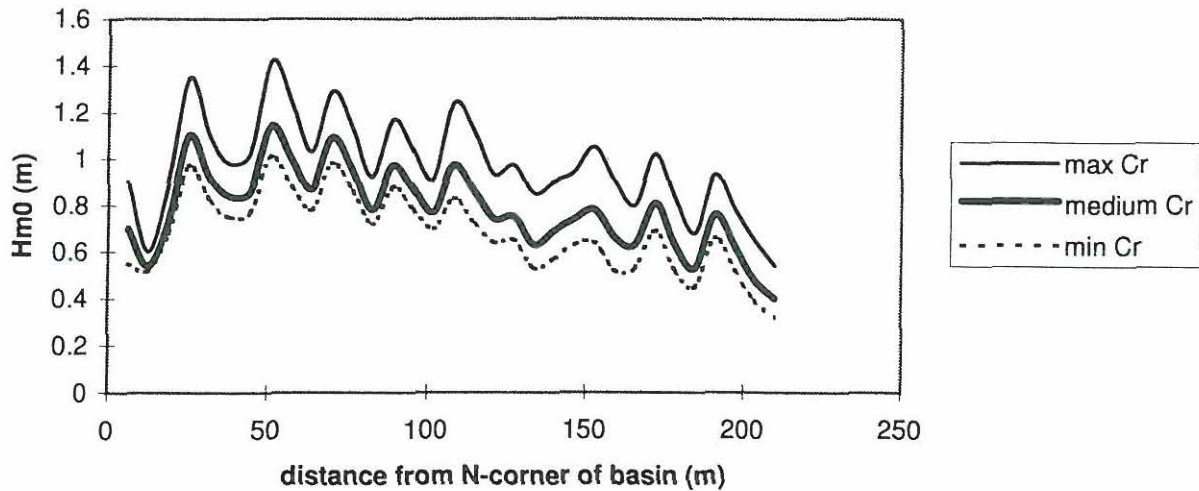
Figure 6.14: Wave disturbance. Cross-section along quay-wall.

6.6 Conclusions

The main result of the present study concerns the influence of reflection on the overall wave disturbance in a selected harbour.

The reflection from the leeward side of the rubble mound breakwater enclosing the outer basin of the harbour (section II, cf. Figure 6.8) could, based on CUR (1995), be predicted to $C_R = 0.47$ with a standard deviation of $\sigma_{C_R} = 0.06$. This standard deviation only covers the uncertainty of the actual prediction formula in case of head on waves. In numerical modelling sponge layers can be designed to model partial reflection of oblique waves from structures with vertical front with good accuracy, if the incident wave field is known. For rubble mound breakwaters, however, the local increase in reflection coefficient for waves with an incident angle of 45 degrees off the normal cannot be described with the sponge layer technique. In order to get an overall estimate of the effect from all uncertainties in the modelling of the reflection, numerical simulations were carried out with reflection coefficients varying within the range ± 0.10 around the value found according to Postma (1989). For the actual harbour it was found that changing the reflection coefficient from minimum to maximum resulted in an increase in the average wave disturbance along the quay-wall from $0.7m$ to $1.0m$.

Furthermore, comparisons of results from physical scale experiments and numerical simulations show that irregular waves can be modelled reasonable accurately with a numerical model based on the linear, time dependent mild-slope equation even in case of moderate non-linear waves and a bathymetry creating considerable gradients in the wave height due to refraction. Notice, however,

that the non-linear transformation of energy at frequencies near f_p to sub- and super-harmonics cannot be described by this linear model. This also applies to forced long waves, which may cause harbour seiching, see e.g. discussion in Kirby, Lee, and Rasmussen (1992). Finally, it should be mentioned that a numerical model as applied here is very robust and therefore easy to use in practice.

7

Summary and Conclusions

Summary

The motivation for the present study has been to improve the reliability in the application of numerical wave propagation models as a tool for assessing the wave disturbance in harbours. This will be valuable in the future as, once developed, numerical models will be a relatively inexpensive design approach. In the introduction of the thesis this is discussed further and the attention is directed towards the modelling of wave reflection. The immediate problems in modelling the wave reflection is discussed, and it is found that the reflection of short-crested waves should be investigated further. Hereafter a general introduction to numerical wave propagation models is given, and the scope of the thesis is outlined.

Following the introduction, methods for estimation of wave reflection coefficients are presented. Starting with the traditional 2D methods some more sophisticated 3D methods are presented. This concerns the Maximum Likelihood Method and the Bayesian Directional Wave Spectrum Estimation Method for estimation of directional wave spectra. The latter method is described in more detail, as it has been the main method used throughout the study.

A number of physical model tests have been carried out and analysed with the purpose of assessing the 3D reflection performance of the considered structures. A vertical face porous structure and a caisson with plain and perforated front were investigated, and surface elevation measurements were analysed with the BDM method. Results were presented mainly as overall reflection coefficients as function of incident main directions.

A large number of field measurements (140) have been made available from the School of Civil and Structural Engineering, Plymouth, UK. By deployment of the School's wave recording system sub-surface pressures have been recorded in an array of gauges mounted on the seabed in front of a breakwater. The data have been analysed with the BDM method, and results on overall reflection coefficients have been presented.

The theory behind the numerical wave propagation model used in this study is presented briefly. The model is based on the mild-slope equation derived using Hamiltons variational principle. The model can be applied for short-crested waves with a narrow wave energy spectrum. Discretization of the governing equations are presented along with the procedure of generating random directional waves according to the double summation principle. More than 40 simulations were carried out for a number of structures (boundaries) involving various incident main directions, directional spreading, and discretization of the structure fronts. The simulations are analysed using the BDM method, and the results are presented.

The thesis ends its main part with a chapter concerning an application of the applied numerical wave propagation model. A harbour for which physical scale measurements was already available were selected and three simulations were carried out. Various boundary conditions were applied as an attempt to model three levels of reflection for the structures involved. The variation of reflection symbolises the uncertainty in predicting the actual reflection for the structures, and also the uncertainty in the implementation of reflection in the numerical model. The results of the simulations were compared and the main differences were emphasised. For validation purposes the simulations were finally compared with results obtained from the physical scale experiments.

Conclusions

Among the considered reflection analysis methods and directional wave spectrum estimation methods, the BDM method has been preferred. The method is not directly including reflection terms when fitting estimated spectral values to the estimated values. In most cases, however, the method is capable of separating a combined wave field. It is mainly when the reflected waves becomes relatively small, that the method appears to neglect the presence of such. A performance analysis have been carried out with synthesised directional wave data in order

to evaluate the capability of the method. The analysis showed, that overall reflection coefficients could be estimated within a range of ±0.1, which is considered sufficiently. In estimating overall incident and reflected main directions, the accuracy depends on the difference between these directions. That is, when the incident main direction becomes too oblique, the peaks of the corresponding directional spreading function are no longer clearly separated, and problems arise for the BDM method to accurately estimate the directions. In general main directions can be estimated within a range of ±5 degrees. It should be emphasised that the performance of the BDM method depends strongly on the available data, and in particular the number of spatially separated gauges.

Estimates of overall reflection coefficients have been obtained based on physical scale measurements. Three structures have been considered. For the vertical face porous structure overall reflection coefficients were estimated in the range $0.6 < C_R < 0.8$, the reflection decreasing with the peak frequency ($0.9Hz < f_p < 1.1Hz$). The influence of incident main direction was not clearly revealed due to the limited number of tests. Thus it can only be concluded, that no difference were observed within the range of incident main directions ($0° < \theta_{M_I} < 30°$) considered. The caisson structure with plain vertical front was subjected to a more comprehensive test programme. The overall reflection coefficient was estimated to 0.95 with only little deviation. No influence of incident main direction, ranging from 0° to 40°, was observed. For the caisson structure with perforated vertical front the overall reflection coefficients were estimated to 0.5 for head on waves decreasing to 0.3 for an incident main direction of 60° off the normal. Altogether the physical experiments indicates a weak increase of the directional spreading of the reflected waves. This effect is clearly larger for the porous/perforated structures.

The analysis of the field measurements concerning the Alderney Admiralty Breakwater (crown wall on mound) resulted in an estimate of the overall reflection coefficient of 0.9 ($\sigma = 0.12$), based on approximately 100 recordings with a high water level. The results were quite scattered, which is believed to be mainly due to high tidal currents, and the possibility of wave refraction and diffraction depending on incident directions. Further, the incident waves often seemed to contain both a swell and locally generated wind waves. For a low water level the breakwater may be considered as a rubble mound structure, as the water level does not reach the crown wall significantly. For this structure reflection coefficients were estimated from 0.5 to 0.8. Plotted as a function of the surf similarity parameter, the reflection appeared to follow the generally accepted trend for such sloping structures. Due to the many uncertainties in the analysis, such as slope angle, incident wave conditions and diffraction, it has not been tried to derive any dependency on incident directions or directional spreading.

The numerical simulations with various sponge layers aimed at clarifying the behaviour of the numerical short-crested waves when approaching such bounda-

ries. The sponge layer technique is in fact a way of establishing a fake structure, which is believed to act in a way similar to the modelled structure, but it is a trial and error process to determine the size and characteristics of a sponge layer. Some aspects were, however, investigated for the general case. The amount of reflection can as expected be controlled by altering the sponge layer coefficients. What is more interesting is that the reflection for a partially reflective structure seems to decrease for oblique wave incidence. This agrees with the results obtained for e.g. the caissons with perforated front.

With respect to main directions, the direction of reflected waves follows Snell's law very well. Small deviations may occur for a very oblique porous structure, but the deviations are considered as insignificant.

Looking at the directional spreading of the reflected waves relative to the incident waves, this ratio increases only for the partially reflective sponge layers. This corresponds very well to the observations from the physical experiments.

It has been the main purpose of the present study to improve the reliability in using numerical wave propagation models as a tool for estimating wave disturbance in harbours. The emphasis was directed towards the implementation of reflection in a particular model. Generally the performance of sponge layers as partially reflective structures appeared satisfactory, but for less simple structures the approach may be unsatisfactory. The more the characteristics of the modelled structure changes with the incident wave conditions, the less applicable the sponge layer technique. By running three simulations with a selected harbour, it has therefore been tried to evaluate the influence that changes in reflection coefficients may have on the estimated wave disturbance. A low-, medium-, and high-reflective model were established, where the difference in overall reflection coefficients for the partially reflective structures were within a range of ± 0.1. The wave disturbance were observed to vary from $0.7m$ to $1.0m$ for exposed areas, which is an increase of almost 50%. Thus the problem is worthwhile to consider. At present, however, there is still a significant need for improving prediction formulae for reflection coefficients, both in the simple 2D case and in the more general 3D case.

Lastly, it can be concluded that the numerical model compared very well with physical measurements. Some deviations appeared, but recalling that the model is based on the linear wave theory, this can be accepted.

Bibliography

Allsop, N. W. H. (1990). Reflection performance of rock armoured slopes in random waves. In *Proc. 22nd International Conference on Coastal Engineering, Delft, The Netherlands*, pp. 1460–1471. ASCE.

Allsop, N. W. H., M. G. Briggs, T. Denziloe, and A. E. Skinner (1991). Alderney Breakwater: The quest for a final solution. In *Proc. Coastal Structures and Breakwaters, London, United Kingdom*, pp. 303–319. ICE.

Allsop, N. W. H. and A. R. Channell (1989). *Wave Reflections in Harbours: Reflection Performance of Rock Armoured Slopes in Random Waves.* Hydraulics Research, Wallingford, Report OD 102.

Allsop, N. W. H. and S. S. L. Hettiarachchi (1988). Reflections from coastal structures. In *Proc. 21st International Conference on Coastal Engineering, Malaga, Spain*, pp. 782–794. ASCE.

Allsop, N. W. H. and M. W. McBride (1994). Reflections from vertical walls: The potential for improvement in vessel safety and wave disturbance. In *Proc. International Workshop on Wave Barriers in Deepwaters*, pp. 101–128. Port and Harbour Research Institute, Japan.

Allsop, N. W. H., M. W. McBride, and D. Colombo (1994). The reflection performance of vertical walls and 'low reflection' alternatives: Results of wave flume tests. In *3rd MCS Project Workshop, MAS2-CT92-0047, Monolithic (Vertical) Coastal Structures*, pp. 22.

Ang, A. H.-S. and W. H. Tang (1975). *Probability Concepts in Engineering Planning and Design.* John Wiley & Sons.

Battjes, J. A. (1968). Refraction of water waves. *Waterways and Harbors Division Vol. 94, No. 4*, pp. 437–451.

Benoit, M. (1992). Practical comparative performance survey of methods used for estimating directional wave spectra from heave-pitch-roll data. In *Proc. 23rd International Conference on Coastal Engineering, Venice, Italy*, pp. 62–75. ASCE.

Benoit, M. (1993). Extensive comparison of directional wave analysis methods from gauge array data. In *Proc. 2nd International Symposium on Ocean Wave Measurement and Analysis*, pp. 740–754.

Benoit, M. and C. Teisson (1994). Laboratory study of breakwater reflection – effect of wave obliquity, wave steepness and mound slope. In *International Symposium on Waves – Physical and Numerical Modelling, Vancouver, Canada*, pp. 1021–1030. IAHR, CSCE.

Berkhoff, J. W. C. (1972). Computation of combined refraction–diffraction. In *Proc. 13th International Conference on Coastal Engineering, Vancouver, Canada*, pp. 471–490. ASCE.

Bird, P. A. D., M. A. Davidson, G. N. Bullock, A. J. Chadwick, P. Axe, and D. A. Huntley (1995). Wave reflection, transformation and attenuation characteristics of rock island breakwaters. In *Proc. Coastal Structures and Breakwaters, London, United Kingdom*, pp. 14. ICE.

Bird, P. A. D., M. A. Davidson, G. N. Bullock, and D. A. Huntley (1994). Wave measurement near reflective structures. In *Proc. Coastal Dynamics, Barcelona, Spain*, pp. 701–711. ASCE.

Brorsen, M. and J. Helm-Petersen (1998). On the reflection of short–crested waves in numerical models. In *Proc. 26th International Conference on Coastal Engineering, Copenhagen, Denmark*. ASCE.

Burg, J. P. (1967). Maximum entropy spectral analysis. In *Paper Presented at 37th Annual International SEG Meeting, Oklahoma City, Oklahoma*.

Capon, J. (1969). High–resolution frequency–wave–number spectrum analysis. *Proc. IEEE Vol. 57*, pp. 1408–1418.

Chadwick, A. J., D. J. Pope, J. Borges, and S. Iliç (1995). Shoreline directional wave spectra. Part 1: An investigation of spectral and directional analysis techniques. *Proc. of the Institution of Civil Engineers, Water Maritime and Energy Vol. 112, Issue 3*, pp. 198–208.

CUR (1995). *Manual on the Use of Rock in Hydraulic Engineering*. A.A. Balkema, CUR Report 169.

Davidson, M. A., P. A. D. Bird, G. N. Bullock, and D. A. Huntley (1994). Wave reflection: Field measurements, analysis and theoretical developments. In *Proc. Coastal Dynamics, Barcelona, Spain*, pp. 642–655. ASCE.

Davidson, M. A., P. A. D. Bird, G. N. Bullock, and D. A. Huntley (1996). A new non–dimensional number for the analysis of wave reflection from rubble mound breakwaters. *Coastal Engineering Vol. 28, No. 1*, pp. 93–120.

Davis, R. E. and L. A. Regier (1977). Methods for estimating directional wave spectra from multi-element arrays. *Journal of Marine Research Vol. 35, No. 3*, pp. 453–477.

Dickson, W. S., T. H. C. Herbers, and E. B. Thornton (1995). Wave reflection from breakwater. *Journal of Waterway, Port, Coastal, and Ocean Engineering Vol. 121, No. 5*, pp. 262–268.

Dingemans, M. W. (1997). *Water Wave Propagation over Uneven Bottoms.* World Scientific.

Frigaard, P., J. Helm-Petersen, G. Klopman, C. T. Stansberg, M. Benoit, M. J. Briggs, M. Miles, J. Santas, H. A. Schäffer, and P. J. Hawkes (1997). Iahr list of sea state parameters - an update for 3d waves. In *Proc. IAHR Seminar on Multidirectional Waves and their Interaction with Structures, San Francisco, California.* IAHR.

Goda, Y. (1985). *Random Seas and Design of Maritime Structures.* University of Tokyo Press.

Goda, Y. and Y. Suzuki (1976). Estimation of incident and reflected waves in random wave experiments. In *Proc. 15th International Conference on Coastal Engineering, Honolulu, Hawaii,* pp. 828–845. ASCE.

Golub, G. E. and C. F. V. Loan (1989). *Matrix Computations.* The Johns Hopkins University Press.

Hansen, E. (1969). *Variationsregning (in Danish).* Polyteknisk Forlag, Copenhagen.

Hashimoto, N. and K. Kobune (1988). Directional spectrum estimation from a Bayesian approach. In *Proc. 21st International Conference on Coastal Engineering, Malaga, Spain,* pp. 62–76. ASCE.

Hashimoto, N., K. Kobune, and Y. Kameyama (1987). Estimation of directional spectrum using the Bayesian approach, and its application to field data analysis. *Report of the Port and Harbour Research Institute, Japan, Vol. 26, No. 5,* pp. 57–100.

Hawkes, P. J., J. A. Ewing, C. M. Harford, G. Klopman, C. T. Stansberg, M. Benoit, M. J. Briggs, P. Frigaard, T. Hiraishi, J. Santas, and H. A. Schäffer (1997). Comparative analyses of multidirectional wave basin data. In *Proc. IAHR Seminar on Multidirectional Waves and their Interaction with Structures, San Francisco, California.* IAHR.

Helm-Petersen, J. (1994). Reflection from caissons in multidirectional seas. In *3rd MCS Project Workshop, MAS2-CT92-0047, Monolithic (Vertical) Coastal Structures,* pp. 37.

Helm-Petersen, J. and M. Brorsen (1997). Wave disturbance in harbours — the importance of a correct modelling of wave reflection. In *Proc. IAHR Seminar on Multidirectional Waves and their Interaction with Structures, San Francisco, California.*

Helm-Petersen, J. and P. Frigaard (1996). Reflection performance of vertical coastal structures in multidirectional seas. In *Proc. 2nd International Conference on Coasts, Ports and Marine Structures, Tehran, Iran,* pp. 221–232. Iran University of Science and Technology.

Hydraulics and Coastal Engineering Laboratory, AAU (1993). Modelforsøg Bagenkop Havn (in Danish). Technical report, Department of Civil Engineering.

Isaacson, M., D. Papps, and E. Mansard (1996). Oblique reflection characteristics of rubble–mound structures. *Journal of Waterway, Port, Coastal, and Ocean Engineering Vol. 122, No. 1*, pp. 1–7.

Isobe, M. and K. Kondo (1984). Method for estimating directional wave spectrum in incident and reflected wave field. In *Proc. 19th International Conference on Coastal Engineering, Houston, Texas*, pp. 467–483. ASCE.

Kim, T., L. Lin, and H. Wang (1993). Comparisons of directional wave analysis methods. In *Proc. 2nd International Symposium on Ocean Wave Measurement and Analysis*, pp. 554–568. ASCE.

Kirby, J. T., C. Lee, and C. Rasmussen (1992). Time-dependent solutions of the Mild-Slope wave equation. In *Proc. 23rd International Conference on Coastal Engineering, Venice, Italy*, pp. 391–404. ASCE.

Kondo, K., M. Akama, and M. Isobe (1986). Measurement of reflection coefficient of seawall in Omura Bay. In *Proc. 20th International Conference on Coastal Engineering, Taipei, Taiwan*, pp. 1987–2001. ASCE.

Larson, H. J. and B. O. Shubert (1979). *Probabilistic Models in Engineering Sciences, Vol. 1: Random Variables and Stochastic Processes*. John Wiley & Sons.

Lee, C. and K. D. Suh (1998). Internal generation of waves for time–dependent mild–slope equations. *Coastal Engineering Vol. 34*, pp. 35–57.

Madsen, P. A. (1983). Wave reflection from a vertical permeable wave absorber. *Coastal Engineering Vol. 7*, pp. 381–396.

Mansard, E. P. D. (1991). Reflection and dissipation characteristics of berm breakwaters. In *Proc. 3rd International Conference on Coastal & Port Engineering in Developing Countries, Mombasa, Kenya*, pp. pp. 482–496.

Mansard, E. P. D. and E. R. Funke (1980). The measurement of incident and reflected spectra using a least square method. In *Proc. 17th International Conference on Coastal Engineering, Sydney, Australia*, pp. 154–172. ASCE.

MAST (1994). *Proceedings of the 3rd MCS Project Workshop, MAS2-CT92-0047, Monolithic (Vertical) Coastal Structures*. Marine Science and Technology.

Mitsuyasu, H., F. Tasai, T. Sabara, S. Mizuno, M. Okusu, T. Honda, and K. Rikiishi (1975). Observation of the directional spectrum of ocean waves using a clover-leaf buoy. *Journal of Physical Oceanography, Vol. 5*, pp. 750–760.

Newland, D. E. (1993). *Random Vibrations, Spectral & Wavelet Analysis, 3rd edition.* Longman.

Ohshimo, T., K. Kondo, and T. Sekimoto (1988). Observation of directional wave spectra and reflection of breakwater in a harbor. In *Proc. 21st International Conference on Coastal Engineering, Malaga, Spain*, pp. 47–61. ASCE.

Postma, G. M. (1989). *Wave Reflection from Rock Slopes under Random Wave Attack.* Unpublished M.Sc. Thesis, Delft University of Technology.

Seelig, W. N. (1983). Wave reflection from coastal structures. In *Proc. Coastal Structures '83, Arlington, Virginia*, pp. 961–973. ASCE.

Suh, K. D., C. Lee, and W. S. Park (1997). Time-dependent equations for wave propagation on rapidly varying topography. *Coastal Engineering Vol. 32*, pp. 91–117.

Suh, K. D. and W. S. Park (1995). Wave reflection from perforated–wall caisson breakwater. *Coastal Engineering Vol. 26, No. 1*, pp. 177–193.

Teisson, C. and M. Benoit (1994). Laboratory measurement of oblique irregular wave reflection on rubble-mound breakwaters. In *Proc. 24th International Conference On Coastal Engineering, Kobe, Japan*, pp. 1610–1624. ASCE.

Tong, Y. L. (1990). *The Multivariate Normal Distribution.* Springer–Verlag.

van der Meer, J. W. (1988). *Rock Slopes and Gravel Beaches under Wave Attack.* Doctoral Thesis, Delft University of Technology; also Delft Hydraulics Communication No. 396.

Yokoki, H., M. Isobe, and A. Watanabe (1992). A method for estimating reflection coefficient in short–crested random seas. In *Proc. 17th International Conference on Coastal Engineering, Venice, Italy*, pp. 765–776. ASCE.

Yourgran, W. and S. Mandelstam (1979). *Variational Principles in Dynamics and Quantum Theory.* Dover Publications, New York.

Zelt, J. A. and J. E. Skjelbreia (1992). Estimating incident and reflected wave fields using an arbitrary number of wave gauges. In *Proc. 23rd International Conference on Coastal Engineering, Venice, Italy*, pp. 777–789. ASCE.

A

Literature Survey on Wave Reflection

Wave data are referring to incident waves. s is denoting wave steepness.

A.1 Vertical Face Structures

Plain Structures

Source:	Helm-Petersen (1994)
Data:	Laboratory
Structure:	Plain vertical caissons
Wave data:	$H_s = 0.14m$; $T_p = 1.5s$; $s = 0.04$
	$\theta_m \in [0°; 40°]$
	$\sigma_\theta : 0°, 15°,$ and $30°$
Reflection:	$C_R = 0.95$; $\sigma_{C_R} = 0.02$
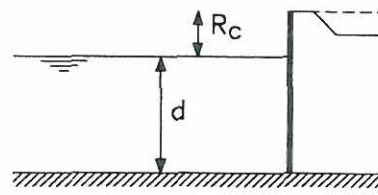
Source:	Kondo, Akama, and Isobe (1986)
Data:	Field measurements
Structure:	Vertical sheet-pile wall
Wave data:	H_s =N/A; $f_p \in [0.34Hz; 0.44Hz]$
	$\theta_m \in [-20°; 30°]$; σ_θ : N/A
Reflection:	$C_R = 0.92$; $\sigma_{C_R} \simeq 0.08$
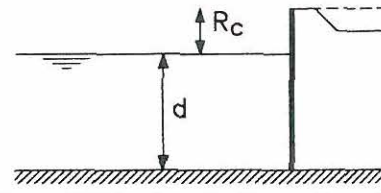
Source:	Ohshimo, Kondo, and Sekimoto (1988)
Data:	Field measurements
Structure:	Composite type, (caisson on berm)
Wave data:	$H_s \in [1.0m; \sim 3.0m]$; $T_p \in [6s; 8s]$
	$\theta_m = \sim 0°$; σ_θ : N/A
Reflection:	$C_R = 0.86$; $\sigma_{C_R} \simeq 0.08$
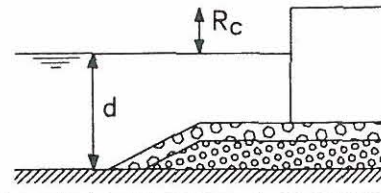
Source:	Allsop, McBride, and Colombo (1994)
Data:	Laboratory
Structure:	Plain vertical wall (caisson)
Wave data:	$H_s \in [0.1m; 0.3m]$; T_p =N/A; $\theta_m = 0°$; $\sigma_\theta = 0°$
	$R_c/H_s \in [0.4; 3.7]$; s_m : 0.02, 0.04, 0.06
Reflection:	$C_R \in [0.85; 0.90]$; σ_{C_R} =N/A
	$C_R = 0.79 + 0.11\frac{R_c}{H_s}$, $R_c/H_s < 1.0$ else $C_R = 0.90$
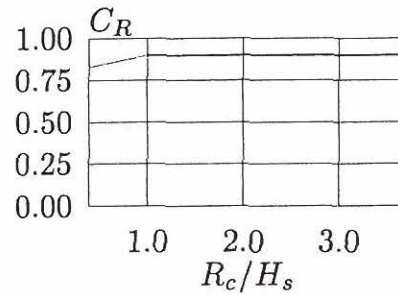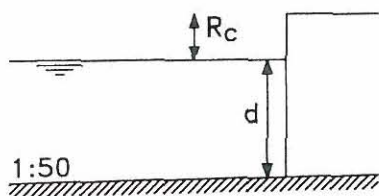
Porous Structures

Source:	Helm-Petersen (1994)
Data:	Laboratory
Structure:	Perforated vertical caissons
Wave data:	$H_s = 0.14m$; $T_p = 1.5s$; $s = 0.04$
	$\theta_m \in [0°; 60°]$
	$\sigma_\theta : 0°, 15°,$ and $30°$
Reflection:	$C_R \in [0.3; 0.55]$

Source:	Allsop, McBride, and Colombo (1994)
Data:	Laboratory
Structure:	Wave screen/perforated caisson, porosity=20%
Wave data:	$H_s \in [0.1m; 0.3m]$; $T_p =$N/A; $\theta_m = 0°$; $\sigma_\theta = 0°$
	$B_w/L_s \in [0.07; 0.33]$
Reflection:	$C_R = \sin\left(k_c(B_w/L_s - k_x)^2\right) + k_y$
	Single screen:
	$k_c = 15.9, k_x = 0.23, k_y = 0.280$ $(d_h = t_s)$
	$k_c = 13.6, k_x = 0.22, k_y = 0.315$ $(d_h = 2t_s)$
	Double screen:
	$k_c = 13.1, k_x = 0.25, k_y = 0.265$ $(d_h = t_s)$
	$k_c = 13.1, k_x = 0.25, k_y = 0.275$ $(d_h = 2t_s)$
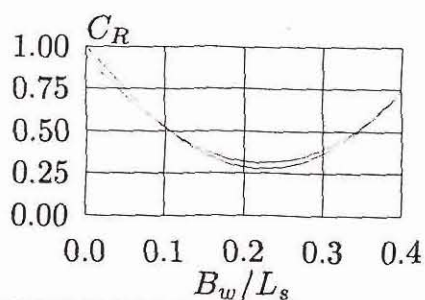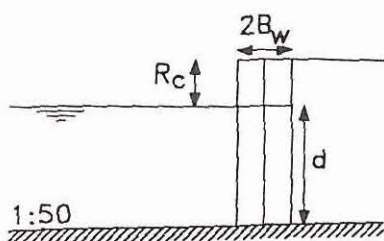
Source: Helm-Petersen and Frigaard (1996)
Data: Laboratory
Structure: Vertical porous structures
Wave data: $H_s = 0.04m$ or $0.06m$
              $T_p \in [0.9s; 1.3s], \quad s \in [0.02; 0.05]$
              $\theta_m \in [0°; 30°]; \quad \sigma_\theta : 25°$
Reflection: $C_R \in [0.6; 0.8]$

A.2   Sloping Structures

For sloping structures the following expression, Seelig (1983), has often been used to fit measured data.

$$C_R = \frac{a\xi^2}{\xi^2 + b} \tag{A.1}$$

Smooth Slopes

Source: Seelig (1983)
Data:
Structure: Smooth slope
Wave data: 2D case
Reflection: Eqn. (A.1) with $a = 1.0$, $b = 5.5$
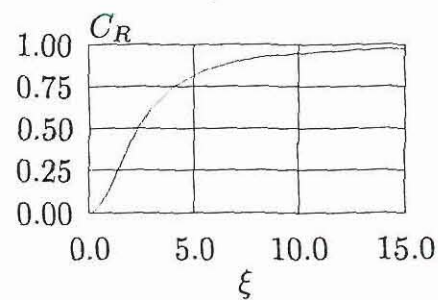
Rubble Mounds

Source: Seelig (1983)
Data:
Structure: Rubble mound (dolos or rock)
Wave data: 2D case
Reflection: Eqn. (A.1) with $a = 0.6$, $b = 6.6$
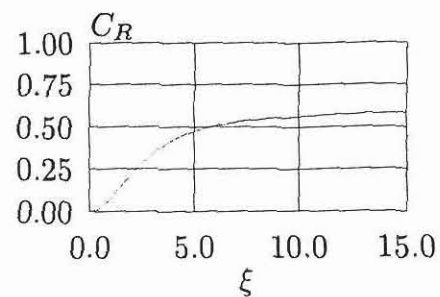
Source:	Benoit and Teisson (1994)
Data:	Laboratory
Structure:	Rubble mound (3:4, 2:3, 1:2)
Wave data:	$H_s \in [0.03m; 0.09m]; \quad T_p = 1.3s$
	$\theta_m \in [0°; 60°]; \quad \sigma_\theta : 0°$
	$d = 0.4m$
Reflection:	For normal incidence the results by Seelig (1983) applies.
	For oblique incidence the reflection is lowest for 15° off the normal and maximum for 45° off the normal.
	Results presented in graphs.

Source:	Davidson et al. (1994)
Data:	Field measurements
Structure:	Rock island breakwater, slope 1:1.1
Wave data:	$H_s > 0.05m$
Reflection:	Eqn. (A.1) with
	$a = 0.65, \; b = 25$ for $d_t > 3.25m$
	$a = 0.60, \; b = 35$ for $2.5m < d_t < 3.25m$
	$a = 0.64, \; b = 80$ for $d_t < 2.5m$
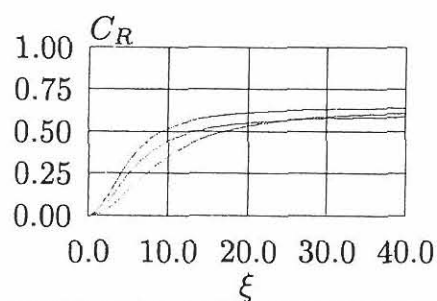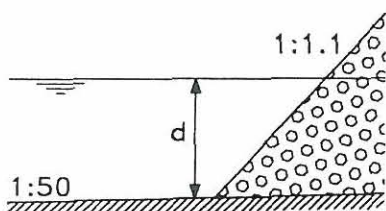
Source: Allsop (1990)

Data: Laboratory

Structure: Armoured slope

Wave data: 2D case; $s_m \in [0.0043; 0.52]$

Reflection: Eqn. (A.1), $\xi_m = \dfrac{\tan(\alpha)}{\sqrt{H_s/(\frac{gT_m^2}{2\pi})}}$

Rock armour:

$a = 0.64,\ b = 8.9$ (two layer)

$a = 0.64,\ b = 7.2$ (one layer)

Large rock:

$a = 0.64,\ b = 9.6$ (two layer)

$a = 0.67,\ b = 7.9$ (one layer)
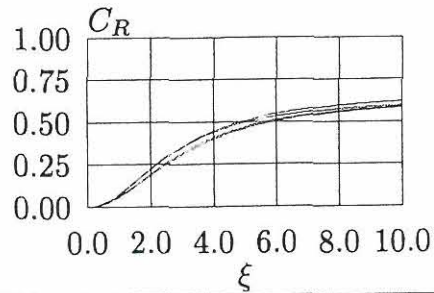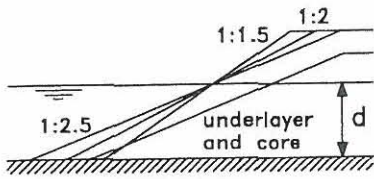
Source: Mansard (1991)

Data: Laboratory

Structure: Berm breakwater, five types

Wave data: 2D case

$s \in [0.006; 0.075]$

Reflection: Given in terms of graphs

Strong   dependence   of   wave steepness
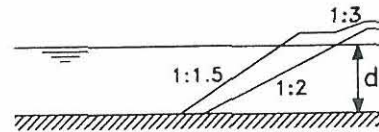
B

The MLM Method

Incident and reflected wave components are defined as

$$\eta_I = \eta_I(\boldsymbol{x}, t) = \sum\sum a_{ij}\cos(\boldsymbol{k}_{ij,I}\boldsymbol{x} - \omega_{ij}t + \Phi_{ij,I}) \tag{B.1}$$

$$\eta_R = \eta_R(\boldsymbol{x}, t) = \sum\sum C_R a_{ij}\cos(\boldsymbol{k}_{ij,R}\boldsymbol{x} - \omega_{ij}t + \Phi_{ij,R}) \tag{B.2}$$

where

$$\boldsymbol{k}_{ij,I} = k\left\{\begin{array}{c} \cos\theta_{ij} \\ \sin\theta_{ij} \end{array}\right\} \tag{B.3}$$

$$\boldsymbol{k}_{ij,R} = k\left\{\begin{array}{c} \cos\theta_{ij} \\ -\sin\theta_{ij} \end{array}\right\} \tag{B.4}$$

Further

$$\Phi_{ij,I} = \Phi_{ij,R} = \Phi_{ij}, \text{ since } \Delta_{ij} = 2y\sin\theta_{ij} \tag{B.5}$$

where Δ_{ij} is the phase difference between the incident and reflected wave component.

Thus

$$\eta = \eta_I + \eta_R \tag{B.6}$$

$$= \sum\sum (a_{ij}\cos(\boldsymbol{k}_{ij,I}\boldsymbol{x} - \omega_{ij}t + \Phi_{ij})$$

$$+ C_R a_{ij}\cos(\boldsymbol{k}_{ij,R}\boldsymbol{x} - \omega_{ij}t + \Phi_{ij})) \tag{B.7}$$

The cross-correlation function between $\eta_m(t)$ and $\eta_n(t)$ is defined as

$$R_{xy}(\tau) \quad = \quad E[\eta_m(t)\eta_n(t+\tau)] \tag{B.8}$$

Further the cross-spectral density function is defined as the Fourier transform of the cross-correlation function, i.e.

$$S_{\eta_m\eta_n}(\omega) \quad = \quad \int_{-\infty}^{\infty} \exp(-i\omega\tau)E[\eta_m(t)\eta_n(t+\tau)]d\tau \tag{B.9}$$

$$E[\eta_m(t)\eta_n(t+\tau)] = \tag{B.10}$$

$$E\left[\sum_j\sum_i (a_{ij}\cos(k_{ij,I}x_m - \omega_{ij}t + \Phi_{ij}) + C_Ra_{ij}\cos(k_{ij,R}x_m - \omega_{ij}t + \Phi_{ij}))\right.$$

$$\left.\sum_j\sum_i (a_{ij}\cos(k_{ij,I}x_n - \omega_{ij}(t+\tau) + \Phi_{ij}) + C_Ra_{ij}\cos(k_{ij,R}x_n - \omega_{ij}(t+\tau) + \Phi_{ij}))\right]$$

$$= \sum_{j_2}\sum_{i_2}\sum_{j_1}\sum_{i_1}\{ \tag{B.11}$$

$$E[a_{i_1j_1}a_{i_2j_2}\cos(k_{i_1j_1,I}x_m - \omega_{i_1j_1}t + \Phi_{i_1j_1})\cos(k_{i_2j_2,I}x_n - \omega_{i_2j_2}(t+\tau) + \Phi_{i_2j_2})] +$$

$$E[C_Ra_{i_1j_1}a_{i_2j_2}\cos(k_{i_1j_1,I}x_m - \omega_{i_1j_1}t + \Phi_{i_1j_1})\cos(k_{i_2j_2,R}x_n - \omega_{i_2j_2}(t+\tau) + \Phi_{i_2j_2})] +$$

$$E[C_Ra_{i_1j_1}a_{i_2j_2}\cos(k_{i_1j_1,R}x_m - \omega_{i_1j_1}t + \Phi_{i_1j_1})\cos(k_{i_2j_2,I}x_n - \omega_{i_2j_2}(t+\tau) + \Phi_{i_2j_2})] +$$

$$E[C_r^2a_{i_1j_1}a_{i_2j_2}\cos(k_{i_1j_1,R}x_m - \omega_{i_1j_1}t + \Phi_{i_1j_1})\cos(k_{i_2j_2,R}x_n - \omega_{i_2j_2}(t+\tau) + \Phi_{i_2j_2})]\}$$

Terms where $i_1 \neq i_2$ or $j_1 \neq j_2$ will cancel out because of independency. Thus

$$E[\eta_m(t)\eta_n(t+\tau)] = \sum_j\sum_i E[a_{ij}^2]\{ \tag{B.12}$$

$$E[\cos(k_{ij,I}x_m - \omega_{ij}t + \Phi_{ij})\cos(k_{ij,I}x_n - \omega_{ij}(t+\tau) + \Phi_{ij})] +$$

$$C_RE[\cos(k_{ij,I}x_m - \omega_{ij}t + \Phi_{ij})\cos(k_{ij,R}x_n - \omega_{ij}(t+\tau) + \Phi_{ij})] +$$

$$C_RE[\cos(k_{ij,R}x_m - \omega_{ij}t + \Phi_{ij})\cos(k_{ij,I}x_n - \omega_{ij}(t+\tau) + \Phi_{ij})] +$$

$$C_r^2E[\cos(k_{ij,R}x_m - \omega_{ij}t + \Phi_{ij})\cos(k_{ij,R}x_n - \omega_{ij}(t+\tau) + \Phi_{ij})]\}$$

Using $\cos u \cos v = (\cos(u+v) + \cos(u-v))/2$ leads to

$$E[\eta_m(t)\eta_n(t+\tau)] = \sum_j\sum_i \frac{1}{2}E[a_{ij}^2]\{ \tag{B.13}$$

$$\overbrace{E[\cos(k_{ij,I}x_m + k_{ij,I}x_n - \omega_{ij}(2t+\tau) + 2\Phi_{ij})]}^{=\,0} +$$

$$E[\cos(k_{ij,I}x_m - k_{ij,I}x_n + \omega_{ij}\tau)] +$$

$$C_R\overbrace{E[\cos(k_{ij,I}x_m + k_{ij,R}x_n - \omega_{ij}(2t+\tau) + 2\Phi_{ij})]}^{=\,0} +$$

$$C_R E[\cos(\boldsymbol{k}_{ij,I}\boldsymbol{x}_m - \boldsymbol{k}_{ij,R}\boldsymbol{x}_n + \omega_{ij}\tau)] +$$

$$\overbrace{C_R\ E[\cos(\boldsymbol{k}_{ij,R}\boldsymbol{x}_m + \boldsymbol{k}_{ij,I}\boldsymbol{x}_n - \omega_{ij}(2t+\tau) + 2\Phi_{ij})]}^{=\ 0} +$$

$$C_R E[\cos(\boldsymbol{k}_{ij,R}\boldsymbol{x}_m - \boldsymbol{k}_{ij,I}\boldsymbol{x}_n + \omega_{ij}\tau)] +$$

$$\overbrace{C_R^2\ E[\cos(\boldsymbol{k}_{ij,R}\boldsymbol{x}_m + \boldsymbol{k}_{ij,R}\boldsymbol{x}_n - \omega_{ij}(2t+\tau) + 2\Phi_{ij})]}^{=\ 0} +$$

$$C_R^2 E[\cos(\boldsymbol{k}_{ij,R}\boldsymbol{x}_m - \boldsymbol{k}_{ij,R}\boldsymbol{x}_n + \omega_{ij}\tau)]\}$$

$$= \ \sum_j \sum_i \frac{1}{2} E[a_{ij}^2]\{ \tag{B.14}$$

$$E[\cos(\overbrace{\boldsymbol{k}_{ij,I}\boldsymbol{x}_m - \boldsymbol{k}_{ij,I}\boldsymbol{x}_n + \omega_{ij}\tau}^{=\ u_1})] + C_R E[\cos(\overbrace{\boldsymbol{k}_{ij,I}\boldsymbol{x}_m - \boldsymbol{k}_{ij,R}\boldsymbol{x}_n + \omega_{ij}\tau}^{=\ u_2})] +$$

$$C_R E[\cos(\overbrace{\boldsymbol{k}_{ij,R}\boldsymbol{x}_m - \boldsymbol{k}_{ij,I}\boldsymbol{x}_n + \omega_{ij}\tau}^{=\ u_3})] + C_R^2 E[\cos(\overbrace{\boldsymbol{k}_{ij,R}\boldsymbol{x}_m - \boldsymbol{k}_{ij,R}\boldsymbol{x}_n + \omega_{ij}\tau}^{=\ u_4})]\}$$

Use $\cos u = (\exp(iu) + \exp(-iu))/2$. Then inserting into (9) yields

$$S_{\eta_m \eta_n}(\omega) = \int_{-\infty}^{\infty} \exp(-i\omega\tau) \sum_j \sum_i \frac{1}{2} E[a_{ij}^2] \frac{1}{2}\{ \tag{B.15}$$

$$(\exp(iu_1) + \exp(-iu_1)) + C_R(\exp(iu_2) + \exp(-iu_2))$$

$$C_R(\exp(iu_3) + \exp(-iu_3)) + C_r^2(\exp(iu_4) + \exp(-iu_4))\}d\tau$$

Set $v_n = u_n - \omega_{ij}\tau$. Then

$$S_{\eta_m \eta_n}(\omega) = \sum_j \sum_i \frac{1}{2} E[a_{ij}^2] \frac{1}{2}\{ \tag{B.16}$$

$$\exp(iv_1) \int_{-\infty}^{\infty} \exp(-i(\omega - \omega_{ij})\tau)d\tau + \exp(-iv_1) \int_{-\infty}^{\infty} \exp(-i(\omega + \omega_{ij})\tau)d\tau$$

$$C_R \exp(iv_2) \int_{-\infty}^{\infty} \exp(-i(\omega - \omega_{ij})\tau)d\tau + \exp(-iv_2) \int_{-\infty}^{\infty} \exp(-i(\omega + \omega_{ij})\tau)d\tau$$

$$C_R \exp(iv_3) \int_{-\infty}^{\infty} \exp(-i(\omega - \omega_{ij})\tau)d\tau + \exp(-iv_3) \int_{-\infty}^{\infty} \exp(-i(\omega + \omega_{ij})\tau)d\tau$$

$$C_r^2 \exp(iv_4) \int_{-\infty}^{\infty} \exp(-i(\omega - \omega_{ij})\tau)d\tau + \exp(-iv_4) \int_{-\infty}^{\infty} \exp(-i(\omega + \omega_{ij})\tau)d\tau\}$$

Applying

$$2\pi\sigma_{ij}^2 \ = \ 2\pi E[a_{ij}^2] \ = \ S_\eta(\omega_{ij}, \theta_{ij})\Delta\omega_{ij}\Delta\theta_{ij} \tag{B.17}$$

and

$$\frac{1}{2\pi} \int_{-\infty}^{\infty} \exp(-i\omega\tau)d\tau \ = \ \delta(\omega) \tag{B.18}$$

$$S_{\eta_m \eta_n}(\omega) = \sum_j \sum_i S_\eta(\omega_{ij}, \theta_{ij}) \Delta\omega_{ij} \Delta\theta_{ij} \{$$

$$\left[\exp(iv_1) + C_R \exp(iv_2) + C_R \exp(iv_3) + C_r^2 \exp(iv_4)\right] \delta(\omega - \omega_{ij}) +$$

$$\left[\exp(-iv_1) + C_R \exp(-iv_2) + C_R \exp(-iv_3) + C_R^2 \exp(-iv_4)\right]$$

$$\delta(\omega + \omega_{ij})\} \tag{B.19}$$

When ω is assumed positive (one-sided spectra) $\delta(\omega + \omega_{ij})$ will always be zero, except for $\omega = \omega_{ij} = 0$ in which case $S_\eta(\omega, \theta) = 0$. Hence

$$S_{\eta_m \eta_n}(\omega) = \int_0^{2\pi} \int_{-\infty}^{\infty} S_\eta(\omega', \theta)\{ \tag{B.20}$$

$$\left[\exp(iv_1) + C_R \exp(iv_2) + C_R \exp(iv_3) + C_R^2 \exp(iv_4)\right]\delta(\omega - \omega')\}d\omega' d\theta$$

And finally

$$S_{\eta_m \eta_n}(\omega) = \int_0^{2\pi} S_\eta(\omega, \theta)\{\exp(iv_1) + C_R \exp(iv_2) + C_R \exp(iv_3)$$

$$+ C_R^2 \exp(iv_4)\} d\theta \tag{B.21}$$

where

$$v_1 = \boldsymbol{k}_{ij,I}\boldsymbol{x}_m - \boldsymbol{k}_{ij,I}\boldsymbol{x}_n = k(x_m - x_n)\cos\theta + k(y_m - y_n)\sin\theta$$

$$v_2 = \boldsymbol{k}_{ij,I}\boldsymbol{x}_m - \boldsymbol{k}_{ij,R}\boldsymbol{x}_n = k(x_m - x_n)\cos\theta + k(y_m + y_n)\sin\theta$$

$$v_3 = \boldsymbol{k}_{ij,R}\boldsymbol{x}_m - \boldsymbol{k}_{ij,I}\boldsymbol{x}_n = k(x_m - x_n)\cos\theta + k(-y_m - y_n)\sin\theta$$

$$v_4 = \boldsymbol{k}_{ij,R}\boldsymbol{x}_m - \boldsymbol{k}_{ij,R}\boldsymbol{x}_n = k(x_m - x_n)\cos\theta + k(-y_m + y_n)\sin\theta$$

The BDM Method

The prior probability distribution function given in (2.24) can be shown to correspond to a multivariate Gaussian distribution. The distribution may be rewritten as shown below.

$$p(x|u,\sigma^2) \;=\; \left(\frac{u}{\sqrt{2\pi}\sigma}\right)^K \exp\left(-\frac{u^2}{2\sigma^2}\sum_{k=1}^{K}(x_{k-1}-2x_k+x_{k+1})^2\right) \quad \text{(C.1)}$$

$$=\; \left(\frac{u}{\sqrt{2\pi}\sigma}\right)^K \exp\left(-\frac{u^2}{2\sigma^2}|Dx|^2\right) \quad \text{(C.2)}$$

$$=\; \left(\frac{u}{\sqrt{2\pi}\sigma}\right)^K \exp\left(-\frac{u^2}{2\sigma^2}x^T M x\right) \quad \text{(C.3)}$$

where

$$D \;=\; \begin{bmatrix} -2 & 1 & 0 & \cdots & 0 & 1 \\ 1 & -2 & 1 & \cdots & 0 & 0 \\ 0 & 1 & -2 & \cdots & 0 & 0 \\ \vdots & \vdots & \vdots & \ddots & \vdots & \vdots \\ 0 & 0 & 0 & \cdots & -2 & 1 \\ 1 & 0 & 0 & \cdots & 1 & -2 \end{bmatrix} \quad \text{(C.4)}$$

$$M \;=\; D^T D \quad \text{(C.5)}$$

In case the inverse of M does exist, it corresponds to the covariance matrix and the distribution is said to be a nonsingular multivariate Gaussian distribution.

If, however, M is singular but positive semidefinite, the distribution is said to be a **singular multivariate Gaussian distribution**. Since $\det(M)$ is 0, the matrix is singular, and the covariance matrix can not be calculated directly. The distribution is still valid though, as the rank of D is less than its dimension (any row is a linear combination of all remaining rows). See e.g. Tong (1990) or Larson and Shubert (1979) for a more detailed mathematical description.

The parameter u is a so–called hyperparameter (or a nuisance parameter) and provides the option of regulating the standard deviation, σ/u. Physically this is better understood by considering the distribution as a smoothing criteria, as mentioned in section 2.5. Changing u to a lower value increases the standard deviation, which for a given vector x yields a higher probability. If instead the probability is considered fixed, then the sum in (C.1) must be larger, which can only be established for a less smooth distribution. Hence decreasing u relaxes the smoothness criteria.

The Householder Method

The problem of optimizing (2.35) may be solved by using the Householder Method. The method is described in the following.

$$
J(x) = |\tilde{A}x - \tilde{B}|^2 + u^2|Dx|^2 \tag{C.6}
$$

$$
= \left| \left\{ \begin{array}{c} \tilde{A} \\ u^2 D \end{array} \right\} x - \left\{ \begin{array}{c} \tilde{B} \\ O_M \end{array} \right\} \right|^2 \tag{C.7}
$$

The system of equations is overdetermined and may be solved in a least squares sense.

How to obtain obtain (C.6) is described in Hashimoto and Kobune (1988) and will not be presented here.

As (C.6) is invariant under orthogonal transformation it can be written as

$$
J(x) = \left| Q^T \left\{ \begin{array}{c} \tilde{A} \\ u^2 D \end{array} \right\} x - Q^T \left\{ \begin{array}{c} \tilde{B} \\ O_M \end{array} \right\} \right|^2 \tag{C.8}
$$

$$
= \left| Q^T \left\{ \begin{array}{cc} \tilde{A} & \tilde{B} \\ u^2 D & O_M \end{array} \right\} \left\{ \begin{array}{c} x \\ -1 \end{array} \right\} \right|^2 \tag{C.9}
$$

where Q is an orthogonal matrix having the dimension $(M + K) \times (M + K)$.

Thus if $Z = \left\{ \begin{array}{cc} \tilde{A} & \tilde{B} \\ u^2 D & O_M \end{array} \right\}$ and $Q^T Z$ is transformed to an upper triangular

matrix, say

$$Q^T Z = \begin{bmatrix} S_{1,1} & \cdots & & S_{1,K} & S_{1,K+1} \\ 0 & \ddots & & \vdots & \vdots \\ \vdots & & \ddots & S_{K,K} & \vdots \\ 0 & & \cdots & 0 & S_{K+1,K+1} \\ & O_{(M-1)\times(K+1)} & & & \end{bmatrix} \qquad (C.10)$$

then (C.8) reduces to

$$J(x) = \left| \begin{bmatrix} S_{1,1} & \cdots & S_{1,K} \\ & \ddots & \vdots \\ O & & S_{K,K} \end{bmatrix} x - \left\{ \begin{matrix} S_{1,K+1} \\ \vdots \\ S_{K+1,K+1} \end{matrix} \right\} \right|^2 \qquad (C.11)$$

$$= \left| \begin{bmatrix} S_{1,1} & \cdots & S_{1,K} \\ & \ddots & \vdots \\ O & & S_{K,K} \end{bmatrix} x - \left\{ \begin{matrix} S_{1,K+1} \\ \vdots \\ S_{K,K+1} \end{matrix} \right\} \right|^2 + S^2_{K+1,K+1} \qquad (C.12)$$

which can be solved by backsubstitution. The matrix Z has the dimensions $(M + K) \times (K + 1)$.

Q^T may be obtained by use of the Householder transformation method. However, only the matrix $Q^T Z$ is needed within this application.

D

Field Measurements

The following set of tables show some basic parameters calculated for the recorded time series. Depths are average values at the deepest and highest positioned gauges. Tide is the average linear trend in the time series. Estimates of H_{m_0} (significant wave height based on m_0, T_z (mean period between zero crossing), T_c (mean period between crests), and ε (spectral width parameter) are based on spectral analysis, assuming

$$H_{m_0} = 4\sqrt{m_0} \tag{D.1}$$

$$T_z = \sqrt{m_0/m_2} \tag{D.2}$$

$$T_c = \sqrt{m_2/m_4} \tag{D.3}$$

$$\varepsilon = \sqrt{1 - \frac{m_2^2}{m_0 m_4}} \tag{D.4}$$

where m_n is the n-th spectral moment.

Hereafter follows a crude graphical presentation of the energy spectra averaged for each recording. This is only to give some qualitative idea of the measured waves in the frequency domain.

The last set of tables show the main results from the directional analysis.

Recording	Depths		Tide	H_{m_0}	T_z	T_c	ε
	m	m	m	m	s	s	
deo4r0.c17	15.53	17.16	−0.06	0.63	4.2	2.5	0.65
deo4r0.c18	13.88	15.50	−0.09	0.64	4.4	2.6	0.65
deo4r0.c19	13.06	14.69	0.02	0.53	3.6	2.6	0.47
deo4r0.c20	14.67	16.28	0.13	0.61	3.8	2.6	0.55
deo4r0.c21	15.65	17.27	−0.04	0.86	5.2	2.7	0.73
deo4r0.c22	14.13	15.75	−0.10	1.02	5.1	3.0	0.66
deo4r0.c23	13.11	14.74	0.01	0.77	4.2	2.9	0.51
deo4r0.c24	14.64	16.25	0.14	0.87	4.4	2.9	0.57
deo4r0.c25	15.69	17.31	−0.03	1.05	5.4	2.9	0.72
deo4r0.c26	14.05	15.67	−0.09	1.29	5.9	3.2	0.71
deo4r0.c27	12.86	14.48	0.01	0.94	4.5	3.2	0.50
deo4r0.c28	14.49	16.11	0.11	0.81	4.4	2.9	0.58
deo4r0.c29	16.10	17.73	0.01	0.68	4.1	2.6	0.59
deo4r1.c21	17.29	18.90	0.05	0.86	4.1	2.5	0.63
deo4r1.c22	15.05	16.68	−0.25	0.59	3.3	2.5	0.42
deo4r1.c23	11.90	13.53	−0.08	0.47	3.2	2.5	0.40
deo4r1.c24	13.77	15.38	0.30	0.63	3.6	2.5	0.51
deo4r1.c25	17.32	18.93	0.02	1.11	4.7	2.7	0.67
deo4r1.c26	15.13	16.75	−0.25	0.73	3.8	2.5	0.56
deo4r1.c27	11.88	13.50	−0.08	0.52	3.5	2.5	0.50
deo4r1.c28	13.89	15.50	0.34	0.74	3.9	2.6	0.57
deo4r1.c29	17.68	19.29	0.05	1.49	5.7	2.8	0.75
deo4r1.c30	15.36	16.98	−0.24	1.56	6.5	2.8	0.81
deo4r1.c31	11.81	13.43	−0.08	0.89	5.0	2.7	0.70
deo4r2.c00	13.66	15.28	0.30	1.29	4.9	3.0	0.62
deo4r2.c01	17.45	19.06	0.05	2.35	5.5	3.2	0.67
deo4r2.c02	15.18	16.80	−0.27	1.25	4.9	2.9	0.65
deo4r2.c03	11.76	13.38	−0.07	0.81	4.7	2.6	0.69
deo4r2.c04	13.83	15.45	0.33	1.04	4.6	2.7	0.64
deo4r2.c05	17.90	19.51	0.05	2.77	5.5	3.5	0.60
deo4r2.c06	15.45	17.07	−0.28	2.23	5.4	3.2	0.64
deo4r2.c07	11.80	13.42	−0.09	1.20	5.3	3.0	0.69
deo4r2.c08	13.64	15.25	0.34	1.56	5.1	3.1	0.63
deo4r2.c09	17.53	19.14	0.03	2.67	5.8	3.4	0.66
deo4r2.c10	15.30	16.92	−0.29	1.82	5.4	3.2	0.65

Recording	Depths		Tide	H_{m_0}	T_z	T_c	ε
	m	m	m	m	s	s	
deo4r2.c11	11.90	13.52	−0.09	1.28	5.8	3.2	0.70
deo4r2.c12	13.81	15.42	0.30	1.39	5.1	3.2	0.62
deo4r2.c13	17.58	19.20	0.06	3.04	6.1	3.6	0.65
deo4r2.c14	15.33	16.95	−0.24	1.33	5.5	3.1	0.68
deo4r2.c15	11.98	13.60	−0.11	1.01	5.8	3.1	0.72
deo4r2.c16	13.91	15.52	0.25	1.55	5.3	3.3	0.62
deo4r2.c17	17.44	19.04	0.11	5.07	5.8	3.7	0.58
deo4r2.c18	15.23	16.84	−0.22	2.93	5.5	3.4	0.62
deo4r2.c19	12.08	13.65	−0.09	1.82	5.7	3.2	0.68
deo4r2.c20	13.98	15.54	0.27	2.07	5.4	3.3	0.63
deo4r2.c21	17.43	19.00	0.03	3.91	6.8	3.4	0.75
deo4r2.c22	15.23	16.81	−0.22	1.67	5.5	3.0	0.69
deo4r2.c23	11.98	13.56	−0.06	1.06	5.8	2.7	0.78
deo4r2.c24	13.76	15.34	0.24	1.36	5.6	3.1	0.70
deo4r2.c25	17.29	18.87	0.04	2.45	6.8	3.4	0.75
deo4r2.c26	15.51	17.09	−0.22	1.25	5.3	3.1	0.64
deo4r2.c27	12.71	14.31	−0.09	1.07	5.4	2.8	0.73
deo4r2.c28	14.33	15.91	0.23	1.62	5.5	3.2	0.67
deo4r2.c29	17.34	18.93	0.01	2.99	5.7	3.3	0.68
deo4r2.c30	15.22	16.83	−0.22	1.86	5.7	3.1	0.69
deo4r2.c31	12.38	14.00	−0.08	1.64	5.8	3.1	0.72
deo4r3.c00	14.03	15.65	0.13	2.11	5.7	3.1	0.70
deo4r3.c01	16.96	18.60	0.00	3.20	6.1	3.5	0.67
deo4r3.c02	15.24	16.89	−0.19	2.08	6.6	3.4	0.73
deo4r3.c03	13.13	14.79	−0.04	1.39	6.0	3.0	0.75
deo4r3.c04	14.89	16.55	0.21	2.09	6.1	3.2	0.72
deo4r3.c05	17.22	18.88	0.03	4.76	6.0	3.5	0.66
deo4r3.c06	15.31	17.01	−0.19	2.29	6.0	3.3	0.71
deo4r3.c07	12.77	14.47	0.01	1.61	6.1	3.0	0.75
deo4r3.c08	14.19	15.89	0.20	1.62	5.5	3.1	0.70
deo4r3.c09	16.53	18.22	0.00	2.71	6.2	3.4	0.69
deo4r3.c10	15.11	16.81	−0.14	1.97	6.3	3.1	0.75
deo4r3.c11	13.27	14.97	−0.03	1.09	5.2	2.9	0.69
deo4r3.c12	14.47	16.17	0.18	1.30	5.5	2.9	0.73
deo4r3.c13	16.58	18.27	0.03	1.67	6.3	2.9	0.79

Recording	Depths		Tide	H_{m_0}	T_z	T_c	ε
	m	m	m	m	s	s	
deo4r3.c14	15.16	16.86	−0.16	0.98	5.4	2.7	0.76
deo4r3.c15	13.18	14.89	−0.04	0.84	5.5	2.6	0.78
deo4r3.c16	14.10	15.80	0.16	0.91	4.7	2.6	0.70
deo4r3.c17	16.04	17.74	−0.01	1.38	5.9	2.9	0.76
deo4r3.c18	14.89	16.59	−0.09	1.11	5.7	2.8	0.76
deo4r3.c19	13.49	15.19	0.02	0.71	4.2	2.5	0.66
deo4r3.c20	14.43	16.12	0.12	1.00	4.9	2.8	0.69
deo4r3.c21	16.12	17.81	0.02	2.06	5.3	3.3	0.62
deo4r3.c22	14.94	16.64	−0.12	1.43	5.0	3.1	0.63
deo4r3.c23	13.34	15.04	−0.03	1.16	5.3	3.1	0.67
deo4r3.c24	14.15	15.85	0.13	1.31	5.2	3.0	0.66
deo4r3.c25	15.87	17.57	0.04	2.03	5.2	3.3	0.61
deo4r3.c26	15.10	16.80	−0.10	1.36	5.0	3.1	0.61
deo4r3.c27	13.77	15.46	−0.05	1.12	5.2	2.9	0.69
deo4r3.c28	14.22	15.91	0.10	1.07	4.7	2.8	0.63
deo4r3.c29	15.82	17.52	0.03	1.73	4.9	3.1	0.60
deo4r3.c30	15.08	16.78	−0.08	2.05	5.7	3.3	0.66
deo4r3.c31	13.61	15.30	−0.04	1.31	5.4	2.9	0.71
deo4r4.c00	14.04	15.73	0.11	1.03	4.8	2.8	0.66
deo4r4.c01	15.71	17.41	0.06	1.84	5.4	3.1	0.68
deo4r4.c02	15.18	16.88	−0.07	1.98	5.8	3.1	0.71
deo4r4.c03	13.77	15.46	−0.04	1.61	6.3	3.2	0.75
deo4r4.c04	13.99	15.68	0.07	1.24	5.3	3.0	0.69
deo4r4.c05	15.66	17.36	0.07	1.55	5.4	3.0	0.69
deo4r4.c06	15.19	16.88	−0.10	1.90	6.2	3.1	0.75
deo4r4.c07	13.60	15.30	−0.06	1.17	5.6	2.8	0.76
deo4r4.c08	13.75	15.45	0.08	1.06	5.2	2.8	0.71
deo4r4.c09	15.57	17.26	0.09	1.26	5.4	2.9	0.71
deo4r4.c10	15.32	17.02	−0.08	1.36	5.6	3.0	0.72
deo4r4.c11	13.69	15.39	−0.08	1.10	5.9	2.7	0.79
deo4r4.c12	13.69	15.38	0.07	0.84	5.0	2.7	0.71
deo4r4.c13	15.61	17.30	0.07	1.03	4.9	2.7	0.69
deo4r4.c14	15.42	17.12	−0.09	1.28	5.1	2.9	0.68
deo4r5.c06	15.70	17.40	−0.13	1.21	6.1	2.9	0.78
deo4r5.c07	13.03	14.74	−0.06	0.76	5.1	2.7	0.72

Recording	Depths		Tide	H_{m_0}	T_z	T_c	ε
	m	m	m	m	s	s	
deo4r5.c08	13.23	14.93	0.15	0.51	3.8	2.6	0.53
deo4r5.c09	16.31	17.99	0.13	0.83	4.8	2.7	0.69
deo4r5.c10	15.74	17.43	−0.14	0.94	4.4	2.8	0.58
deo4r5.c11	12.98	14.68	−0.08	0.81	5.0	2.8	0.70
deo4r5.c12	13.16	14.86	0.14	0.84	4.7	3.0	0.60
deo4r5.c13	16.33	18.02	0.11	1.27	5.0	3.2	0.58
deo4r5.c14	15.67	17.37	−0.16	1.51	5.5	3.2	0.66
deo4r5.c15	12.94	14.65	−0.09	1.05	5.5	3.0	0.71
deo4r5.c16	13.56	15.26	0.17	1.22	5.7	3.3	0.67
deo4r5.c17	16.83	18.52	0.13	2.23	5.6	3.3	0.65
deo4r5.c18	15.78	17.48	−0.17	1.82	5.9	3.4	0.67
deo4r5.c19	12.97	14.67	−0.11	1.13	4.9	3.1	0.61
deo4r5.c20	13.36	15.06	0.19	1.20	5.0	3.0	0.63
deo4r5.c21	16.59	18.28	0.09	2.48	5.7	3.4	0.64
deo4r5.c22	15.62	17.32	−0.16	1.93	6.2	3.1	0.75
deo4r5.c23	12.88	14.59	−0.07	2.24	7.0	3.3	0.78
deo4r5.c24	13.66	15.35	0.21	1.79	5.9	3.2	0.70
deo4r5.c25	16.83	18.51	0.06	1.99	5.6	3.2	0.68
deo4r5.c26	15.43	17.12	−0.18	1.98	6.1	3.4	0.69
deo4r5.c27	12.55	14.25	−0.09	1.20	5.1	3.0	0.66
deo4r5.c28	13.36	15.06	0.21	1.35	4.7	2.9	0.62
deo4r5.c29	16.61	18.30	0.08	1.86	5.2	3.2	0.62
deo4r5.c30	15.28	16.98	−0.19	1.53	5.4	3.5	0.59
deo4r5.c31	12.55	14.25	−0.07	1.13	4.7	3.1	0.55
deo4r6.c00	13.80	15.50	0.23	1.20	4.4	3.0	0.55
deo4r6.c01	16.92	18.61	0.05	1.50	5.0	2.9	0.66
deo4r6.c02	15.22	16.92	−0.21	1.25	5.2	3.2	0.62
deo4r7.c09	16.30	17.99	−0.01	1.22	4.6	3.1	0.55
deo4r7.c10	14.46	16.15	−0.15	1.36	5.3	3.3	0.62
deo4r7.c11	12.97	14.67	−0.01	0.96	4.8	2.8	0.65
deo4r7.c12	14.49	16.18	0.18	0.94	4.7	2.8	0.65
deo4r7.c13	16.04	17.73	−0.03	1.78	5.2	3.3	0.61
deo4r7.c14	14.57	16.26	−0.14	1.62	5.7	3.4	0.65
deo4r7.c15	13.23	14.93	−0.02	0.91	4.6	2.9	0.62
deo4r7.c16	14.63	16.32	0.19	0.85	4.3	2.7	0.61
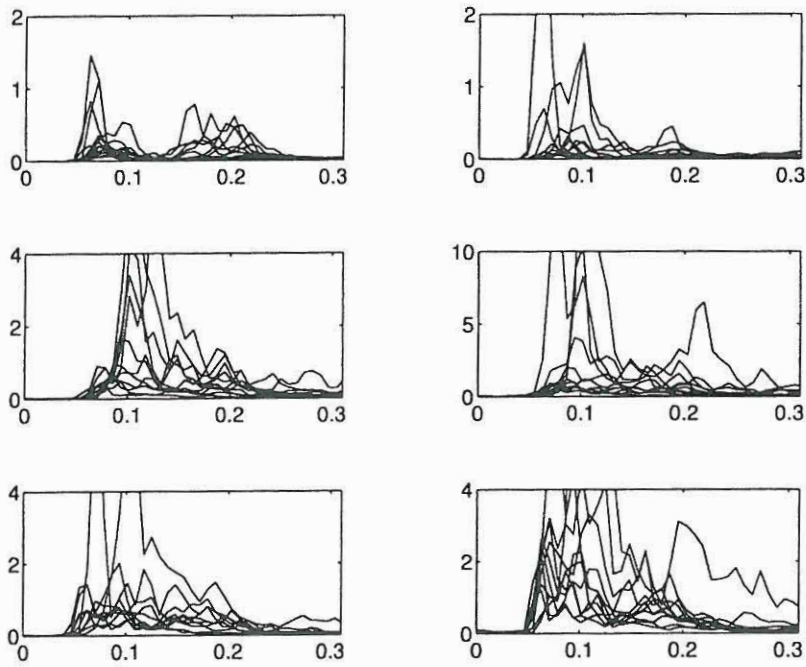
Figure D.1: *Raw energy spectra.*
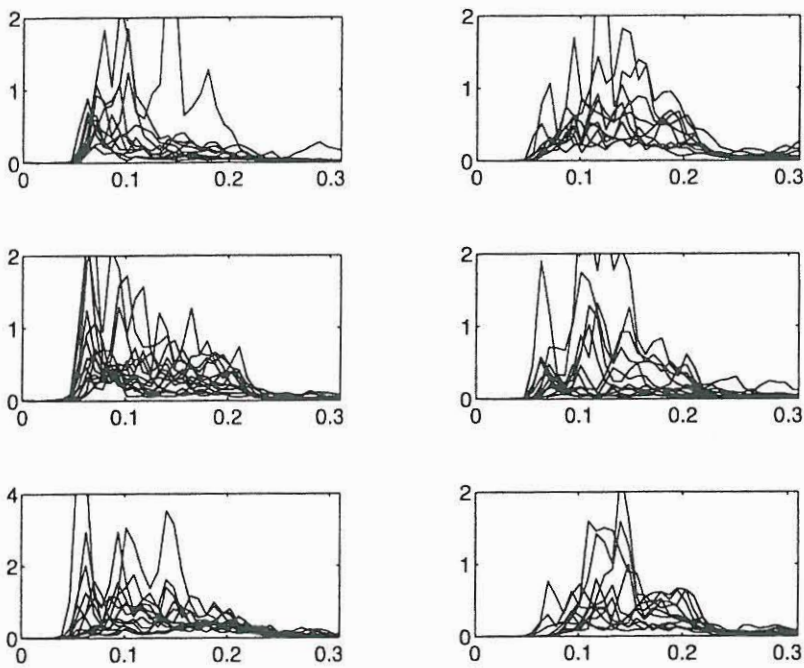
Figure D.2: *Raw energy spectra.*

Datafile	Depth m	$H_{s,I}$ m	$H_{s,R}$ m	$\theta_{m,I}$ deg.	$\sigma_{\theta,I}$ deg.	$\theta_{m,R}$ deg.	$\sigma_{\theta,R}$ deg.	C_R
deo4r0.r17	16.0	0.525	0.349	260.4	30.4	98.2	32.4	0.603
deo4r0.r18	14.4	0.455	0.331	254.7	29.6	104.4	30.5	0.733
deo4r0.r19	13.6	0.367	0.346	255.6	28.2	101.9	27.8	0.902
deo4r0.r20	15.2	0.360	0.421	268.0	32.1	87.3	31.4	1.149
deo4r0.r21	16.2	0.533	0.455	255.9	26.9	94.0	30.1	0.886
deo4r0.r22	14.6	0.736	0.506	237.2	27.7	112.6	32.3	0.692
deo4r0.r23	13.6	0.546	0.410	230.0	24.5	120.1	30.9	0.751
deo4r0.r24	15.1	0.478	0.576	232.2	32.2	114.7	32.8	1.192
deo4r0.r25	16.2	0.684	0.630	239.7	31.1	115.8	32.2	0.923
deo4r0.r26	14.6	0.810	0.595	234.2	24.3	111.8	32.7	0.715
deo4r0.r27	13.4	0.576	0.532	231.7	19.5	108.8	32.2	0.861
deo4r0.r28	15.0	0.569	0.518	236.8	32.7	106.5	35.4	0.921
deo4r0.r29	16.6	0.463	0.536	253.2	29.2	103.8	29.9	1.096
deo4r1.r21	17.8	0.576	0.521	269.8	26.8	93.6	33.1	0.961
deo4r1.r22	15.6	0.337	0.468	281.0	27.5	83.3	28.0	1.293
deo4r1.r23	12.4	0.295	0.318	262.4	29.7	96.8	30.3	1.113
deo4r1.r24	14.3	0.379	0.400	255.5	22.6	93.1	23.6	0.952
deo4r1.r25	17.8	0.599	0.605	277.0	21.8	82.9	22.8	0.947
deo4r1.r26	15.6	0.393	0.527	271.8	28.6	77.3	27.3	1.232
deo4r1.r27	12.4	0.358	0.334	260.2	26.6	105.3	28.4	0.856
deo4r1.r28	14.4	0.456	0.504	266.5	25.9	93.5	26.8	1.045
deo4r1.r29	18.2	1.017	0.903	271.0	27.1	80.3	28.5	0.901
deo4r1.r30	15.9	0.859	0.754	270.2	23.9	86.5	27.3	0.914
deo4r1.r31	12.3	0.728	0.341	253.1	27.0	116.3	33.6	0.418
deo4r2.r00	14.2	0.908	0.862	272.1	28.9	84.2	26.4	0.979
deo4r2.r01	18.0	1.551	1.500	272.3	22.4	82.6	27.0	1.014
deo4r2.r02	15.7	0.900	0.827	271.6	30.6	85.7	30.0	0.931
deo4r2.r03	12.3	0.627	0.385	253.8	27.6	105.6	33.5	0.560
deo4r2.r04	14.3	0.757	0.645	271.6	28.8	84.3	30.0	0.872
deo4r2.r05	18.4	1.896	1.681	276.6	24.0	85.9	26.9	0.875
deo4r2.r06	16.0	1.802	1.405	265.8	28.6	86.7	30.9	0.799
deo4r2.r07	12.3	0.955	0.515	262.5	20.7	91.9	29.4	0.449
deo4r2.r08	14.1	1.100	0.881	268.1	23.5	91.4	22.6	0.758
deo4r2.r09	18.0	1.647	1.647	269.4	30.5	76.0	23.4	1.066
deo4r2.r10	15.8	1.209	1.183	271.2	29.4	80.2	30.3	0.994

Datafile	Depth	$H_{s,I}$	$H_{s,R}$	$\theta_{m,I}$	$\sigma_{\theta,I}$	$\theta_{m,R}$	$\sigma_{\theta,R}$	C_R
	m	m	m	deg.	deg.	deg.	deg.	
deo4r2.r11	12.4	0.973	0.476	260.2	21.2	102.1	31.8	0.549
deo4r2.r12	14.3	1.023	0.929	274.2	25.0	83.5	23.1	0.916
deo4r2.r13	18.1	1.909	1.008	272.8	25.6	82.9	23.7	0.986
deo4r2.r14	15.8	0.834	1.112	256.5	28.1	85.3	34.5	1.074
deo4r2.r15	12.5	0.773	0.538	259.5	25.0	107.9	33.0	0.527
deo4r2.r16	14.4	1.021	0.909	277.2	26.8	82.4	22.8	0.893
deo4r2.r17	17.9	3.437	0.855	284.6	24.0	75.6	23.2	0.845
deo4r2.r18	15.7	1.940	1.140	269.4	28.1	87.6	24.3	1.035
deo4r2.r19	12.6	1.519	0.436	264.3	20.3	96.4	31.6	0.465
deo4r2.r20	14.4	1.407	0.868	271.9	22.6	85.6	21.5	0.937
deo4r2.r21	17.9	2.846	0.764	267.6	25.5	97.5	28.7	0.766
deo4r2.r22	15.7	1.183	0.866	272.8	27.2	87.4	29.4	0.894
deo4r2.r23	12.5	0.788	0.478	255.1	25.6	107.4	29.0	0.512
deo4r2.r24	14.3	1.008	0.925	267.8	30.0	90.7	27.8	0.862
deo4r2.r25	17.8	1.604	0.749	273.1	24.4	89.5	20.8	0.746
deo4r2.r26	16.0	0.851	0.924	274.1	28.9	78.4	29.1	0.885
deo4r2.r27	13.2	0.724	0.771	268.0	22.7	93.4	25.2	0.731
deo4r2.r28	14.8	1.200	0.921	273.0	25.7	86.8	25.3	0.888
deo4r2.r29	17.8	2.038	0.952	275.9	24.3	81.8	27.4	0.937
deo4r2.r30	15.7	1.283	1.135	275.0	27.1	85.2	25.8	0.957
deo4r2.r31	12.9	1.238	0.534	265.0	18.3	89.5	27.7	0.519
deo4r3.r00	14.5	1.390	1.027	279.7	26.2	83.9	23.3	0.948
deo4r3.r01	17.5	2.255	0.926	273.3	22.2	79.9	26.1	0.898
deo4r3.r02	15.7	1.476	0.944	278.5	26.2	85.6	25.9	0.927
deo4r3.r03	13.6	0.927	0.788	268.2	16.9	89.9	21.1	0.871
deo4r3.r04	15.4	1.255	1.219	275.3	20.3	85.5	18.3	1.133
deo4r3.r05	17.7	3.522	0.864	267.5	24.4	93.6	26.1	0.809
deo4r3.r06	15.8	1.586	0.986	267.5	29.4	80.4	25.6	0.957
deo4r3.r07	13.3	1.211	0.615	262.4	21.6	102.6	25.9	0.597
deo4r3.r08	14.7	1.230	0.812	272.3	26.6	86.8	25.8	0.804
deo4r3.r09	17.0	1.735	1.027	277.0	26.0	78.0	27.5	0.974
deo4r3.r10	15.6	1.231	0.973	266.1	30.3	88.1	28.5	0.946
deo4r3.r11	13.8	0.809	0.737	257.1	28.4	92.3	29.8	0.727
deo4r3.r12	15.0	0.796	1.037	264.6	31.0	86.6	27.8	1.003
deo4r3.r13	17.1	1.236	0.867	271.3	26.3	81.6	27.5	0.849

Datafile	Depth m	$H_{s,I}$ m	$H_{s,R}$ m	$\theta_{m,I}$ deg.	$\sigma_{\theta,I}$ deg.	$\theta_{m,R}$ deg.	$\sigma_{\theta,R}$ deg.	C_R
deo4r3.r14	15.7	0.638	0.587	266.5	27.2	82.7	28.4	0.932
deo4r3.r15	13.7	0.546	0.356	256.0	27.5	107.0	30.2	0.662
deo4r3.r16	14.6	0.625	0.566	274.5	27.7	81.2	25.7	0.927
deo4r3.r17	16.6	0.863	0.890	276.7	25.6	71.6	27.3	1.077
deo4r3.r18	15.4	0.696	0.629	270.6	25.0	83.5	24.6	0.977
deo4r3.r19	14.0	0.484	0.447	270.1	28.9	84.6	27.6	0.902
deo4r3.r20	15.0	0.674	0.636	280.0	28.0	83.2	28.4	0.959
deo4r3.r21	16.6	1.612	1.262	284.7	20.2	82.5	24.3	0.816
deo4r3.r22	15.5	0.993	0.894	267.5	30.8	86.2	29.3	0.934
deo4r3.r23	13.9	0.913	0.678	273.7	20.0	90.2	23.1	0.766
deo4r3.r24	14.7	0.932	0.793	284.2	26.6	75.0	27.4	0.864
deo4r3.r25	16.4	1.452	1.082	282.6	22.9	80.5	26.3	0.745
deo4r3.r26	15.6	1.086	0.828	270.4	30.3	82.1	30.9	0.787
deo4r3.r27	14.3	0.894	0.613	272.9	20.8	89.7	24.8	0.704
deo4r3.r28	14.7	0.761	0.693	274.1	25.9	83.5	24.2	0.917
deo4r3.r29	16.3	1.212	1.070	285.7	25.0	71.3	24.2	0.915
deo4r3.r30	15.6	1.348	1.164	273.6	27.7	87.7	26.2	0.871
deo4r3.r31	14.1	1.012	0.755	272.3	25.0	91.4	29.7	0.793
deo4r4.r00	14.6	0.724	0.571	280.2	27.7	84.4	25.7	0.804
deo4r4.r01	16.2	1.354	1.059	284.9	21.3	81.1	27.0	0.789
deo4r4.r02	15.7	1.506	1.187	268.2	26.3	97.1	27.2	0.698
deo4r4.r03	14.3	1.062	0.826	270.4	24.3	81.1	26.0	0.811
deo4r4.r04	14.5	0.809	0.659	278.4	25.2	84.7	25.0	0.837
deo4r4.r05	16.2	1.043	0.939	280.0	25.8	75.6	27.2	0.918
deo4r4.r06	15.7	1.344	1.344	272.0	23.9	84.5	22.3	1.038
deo4r4.r07	14.1	0.780	0.680	274.7	22.5	83.9	22.8	0.738
deo4r4.r08	14.3	0.735	0.651	279.5	29.6	82.1	27.7	0.897
deo4r4.r09	16.1	0.791	0.848	281.0	26.1	69.1	24.4	0.979
deo4r4.r10	15.9	0.992	0.799	260.7	28.2	84.6	32.1	0.826
deo4r4.r11	14.2	0.685	0.534	264.8	22.6	99.7	21.7	0.778
deo4r4.r12	14.2	0.558	0.516	271.1	26.0	84.0	28.1	0.945
deo4r4.r13	16.1	0.628	0.609	283.0	30.0	74.2	27.0	0.984
deo4r4.r14	16.0	0.943	0.834	269.6	33.0	74.5	31.5	0.918
deo4r5.r06	16.2	0.718	0.547	262.0	30.7	98.0	33.4	0.781
deo4r5.r07	13.6	0.526	0.364	252.7	28.1	105.2	33.3	0.628

Datafile	Depth	$H_{s,I}$	$H_{s,R}$	$\theta_{m,I}$	$\sigma_{\theta,I}$	$\theta_{m,R}$	$\sigma_{\theta,R}$	C_R
	m	m	m	deg.	deg.	deg.	deg.	
deo4r5.r08	13.8	0.306	0.371	275.5	28.8	86.8	26.3	1.248
deo4r5.r09	16.8	0.494	0.518	271.0	28.8	81.4	29.9	1.037
deo4r5.r10	16.3	0.580	0.555	282.6	27.8	82.4	28.1	0.934
deo4r5.r11	13.5	0.568	0.388	253.9	28.0	100.5	29.5	0.664
deo4r5.r12	13.7	0.543	0.458	273.0	27.9	84.4	27.5	0.830
deo4r5.r13	16.9	0.826	0.905	284.6	23.4	73.3	25.4	1.151
deo4r5.r14	16.2	0.865	0.928	275.9	30.8	80.3	31.5	1.115
deo4r5.r15	13.5	0.752	0.527	274.3	25.1	88.9	26.8	0.757
deo4r5.r16	14.1	0.806	0.674	288.1	25.2	84.8	24.4	0.822
deo4r5.r17	17.4	1.597	1.437	278.6	22.8	80.4	28.5	0.914
deo4r5.r18	16.3	1.236	1.223	269.4	25.0	75.5	25.4	1.013
deo4r5.r19	13.5	0.861	0.646	262.9	25.6	91.2	30.7	0.771
deo4r5.r20	13.9	0.951	0.681	273.5	26.1	85.9	27.8	0.735
deo4r5.r21	17.1	1.737	1.424	279.0	23.0	73.6	26.7	0.817
deo4r5.r22	16.2	1.300	1.175	270.9	27.8	79.8	29.0	1.025
deo4r5.r23	13.4	1.587	0.924	263.0	21.0	97.5	27.7	0.542
deo4r5.r24	14.2	1.250	1.019	272.9	25.2	89.0	26.0	0.830
deo4r5.r25	17.3	1.336	1.372	268.0	25.5	80.7	24.1	1.061
deo4r5.r26	16.0	1.269	1.254	268.3	26.4	85.6	23.8	1.058
deo4r5.r27	13.1	0.922	0.546	263.2	22.4	100.9	31.3	0.567
deo4r5.r28	13.9	1.047	0.772	275.0	25.7	85.4	29.4	0.756
deo4r5.r29	17.1	1.312	1.276	273.5	24.8	87.1	28.7	1.021
deo4r5.r30	15.8	1.103	0.907	263.5	28.7	85.7	28.5	0.848
deo4r5.r31	13.1	0.899	0.528	265.0	23.5	96.3	30.0	0.565
deo4r6.r00	14.3	0.912	0.721	278.5	29.9	82.1	30.1	0.740
deo4r6.r01	17.4	0.993	0.976	271.8	30.8	73.6	30.4	1.028
deo4r6.r02	15.8	0.907	0.775	266.2	28.8	90.9	29.8	0.858
deo4r7.r09	16.8	0.910	0.745	274.7	29.2	75.8	29.5	0.827
deo4r7.r10	15.0	0.953	0.582	261.3	25.6	84.7	32.8	0.596
deo4r7.r11	13.5	0.671	0.544	278.9	22.3	84.1	25.1	0.817
deo4r7.r12	15.0	0.646	0.529	281.1	26.0	81.8	26.8	0.815
deo4r7.r13	16.6	1.291	1.028	276.0	26.8	78.9	27.3	0.812
deo4r7.r14	15.1	1.076	0.904	273.4	27.0	84.3	27.0	0.856
deo4r7.r15	13.8	0.661	0.482	268.2	18.9	82.8	22.3	0.741
deo4r7.r16	15.2	0.604	0.523	273.3	28.1	79.6	29.4	0.868

E

Simulations

The following tables show the results from the directional analysis of the simulations described in Chapter 5.

For comparison the following variables are introduced.

$$\Delta_T = 90° - \theta_{m,I} = \theta_{m,R} - 270° \qquad \text{(E.1)}$$

$$\Delta_{E,I} = 90° - \theta_{m,I} \qquad \text{(E.2)}$$

$$\Delta_{E,R} = \theta_{m,R} - 270° \qquad \text{(E.3)}$$

Δ_T denotes the difference between main directions and the normal to the structure according to target values. $\Delta_{E,I}$ and $\Delta_{E,R}$ denote the same difference according to estimated values for incident and reflected waves respectively.

Model	Target [°]			Estimated [°]			
Test	$\theta_{m,I}$	$\theta_{m,R}$	Δ_T	$\theta_{m,I}$	$\Delta_{E,I}$	$\theta_{m,R}$	$\Delta_{E,R}$
2f 5	90	270	0	90.5	-0.5	270.2	0.2
6	80	280	10	80.5	9.5	279.6	9.6
7	70	290	20	73.3	16.7	286.7	16.7
8	60	300	30	68.9	21.1	289.8	19.8
9	90	270	0	90.1	-0.1	270.0	0.0
10	80	280	10	79.9	10.1	279.5	9.5
11	70	290	20	70.3	19.7	289.2	19.2
12	60	300	30	63.7	26.3	296.4	26.4
2h 23	90	270	0	90.0	0.0	270.8	0.8
24	80	280	10	82.5	7.5	277.8	7.8
25	70	290	20	73.4	16.6	286.9	16.9
26	60	300	30	66.5	23.5	290.8	20.8
2l 30	90	270	0	89.7	0.3	270.1	0.1
31	80	280	10	80.5	9.5	276.9	6.9
32	70	290	20	72.6	17.4	285.2	15.2
33	60	300	30	63.3	26.7	293.2	23.2
34	90	270	0	90.1	-0.1	274.2	4.2
35	80	280	10	80.3	9.7	286.2	16.2
36	70	290	20	78.1	11.9	295.5	25.5
37	60	300	30	69.6	20.4	297.2	27.2
38	50	310	40	64.1	25.9	309.1	39.1

Table E.1: Model-2f/h/l.

| Model | | Target [°] | | | Estimated [°] | | | |
Test		$\theta_{m,I}$	$\theta_{m,R}$	Δ_T	$\theta_{m,I}$	$\Delta_{E,I}$	$\theta_{m,R}$	$\Delta_{E,R}$
3l	15	89.5	270.5	0.5	91.4	−1.4	282.2	12.2
	16	99.5	260.5	−9.5	101.3	−11.3	272.0	2.0
	17	109.5	250.5	−19.5	110.3	−21.3	258.4	−11.6
	18	119.5	240.5	−29.5	117.8	−27.8	251.9	−18.1
	19	129.5	230.5	−39.5	125.9	−35.9	244.5	−25.5
4l	20	88.4	271.6	1.6	90.7	−0.7	291.2	21.2
	21	98.4	261.6	−8.4	100.7	−10.7	276.1	6.1
	22	108.4	251.6	−18.4	109.5	−19.5	256.4	−13.6
	23	118.4	241.6	−28.4	118.3	−28.3	253.8	−16.2
	24	128.4	231.6	−38.4	126.3	−36.3	238.2	−31.8
	25	138.4	221.6	−48.4	134.0	−44.0	225.9	−44.1
5l	26	86.6	273.4	3.4	87.6	2.4	289.1	19.9
	27	96.6	263.4	−6.6	97.6	−7.6	273.5	3.5
	28	106.6	253.4	−16.6	107.6	−17.6	255.8	−14.2
	29	116.6	243.4	−26.6	116.7	−26.7	234.5	−35.5
	30	126.6	233.4	−36.6	125.0	−35.0	209.3	−60.7
	31	136.6	223.4	−46.6	132.9	−42.9	211.5	−58.5
	32	146.6	213.4	−56.6	139.7	−49.6	203.4	−66.6

Table E.2: Model-3l, -4l, -5l.

F

Performance Analysis of the BDM Method

F.1   Introduction

F.1.1   Purpose

In order to evaluate the ability of the BDM method, Hashimoto et. al. 1988, when applied to reflected shortcrested waves, some numerical simulations have been carried out. This note presents the estimates of the directional wave spectra and reflection coefficients, which have been obtained by use of the BDM method. The results are presented as graphs showing the estimated reflection coefficients together with the estimated main directions and directional spreading of the incident and reflected waves respectively. The results are shown in the frequency domain.

The method has been used to estimate the reflection from various caisson structures in a physical model, Helm–Petersen 1994. The results are believed to be reliable in most cases. The numerical simulations presented here also aim at an evaluation of the reliability of these results.

F.1.2 The BDM Method

The BDM method is used for the estimation of directional wave spectra. Subsequently it may be used for estimating the reflection from coastal structures exposed to short-crested waves. This implies that the ranges of directions, where incident and reflected waves may occur respectively, are known.

The BDM method, in the present implementation, does not account for the reflected waves directly. That is, the distance from the measurering points to the reflecting structure is not assumed known. This is an advantage in cases, where the reflection points is not a unique well defined line, which is only the case for a non perforated vertical wall type of structure.

F.2 Test Conditions

In general the simulation parameters correspond to the configuration in the *'Caisson Investigations'*, Helm-Petersen (1994).

F.2.1 Numerical Simulation of Waves

A white-noise filtering method has been used for numerical generation of wave-fields. The filter length was 245 elements. Incident waves were generated in 40 directions in the range $[180°; 360°]$, cf. Figure F.1. Timeseries, with a duration of 12 minutes were generated with a sampling frequency of $5Hz$.

F.2.2 Wave Parameters and Test Set–Up

The JONSWAP wave spectrum ($\gamma = 3.3$) and the Mitsuyasu directional spreading function were used in the simulations. The depth of water was $0.61m$. The wave elevations were simulated in a 5×2 array of wave gauges. The mutually distances were $0.5m$, and the distance to the reflection line was $1.0m$, except when something else is stated. The following two tables show the main direction and spreading of the simulated waves and the reflection coefficient applied in the various tests.

Label	$\theta_{m,I}$	$\theta_{m,R}$	s	C_R
Test1	270°	90°	7	0.0
Test2	270°	90°	7	0.4
Test3	270°	90°	7	0.9
Test4	250°	110°	7	0.4
Test5	250°	110°	7	0.9
Test6	230°	130°	7	0.4
Test7	210°	150°	7	0.9

Test series 1.

Label	$\theta_{m,I}$	$\theta_{m,R}$	s	C_R
Test1x	270°	90°	29	0.0
Test3x	270°	90°	29	0.9
Test5x1	230°	130°	3	0.4
Test5x2*	230°	130°	7	0.4
Test5x3†	230°	130°	7	0.4

* denotes alternative wave gauge array

† denotes spatial errors in input

Test series 2.
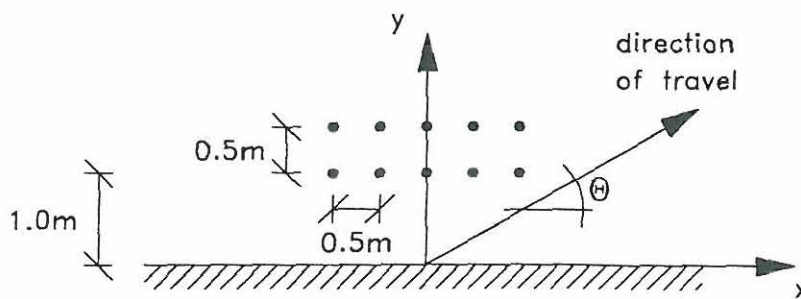
Figure F.1: Set-up of wave gauges.

F.3   Analysis

F.3.1   Spectral Analysis

The BDM method is based on a spectral analysis of the measured wave elevation timeseries. The spectral estimates are derived by use of Fast Fourier Transformation. The timeseries are divided into subseries, which have been tapered over 10% in each end using the cosine–squared function. The subseries contain 256 elements, which result in 14 subseries. The loss in variance due to tapering are regained by proper amplification of the timeseries. Overlapping of subseries has not been applied.

Only frequencies containing more variance than 5% of the maximum variance were analysed. The directional spreading functions were discretized into 36 intervals causing a directional resolution of 10°.

F.3.2   Results

Table F.1 shows the results from the directional analysis.

Label	H_{s_I}	H_{s_R}	C_R	$\theta_{m,I}$	$\sigma_{\theta,I}$	$\theta_{m,R}$	$\sigma_{\theta,R}$
Test1	0.131	0.036	0.25	269.4	22.6	87.3	35.3
Test2	0.132	0.067	0.51	269.9	22.7	88.1	28.9
Test3	0.136	0.125	0.92	270.4	23.8	89.0	24.7
Test4	0.131	0.065	0.49	254.6	23.1	110.3	30.3
Test5	0.134	0.123	0.93	254.4	25.1	106.2	25.5
Test6	0.127	0.066	0.52	239.7	23.7	129.3	32.5
Test7	0.128	0.124	0.97	224.7	24.2	138.7	24.2
Test1x	0.137	0.008	0.02	269.8	11.4	84.1	36.1
Test3x	0.144	0.128	0.89	269.8	15.6	90.8	17.3
Test5x1	0.125	0.076	0.60	241.8	31.8	131.6	35.5
Test5x2	0.127	0.070	0.55	241.2	24.5	122.1	34.6
Test5x3	0.128	0.066	0.52	239.0	24.0	127.8	33.8

Table F.1: *Results of analysis with BDM.*

Wave Spectra — Reflection — Incident waves — Reflected waves

Test: run2.bdm

Wave Spectra — Reflection — Incident waves — Reflected waves

Test: run3.bdm

Wave Spectra

Test: run4.bdm

Reflection

Incident waves

Reflected waves

Wave Spectra

Test: run5.bdm

Reflection

Incident waves

Reflected waves

Wave Spectra

Reflection

Test: run6.bdm

Incident waves

Reflected waves

Wave Spectra

Reflection

Test: run7.bdm

Incident waves

Reflected waves

Wave Spectra

Reflection

Test: run1x.bdm

Incident waves

Reflected waves

Wave Spectra

Reflection

Test: run3x.bdm

Incident waves

Reflected waves

Wave Spectra

Reflection

Test: run5x1.bdm

Incident waves

Reflected waves

Wave Spectra

Reflection

Test: run5x2.bdm

Incident waves

Reflected waves

Wave Spectra

Test: run5x3.bdm

Reflection

Incident waves

Reflected waves

F.4 Evaluation

The BDM method has been applied to numerically generated reflected shortcrested waves. The tests conditions were adapted from the 'Caisson Investigations'. Only test concerning a non perforated vertical wall were performed in order to reduce the amount of tests. The vertical wall type of structure was chosen, since simulation of reflection from such a structure is relatively simple and close to reality. A possible influence of the wave steepness ($H_{s0}/L_{0p} = 0.04$) on the reflection was ignored.

Considering the difficulties in estimating reflection from a structure exposed to shortcrested waves, the ability of the BDM method is reasonable. The estimated reflection coefficient as a function of frequency is contaminated with some scatter, but the total weighted reflection coefficients is estimated quite well, although always slightly higher than the target value. Main directions of both incident and reflected waves are estimated within a range of $\pm 10°$ ($5°$ in most cases). The directional spreading is also estimated close to the target values, but some fluctuations do occur, which is reflected in the scatter of the estimated reflection coefficients. This consideration encourages to perform some averaging of the reflection coefficients, which has not been done in the presented results.

Additional conditions subjected to analysis.

- **Number of gauges and type of array.**
  The number of gauges are important to the performance of the BDM method. This is believed mainly to be due to the inhomogeneous conditions occuring in front of the reflecting structure due to phase locking. Simulations have been performed with a varied number of gauges and various types of arrays. These are not presented within this note, but the number of gauges is found to be more important than the type of array. If only a few gauges are available the type of array should be chosen carefully.

- **Duration of timeseries.**
  The duration of the tests are relatively short. A few tests have been performed having twice the duration. The influence on the results were negligible, indicating that the duration beyond a certain limit (here approx. 500 waves) has only little influence on the results.

- **Sample frequency.**
  The sample frequency should be high enough, in order to achieve a Nyquist frequency higher than the highest frequency having any significant wave energy in the wave energy spectrum. A higher sample frequency does not improve the results.

Series Papers
Hydraulics and Coastal Engineering Laboratory
ISSN 0909-4296